Experimental Analysis of Boundary Layer Dynamics in Plunging Breaking Wave

TOOMAS LIIV

TALLINN UNIVERSITY OF TECHNOLOGY
Faculty of Civil Engineering
Department of Mechanics

The dissertation was accepted for the defence of the degree of Doctor of Philosophy on May 18, 2011

Supervisor: Prof. Aleksander Klauson, Department of
                               Mechanics, Tallinn University of Technology,
                               Estonia

Co-supervisor   Prof. Emeritus Klas Cederwall, Department of
                               Land and Water Resources Engineering, Royal
                               Institute of Technology, Stockholm, Sweden

Opponents: Dr. Rolf Deigaard, Chief Engineer, Danish
                               Hydraulic Institute, Denmark

                               Prof. Jüri Elken, Institute of Marine Systems,
                               Tallinn University of Technology, Estonia

Defence of the thesis: May 24, 2011 Lecture hall VII-226, Tallinn
                               University of Technology, Ehitajate tee 5,
                               Tallinn

Declaration:

Hereby I declare that this doctoral thesis, my original investigation and achievement, submitted for the doctoral degree at Tallinn University of Technology has not been submitted for any academic degree.

Toomas Liiv

Sukelduva murdlaine piirikihi dünaamika eksperimentaalne analüüs

TOOMAS LIIV

Contents

List of original publications

This thesis is mainly based on the data presented in the following publications in peer-reviewed journals:

I   T. Liiv, 2001. Investigation of Turbulence in a Plunging Breaking Wave. Proceedings of the Estonian Academy of. Sciences. Engineering; 7(1), 58-78.

II T.Liiv, 2007. An Experimental Investigation of the Oscillatory Boundary Layer Around the Breaking Point. Proceedings of the Estonian Academy of. Sciences. Engineering; 13(3), 215-233.

III T. Liiv, P. Lagemaa, 2008. The Variation of the Velocity and Turbulent Kinetic Energy Field in the Wave in the Vicinity of the Breaking Point. Estonian Journal of Engineering; 14(1), 42-64.

and on the following conference publications:

IV T. Liiv, (1995) An Experimental Investigation of the Breaking Wave Characteristics in Coastal Region. International Conference on Coastal and Port Engineering in Developing Countries, Proceedings of the COPEDEC IV, Rio de Janeiro, Brazil; 1995; 1995, 3, 2334-2343.

V T. Liiv, U. Liiv, 1998. Shear Investigations of the Breaking Waves in the Flume. Proceedings of the 3rd International Conference on Hydro-Science and Engineering; Cottbus/Berlin, Germany; CD-ROM, 12 p.

V T. Liiv, U. Liiv, 1999. Laboratory Study of the Breaking Wave Characteristics; Proceedings of the XXVIII IAHR Congress 22-27 August, Graz, Austria, CD-ROM

VI T. Liiv, 2001. The effect of bottom roughness on the flow quantities under plunging breaking wave motion, 29th Annual Congress of the International-Association-of-Hydraulic-Engineering-and-Research (IAHR), Hydraulics for Maritime Engineering, Theme E, Proceedings   pp 313-319

VII   T. Liiv, 2005. The Effect of Bottom Roughness on the Flow Structure under Wave Breaking Condition in the Surf Zone. Transactions of the Conference Dedicated to the 100th Birthday prof. R.R. Chugajev; SPbGTY Nautšno-tehnitšeskie vedomosti; Sankt Petreburg, 19-25. (In Russian).

ACRONYMS, ABBREVIATIOS AND NOTATIONS

CFD   Computational Fluid Dynamics
CTA   Constant Temperature Anemometer
DNS   Direct Numerical Simulation Method
LDA   Laser Doppler Anemometer
LES   Large Eddy Simulation
PIV   Particle Image Velocimeter
RANS   Reynolds Averaged Navier-Stokes equations
SAV   Sontek Acoustic Velocimeter
MAC   Marker and Cell Method

Introduction

Background

Everything connected with the sea has been of utmost importance to mankind already since the dawn of times. It has been the divider and connector between people, continents and cultures. Famous seafarers have set sail from their native shores to discover new lands and cultures, so enhancing the life of the whole mankind. Throughout the centuries, the sea has been a rich source of food to millions of people.

On the other hand, sea has been a source of fear and terror for people living on its coasts or sailing it. The main source of these catastrophes is the various natural phenomena that might occur on the coastline. These phenomena are usually caused by various natural processes ranging from earthquakes to wind driven storms. Even a moderate storm in favourable conditions can cause unpredictable changes on the coastline that result in damage to nature or humans.

The last centuries have seen intensive growth in the usage of coastline. The construction of ports and various other hydro-technical structures has resulted in the shift in the hydrodynamic balance that has been achieved over thousands of years. Another important aspect is also the climate change. These processes have caused intensive coastline deformation processes all over the world.

The present work is focused on the experimental investigation of the complicated phenomena – wave breaking in the surf zone. The physical modelling of this process that forms a basis for mathematical modelling has not been systematic and has given ambivalent results. This seems to be caused by the non–stationary behaviour of wave breaking that presents higher demands to the experimental setup, equipment and processing of measured data.

The morphological processes on the coastline are mainly connected with the wind generated waves and the corresponding wave generated current. Depending on the geographical location there is a balance on the coastline that has developed over the centuries and the coastline is more or less stable. Severe storms can cause temporary changes in this stability and result mainly in seasonal variation of the coastline.

One of the main agents of coastline change is the breaking process of the waves and the accompanying generation of cross- and long-shore currents. In the surf zone these processes result in shear stresses on the bed and consequently in re-suspension of material from the bed. The suspended material is carried along with the currents.

The hydrodynamic and morphologic processes are closely related to the wave breaking. Although the breaking phenomenon has been studied already for decades, there are still cases that lack generalized correlations based on systematic investigations.

As the trend on the coastline is to build ever more and larger structures, there is an ever-growing need to solve the engineering problems connected with wave breaking and the hydrodynamic and morphologic processes around new infrastructures on the coastline. The need to protect the marine environment from the impact of these developments has led to several restrictions in the time frame of these works. For instance in Estonia all marine works have to be stopped during the spawn period of the coastal fish. Unfortunately the period happens to be the time with smallest winds and waves. As the environmentally sensitive areas are relatively well mapped, a high precision modelling tool would be capable of demining potential risks to these areas. The mathematical models at present day can not resolve the breaking process and the associated flows adequately due to the non-stationary nature of the phenomena. This is mainly due to the necessity of large computer resources. The lack of computer power is the reason why main hydrodynamic models treat the flow in the surf zone as a field, instead on following an individual wave. The advances in computer technology will soon make it possible to do it. The need is urgent as the breaking process itself is an extremely complicated time dependent process and its investigation even in controlled laboratory environment sets high demands to the experimental setup and processing of measured data. The experimental investigation of wave breaking in nature, i.e. on the coast of the ocean, is only taking its first steps, as the data processing and measuring equipment is getting smaller and more reliable, allowing its transportation.

The results of the publications from the past two or three decades cover investigations carried out for various initial and boundary conditions and in many cases assumptions have been made on the basis of stationary hydrodynamics. These assumptions may not always be adequate to depict the content of the non–stationary process.

The aim of the present study was to clarify the physical properties of the flow in the vicinity of the breaking point of the wave. The results could be the basis for refining of the present mathematical models.

Problem setting

Although the various mathematical models describing the processes on the coastline have reached micro scales, i.e. to the level of turbulent fluctuations, there is still a lack of general concepts based on experimental investigations. In the absence of these concepts, modellers have used various parameters that have been acquired using similar experiments in a stationary flow or in the best case unsteady oscillating flows in pipes. The main drawback of these experiments is that the data obtained in this way neglects the time dependent character of the breaking wave motion.

There is a particularly wide gap between real needs and available data in the intermediate vicinity of the wave breaking point. The behaviour of flow in this region has a fundamental effect on the diffusion and dissipation processes in the wave and also contributes much to the energy balance in the surf zone. The

wave breaking and the associated unsteady flow in the wave boundary layer are the key agents that contribute to the settling and re-suspension of material from the seabed, which is the main reason for coastline change.

Main objectives

The present study was initiated to make thorough experimental investigations around the wave breaking point. The goal was to use a wave flume to measure two-dimensional flow fields inside the breaking wave and perform a qualitative comparison with similar experimental studies. The aim was to get an insight into the boundary layer flow and turbulent kinetic energy of the breaking wave.

In order to achieve the goals the following problems had to be solved:
- The creation of the experimental setup that would enable regular waves to be created with a constant wave period and provision of a system for the measurement and simultaneous saving of the measured data.
- The measurement of the two-dimensional flow field and the statistical analysis of the measured data.
- The calculation of the time dependent flow and turbulent energy field inside the breaking wave.
- The calculation of the boundary layer properties of the time dependent wave.

1 Overview of the existing experimental studies

1.1 Experimental studies of breaking waves

The experimental investigation of the processes that govern the behaviour of sediment and waves in the surf zone has been a gradual process that has taken decades. The first investigations concentrated on the measurements of the free surface of the surf zone during wave action. Svendsen and Hansen (1976) focused on the average physical values of the wave, whereas the turbulent structures inside the wave were not discussed.

The first insights into the mechanism of the breaking wave were gained with the introduction of different contact free measuring techniques, such as LDA (Laser Doppler Anemometer) and PIV (Picture Image Velocimeter). Various investigators have used the mentioned systems for measuring the velocity fields and turbulent characteristics in the waves. Chang and Liu (1999) measured the kinematics of the breaking waves and found that the velocity of the water particles in the wave crest exceeds the wave phase velocity 1.7 times. This phenomenon was even more complicated by the areas of high entrainment due to the breaking process as the air bubbles block the laser beams.

As the knowledge of the breaking process has increased, the mathematicians have proposed several mathematical models to describe the process phenomena. The common problem encountered with the models is that of an accurate representation of the physical phenomenon, the models need to overcome the nonlinearity of certain parts of the equations and that empirical relations are required that can only be obtained through experiments. The breaking process by nature is an unsteady process, but in most cases due to lack of information the data used is obtained from the investigations of similar stationary processes. The most widely used coefficients for closing the nonlinear terms of the equations are the coefficients of turbulent viscosity or tensor turbulent shear stress. As data on a unsteady flow is scarce, there is a great need for further experimental investigations.

The most widely used method of the determination of the velocity field and its turbulent characteristics in the breaking waves is the Laser Doppler Anemometry. The first to publish a paper on LDA measurements in the breaking waves was Stieve (1980). Nadaoka and Kondoh (1982) defined the inner and outer surf zone based on the measured characteristics of the breaking waves in these regions. The most comprehensive studies this far have been published by Ting and Kirby (1994, 1995, 1996). The data obtained by the authors has been used for comparison and measurement verification by most other authors. Ting and Kirby found that in the case of plunging breaking wave there is an area of high turbulent intensity in front of the wave crest. This area was found to move perpendicular to the coastline.

The advantage of the PIV method is that this method enables one to investigate the coherent structures inside the flow. The first to publish papers on PIV measurements were Haydon et al. (1996) and Chang & Liu (1996). Haydon et al. used local averaging to determine average velocity and velocity fluctuations, whereas Chang & Liu used ensemble averaging.

The shear stresses on the bottom have been mainly measured using CTA (Constant Temperature Anemometer) techniques. The most comprehensive studies under the breaking waves have been carried out by Deigaard et al.(1991) and Cox et al.(1996).

In recent years there have been numerous experiments carried out in the surf zone and not only in the laboratory. In the measuring instruments, mainly LDA, a mechanical profiling system, acoustic pressure sensors, video cameras, current meters etc, are mounted on tripods. Feddersen & Trowbridge (2005) measured the wave generated turbulence in the surf zone and eventually developed a model that is able to reproduce the production and dissipation of turbulence during wave breaking. Trowbridge & Agraval (1995) measured the wave boundary layer. Their measurements indicate that there is a reduction in variance and the increase in phase relative to the flow outside the boundary layer. Feddersen & Williams (2007) measured the distribution of Reynolds stresses and Bryan et al. (2003) investigated dissipation near the surf zone. Feddersen et al. (2003) investigated drag coefficients, bottom roughness and wave breaking in the near shore area during a two-month campaign.

1.2 Overview of the studies on boundary layer flows under breaking waves

Today there are several quasi-stationary models that describe processes in the boundary layer in the case of oscillatory flow over horizontal bottom. These models can roughly be divided into three groups.

The simplest model assumes that the velocity distribution in the boundary layer is logarithmic during the whole period of oscillation, whereas the boundary layer thickness varies. Viability of these models depends on the roughness of the bottom. The first of these classical models was presented by Jonsson (1966).

The second type of models on boundary layer flows assumes that the flow distribution during the horizontal oscillatory flow resembles the flow distribution of a laminar oscillatory flow. The main models were derived by Kalkanis (1957, 1966), Sealth (1987) and Nielsen (1985, 2005). These models are derived to describe the harmonic mode of the flow.

The velocity distribution in this case is calculated as

$$u(z,t) = A\omega[1 - D_1(z)]e^{i\omega t}, \qquad (1)$$

And here

$$D_1(z) = \exp\left[-(1+i)\frac{z}{\sqrt{2\nu/\omega}}\right]. \qquad (2)$$

In the first equation $u(z,t)$ is the variation of velocity over the vertical coordinate z and time t. The variable A is the amplitude of motion, ω is radian frequency, $D_1(z)$ is the velocity defect function for a smooth laminar flow and ν is kinematic viscosity. The vertical length scale of this velocity distribution is called the Stokes length δ_S and can be expressed for the turbulent flow both for rough and smooth boundaries as

$$\delta_s = \sqrt{2\nu/\omega} \ , \qquad (3)$$

According to Nielsen (1985) the velocity defect is nearly constant throughout the boundary layer, so Equation (1) can be rewritten as:

$$D_1 = \exp\left[-(1+i)(z/z_1)^p\right]. \qquad (4)$$

Here D_1 is the velocity defect function for a turbulent oscillatory flow and the parameters z_1 and p are derived using special graphs by Jonsson and Carlsen (1976). Both parameters depend on the relative roughness of the wall and the Reynolds number.

According to Jensen (1989) Eqs. (1) and (4) describe both the turbulent and the transitional boundary layers well, provided that the relative roughness is greater than 0.01.

The third type of the boundary layer models combine eddy viscosity with the equation of motion

$$\rho \frac{\partial u}{\partial t} = -\frac{\partial p}{\partial x} + \frac{\partial \tau}{\partial z}.$$ (5)

Here u is the velocity, p is the pressure, x is the horizontal coordinate, and τ is the shear stress.

When vertical accelerations are negligible in comparison with the acceleration of gravity and assuming that the shear stresses vanish outside the boundary layer, Eq. (5) can be rewritten as

$$\rho \frac{\partial}{\partial t}(u - u_\infty) = \frac{\partial \tau}{\partial z}.$$ (6)

Here u_∞ is the velocity infinitely remote from the boundary. If we assuming that all eddy viscosity ν_t models depend only on z, but not t, shear stresses can be expressed as $\tau = \rho \nu_t (\partial u / \partial z)$ and Eq. (6) can be rewritten as

$$\frac{\partial}{\partial t}(u - u_\infty) = \frac{\partial}{\partial z}(\nu_t \frac{\partial u}{\partial z})$$ (7)

Different types of eddy viscosity ν_t models have been developed by Kaijura (1968), who proposed a three layer eddy viscosity distribution.

In order to close the equations of the mathematical models describing coastal processes, source terms are required to depict the velocity distribution in the boundary layer during the breaking process.

Using eddy viscosity models the velocity distribution in the oscillatory boundary layer was mathematically derived by Kajura (1968) and Grant and Madsen (1979, 1982). Brevik (1981) proposed another model to determine two layer eddy viscosity distribution. He simplified the model by omitting the inner layer. Rodi (1980) published a book that dealt with all possible eddy viscosity schemes, including k-ε scheme for solving turbulent boundary layer problems. Christensen and Deigaard (2001) calculated the flow fields, large eddies and turbulent kinetic energy fields of plunging and spilling breakers.

The first model that took into account the time dependence of the eddy viscosity was derived by Trowbridge and Madsen (1984).

In 1985 Fredsoe et al (1985) proposed a time dependent turbulence model that assumed parabolic viscosity distribution over the boundary layer. The governing equation presented was

$$v_t(z,t) = k|U_f(t)|z\left(1 - \frac{z}{\delta(t)}\right) \qquad (8)$$

where U_f is shear velocity, $\delta(t)$ is the width of the boundary layer and k is the von Karman coefficient. Absi (2001) proposed two models for predicting time dependent turbulent eddy viscosity:

1. based on measurements of the Reynolds stresses by Jensen et al (1989) $R_{12} = -\overline{u'w'}$;
2. based on turbulent viscosity concept, similar to the $k - \varepsilon$ model that is averaged over the oscillation period.

The increase of computer speed during the last decades has led to more intensive use of models, based on Navier–Stokes equations. This has initiated a separate branch of mathematical modelling, computational fluid dynamics (CFD). CFD allows modelling of different flows with utmost complicated flow kinematics, whereas the result of calculations is relatively accurate. The advantage of CFD is its high precision but the main drawback is the necessity of large computer resources. The method is based on the Navier–Stokes equations that describe the evolution of the momentum of the water volume. The set of equations consists of the continuity equation and equations for the components of the momentum.

The models that describe the processes on the inclined bottom profile usually also take into account the generation of bottom ripples that are responsible for the generation of vorticity in the bottom boundary layer. Already in 1982 Sealth (1991, 1982) presented several numerical methods with rounded ripple profiles which described shear stress on the wall definitely well. Blondeaux and Vittori (1990) have presented different methods of vorticity generation and prediction of suspended sediment around these vortices. Different types of eddy viscosity models have been used to describe an oscillatory flow on the inclined bottom Xing (2004). Feddersen et al. (2003) measured the shear coefficient, bottom roughness and wave breaking on the ocean beach. Wave breaking on the natural beach and its boundary layer were investigated by Trowbridge and Agrawal (1995).

Theoretical results of Trowbridge and Madsen (1984) agreed well with the measurements of Jonsson and Carlsen (1976) that determined the near bottom velocity in an oscillating water tunnel using a micropropeller. Bottom shear stress was estimated by a logarithmic fit. Jensen (1989) and Jensen et al. (1989) measured the turbulent boundary layer in an oscillatory water tunnel at large Reynolds number, studying smooth and rough bottoms. Flush mounted hot film sensors were used for direct measurements of the bottom velocities.

All the studies on the mathematical models describing bottom boundary layer flows use data obtained in oscillatory flows in pressure pipes, an example can be work by Jonsson and Carlsen (1976). One of the last works that depict the results of Jonsson, I.G. & Carlsen (1976) is the one by Heinloo and Toompuu (2009)

It should be noted that although most experiments have been carried out with unsteady and oscillating flow, the flow in pressure pipes differs greatly from oscillatory free surface flows. In essence, the first reliable investigations of flow structure and boundary layer in free surface flows started with the introduction LDA technology. The first works were published in the 1980s by Stieve (1980). He measured both vertical and horizontal coordinates of velocity. In 1982 Nadaoka and Kondoh's (1982) laboratory measurements proved the existence of large-scale vortices and associated long shore vorticity in the flow.

Most of the mathematical models of the oscillatory wave boundary layer make an assumption based on the previously mentioned experimental investigations by Jonsson and Carlsen (1976). Their experiments showed that the velocity infinitely far away from the solid boundary, u_∞ varies with a sinusoidal pattern in time and the shear stress $\tau(0,t)$ follows the same trend with a slight phase shift. This phase shift was initiated by the hydrodynamic processes in the wave. The same phase lag was also observed in the case of the present experimental run by Liiv and Lagemaa (2008).
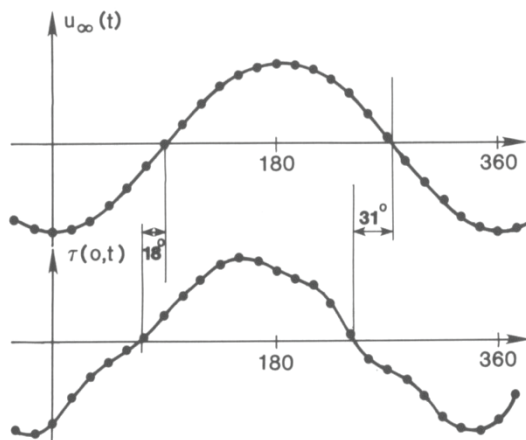
Figure 1 Time variations of the bed shear stress $\tau(0,t)$ for a rough turbulent flow over relatively small roughness elements Svendsen (1976).
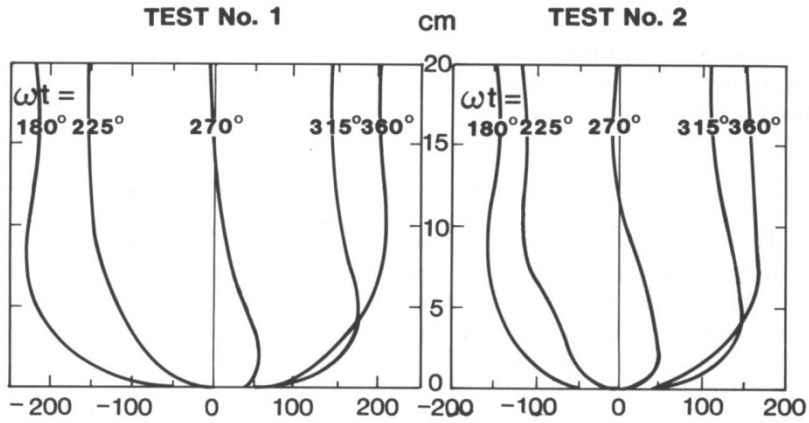
Figure 2 Instantaneous velocities u(z,t) plotted against elevation from the top of the roughness elements. Numbers on the curves refer to the phase of the free stream velocity $A\omega\sin\omega t$ Jonsson (1966)

As Figure 1 shows, the velocity near the bed turns back before the free stream velocity. The maximum value of the velocity is not on the free surface, but near the bottom, at the level of about ¼ of the stream height. The velocity profiles for different ωt that correspond to Fig. 1 are presented in Fig. 2.

Many of the mathematical models that calculate the time dependent velocity distribution of flow velocity in the boundary layer use the non-dimensional velocity profiles derived by Jensen (1989) and Jensen et al. (1989). Their experiments were conducted in a U – tube with a rectangular cross-section. The free stream velocity changes according to the pattern $A\omega\sin\omega t$. Figure 3 shows the semi-log plot of the mean velocity distribution. The orbital amplitude over the boundary layer $A = 3.1$ m, oscillation period $T = 9.72$ s. The dimensionless quantities u^+ and y^+ were calculated as

$$y^+ = z\langle u*\rangle / v \text{ and } u^+ = \langle u\rangle(z,t)/\langle u*\rangle(t) \tag{9}$$

As the flow is in the boundary layer on the smooth flat surface, the values in the equation do not change along the flow. Here z is the vertical coordinate, $\langle u*\rangle$ - shear velocity, v - kinematic viscosity and t is time.
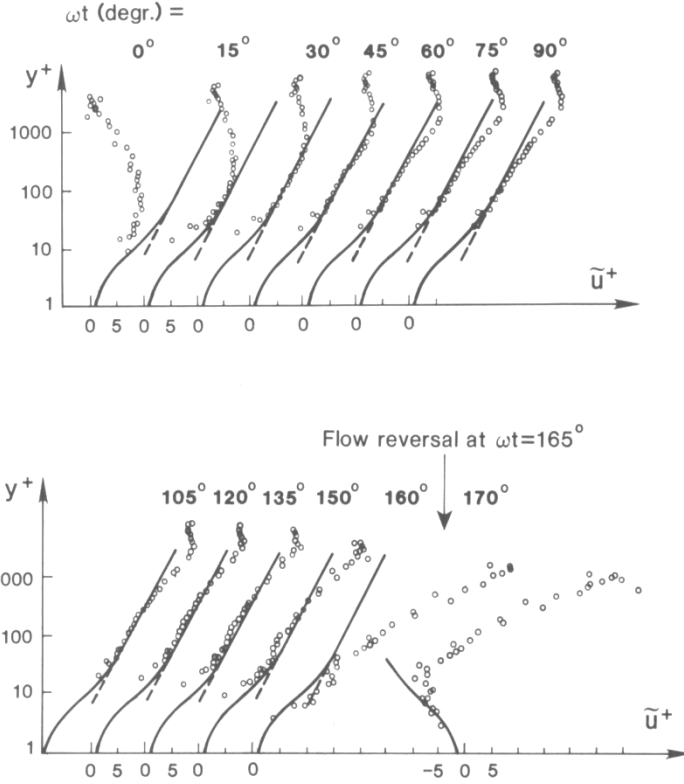
Figuer 3 Dimensionless velocity profiles for smooth turbulent oscillatory flows at different phases of the free stream velocity $A\omega \sin \omega t$ Jensen (1989)

Here and below u^+ is given by logarithmic distribution

$$u^+ = (1/k)\ln y^+ + 5,$$ (10)

at large values of y^+. k is the von Karman constant (equal to 0.4).

Numerous experimental studies are dedicated to the determination of oscillatory velocity distribution, both for two- and three-dimensional flows and for smooth and rough boundaries, for example, Nadaoka and Kondoh (1982), Lin and Liu (1998), Pedersen et al. (1998), Arnskov et al. (1993), Stansell (2002), Rogers and Dalrympe (2004), Liu and Babanin (2004), and Sugihara et al. (2005). Here it is suitable also to mention that no systematic investigations of the oscillatory boundary layer flow around the breaking point have been performed, and therefore usually boundary layer calculations are based on works by Nielsen (2005).

Cox et al. (1996) investigated the shear stresses measured in the wave flume on the inclined bottom profile. Krstic & Fernando (2001)investigated the effect of artificial roughness on the bottom boundary layer. Bryan et al. (2003) used Sontek Acoustic Velocimeter (SAV) to measure wave energy and energy dissipation in the breaking waves on the coast of New Zealand.

2   Experimental setup and procedures

2.1   Experimental setup

The experimental work of the present study aims at the determination of the unsteady two-dimensional flow field parameters in the wave breaking point and around its immediate vicinity. Based on the experiments performed in the wave flume of Tallinn University of Technology, the variation of the two-dimensional flow fields during the breaking process perpendicular to the shoreline have been investigated. For this purpose regular waves were generated in the wave flume. Vertical and horizontal velocity components under the weakly plunging breaking wave were measured with LDA. As a result of the measurements in 29 profiles and 1852 points along the surf zone model slope perpendicular to the shoreline, the time dependent two-dimensional flow field was measured.

2.1.1   Description of the experimental setup

The wave flume used was 0.6 meters wide, 0.6 meters deep and 22 meters long (Fig. 4). The transparent walls of the flume were made of glass and the bottom was made of vinyl plates. Waves were generated in the constant depth section of the wave flume, which was 12.45 meters long. The average water depth in the constant depth section was kept at 0.3 meters. Regular waves were generated with the flap type wave generator. During current experimental
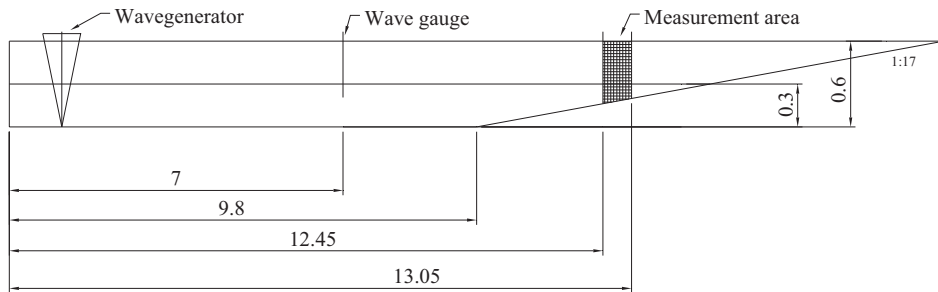
Figure 4 Wave flume (measurements in meters)

run waves were generated with a constant wave period $T = 2.03$ seconds. The wave parameters describing the breaking wave are listed in Table 1. The electric motor that drove the wave generator was controlled with a frequency controller. Before measurement procedures were initiated, the waves were let run for 30 minutes to allow for a decrease of the reflection caused by second harmonic waves and for the generation of adequate wave set up.

Table 1. Parameters describing a weak plunging breaker

T, s	h_b, m	d_b, m	x_b, m	H_0, m	H_0/L_0	H_b, m	H_b/d_b
2.0	0.106	0.111	2.90	0.072	0.012	0.118	1.06

Here T is the wave period, h_b is water depth at the breaking point, including the change of water level due to wave set-up, d_b still water depth at the breaking point, H_0 is deep water wave height, L_0 is deepwater wave length, H_b is wave height at the breaking point.

The measurement section was chosen such that it would incorporate also the breaking point. Wave breaking was investigated on a surf zone model made of vinyl plates. The model had a constant slope of 1 to 17. The velocity field inside the breaking waves was measured with a two-component argon-ion Laser Doppler Anemometer (LDA) with an output power of 1.3 W. Forward scatter mode was used throughout the experiments.

As the LDA system allows measurement only in one point, the measurements were repeated over the vertical for all 29 profiles and with a total number of 1852 measuring points. The measuring net had a variable step. The measuring profiles were one centimetre apart before the breaking point and three centimetres after the breaking point. The measuring step along the vertical was 1 mm in the near–bed zone, 3 mm in the intermediate zone and 2 mm in the zone affected directly by wave action. During the experiments the measuring point closest to the bottom was 0.05 mm away from the bottom.

The aim of the investigation was to get an insight into the flow structure and different hydrodynamic processes in the vicinity of the wave breaking point. The total number of wave cycles sampled in each measuring point was N=151. The data processing procedures and main results of investigations are given in Liiv and Lagemaa (2008). Main attention in the study was focused on the determination of the velocity field inside the breaking wave. Investigations were concentrated to the area close to the bottom of the surf zone model, where data was collected in each measuring profile with the vertical density of 1 mm. The closest measuring point to the bottom was considered to be the bottom shear velocity. The reasoning behind this claim is that as the laser beams measuring the horizontal velocity component entered the flume under an angle (cf. Fig. 5), it was possible to project the measuring volume to the very bottom of the flume. Thus, it can be said that the height of the first measuring point is equal to one half of the shorter half axis of the measuring volume. Generally, the dimensions of the measuring volume can be calculated using the formulas:

$$\delta_x = \frac{4F\lambda}{\pi E D_L \cos\left(\dfrac{\theta}{2}\right)} \quad \text{and} \quad \delta_z = \frac{4F\lambda}{\pi E D_L \sin\left(\dfrac{\theta}{2}\right)}, \tag{11}$$

where δ_x and δ_z are the measures of the shorter and longer axes of the measuring volume, λ is the wave length of the laser beam, the rest of the notation is illustrated in Fig. 5. This will give the value of the shorter half axis as 0.12 mm, which is of the same precision as the precision of mounting a hot film probe. The horizontal velocity measured closest to the model bottom was taken to be shear velocity $u*$.
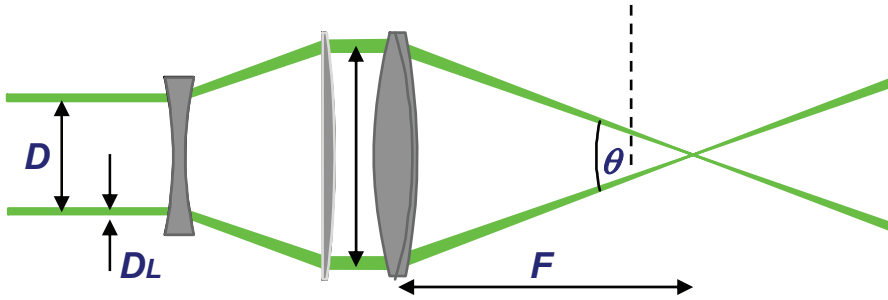
Figure 5 Explanation to Equation (11). D is the distance between the laser beams, D_L is the diameter of the laser beam, F is the focal distance of the frontal lens and θ is the angle between the laser beams

In order to evaluate the values of the shear velocity measured in the abovementioned way, calibration calculations were made using the method proposed by Shin (2004). This method enables one to evaluate the values of shear velocity in the case of shallow water wave action. The analysis showed that the results achieved were satisfactory and the concurrency of measurements with existing information was good.

Wave parameters were kept constant throughout the experiments. Wave similarities were controlled with the synchronizing mechanism and analyzed with the methods depicted below. The working principle of the synchronizing mechanism is described by Liiv (2001). Probably the best representation of the location of the measuring points can be obtained from Figures 25 to 30. The wave parameters and location of the measuring points are given in Table 2.

2.1.2 Procedures

Experimental data from six channels were stored in a computer simultaneously. The channels were connected to the computer through an analog-digital converter. During the experimental run both, horizontal and vertical components of the velocity, the corresponding signal dropouts, water level variation and signals from the synchronizing mechanism were saved. In

order to achieve reliable results during ensemble averaging, data were collected for 151 wave periods (T=2.03s). Sampling frequency was 1000 Hz, that means that for each measuring location 6 x 306 530 data points were saved. The total number of measuring points was 1852.

In order to filter the experimental results, dropout signals were used. In the case of measurements with the LDA system, dropouts occur, when the measuring volume is not formed of the laser beams or the beam is blocked by a solid object, for instance, by a sediment particle or air bubble. This means that the dropout signal showed if the measured value was true.

The use of the signal from the synchronizing mechanism is mostly necessary for the synchronization of the measured data. The synchronizing mechanism was made of two stainless steel wires. The existence of electric conductivity between the wires showed if the synchronizing mechanism was in water or not. The signal was considered as a truth – value, i.e. if the synchronizing mechanism was in water, the value was 1 and if out of water, then 0. The location of the synchronizing mechanism was kept constant during the whole experimental arrangements. Experimental runs were started, when the value of the signal had been 1 for at least 50 ms to avoid false information from possible water sprays.

A common problem with the experiments in the wave flume is how the generation of waves with a constant period can be achieved and which methods have to be used. The most common shortcoming of the wave flume is usually the generation reflected waves between the wave generator and the surf zone model. The easiest way to deal with the problem is to perform experiments before the reflected waves occur. In the present case it was impossible, as the number of wave periods in the experimental run was 151. For this reason the reflected wave was taken as part of the wave. The next analysis investigates the behaviour of the reflected wave. 1250 wave periods were measured from the start up of the generator. The result is depicted in Fig. 6. The vertical axis is the synchronizing mechanism based wave period, the upper horizontal axis is time and the lower the wave number. It can be seen from the figure that after the initial stabilization the wave period is approximately 2.02 seconds. After wave number 500 the reflected waves arrive and within 200 waves the wave period stabilizes at 2.03 seconds. This new wave period will stay virtually unchanged for the rest of the working time of the generator. The upper axis gives us the wave flume stabilization time. The mean wave period is achieved at wave 1680, i.e. 28 minutes after starting the wave generator. For this reason waves were always let run at least 30 minutes before starting the measuring procedures.

The flow velocity inside the turbulent flow can be described as the sum of an averaged velocity and the fluctuating component.

$$u_i(t) = \langle u_i(t) \rangle + u'_i(t), \tag{12}$$

where $u_i(t) = (u(t); v(t); w(t))$ is the measured velocity, $\langle u_i(t) \rangle$ is the averaged velocity and $u'_i(t)$ is the turbulent fluctuations. As mentioned in the introduction, the most common way of defining the averaged velocity is

ensemble (phase) averaging. The ensemble-averaged velocity is then derived from the equation

.

Table 2. Location of measuring points and corresponding wave parameters

Cross section no.	No. of measuring points on the vertical	Distance from the origin x, m	Water depth d, m	Water depth h, m	Wave celerity C, m/s
29	47	3.21	0.089	0.089	0.933
28	47	3.18	0.091	0.091	0.944
27	48	3.15	0.093	0.093	0.955
26	50	3.12	0.095	0.095	0.964
25	51	3.09	0.098	0.097	0.975
24	51	3.06	0,100	0.099	0.983
23	53	3.03	0.102	0.100	0.990
22	54	3.00	0.104	0.101	0.997
21	55	2.97	0.106	0.102	1.001
20	58	2.94	0.108	0.104	1.010
19	58	2.91	0.110	0.104	1.012
18	61	2,82	0.117	0.114	1.059
17	61	2.81	0.118	0.115	1.064
16	62	2.80	0.118	0.116	1.069
15	62	2.79	0.119	0.117	1.071
14	65	2.78	0.120	0.118	1.077
13	65	2.77	0.120	0.119	1.079
12	64	2.76	0.121	0.119	1.082
11	66	2.75	0.122	0.120	1.086
10	63	2.74	0.123	0.121	1.090
9	67	2.73	0.123	0.121	1.091
8	69	2.72	0.124	0.122	1.094
7	69	2.71	0.125	0.123	1.098
6	70	2.70	0.125	0.124	1.101
5	70	2.69	0.126	0.124	1.104
4	70	2.68	0.127	0.125	1.108
3	69	2.67	0.128	0.126	1.111
2	76	2.66	0.128	0.127	1.115
1	151	2.65	0.129	0.127	1.117

$$\langle u_i(t) \rangle = \frac{1}{N} \sum_{k=0}^{N-1} u_i(t+kT) \qquad 0 \le t \le T, \qquad (13)$$

where N is the number of averaged waves and T is the wave period. This method, however, requires very precise repetitions of the phenomena under investigation. Although the wave period stabilized in 30 minutes, this did not mean that all the waves entering the measuring section had had the same period. As seen in Fig. 6, the wave periods have a random character and have a distribution, as shown in Fig. 7. In the figure a wave spectra of 12 consequent

experimental runs, i.e. 1812 waves, is depicted. The vertical axis gives the number of occurrences and the horizontal axis shows the wave period. Although it might seem on the first glance that the experiments were performed with irregular waves, with an average period of 2.03 seconds, in reality, the deviation from the mean period is only ~±0.03 seconds that makes only ~1.5% of the whole wave period. Thus, the waves can be considered to be regular.
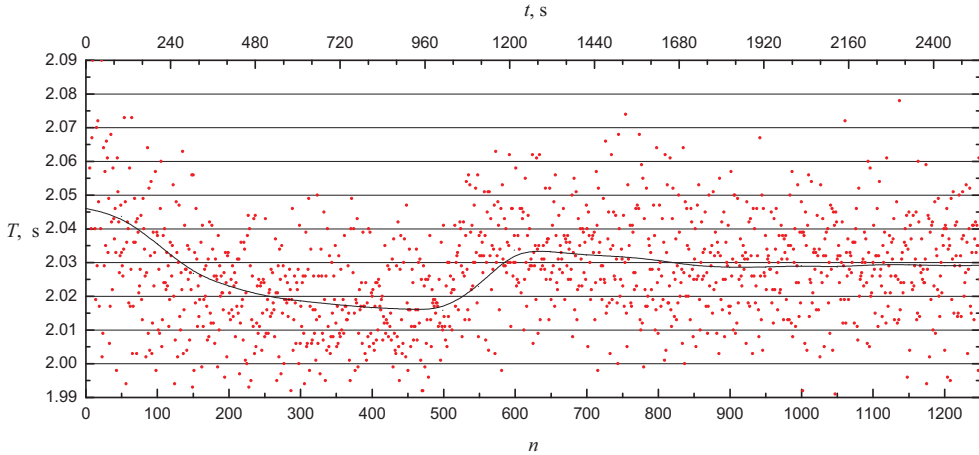
Figure 6 Stabilization of the wave periods after the start of the wave generator

It was shown that not all of the waves were with the same period, thus the usual way of ensemble averaging was not applicable. Instead, a modified ensemble-averaging method was derived. The similar method has also been used by Petti & Longo (2001).
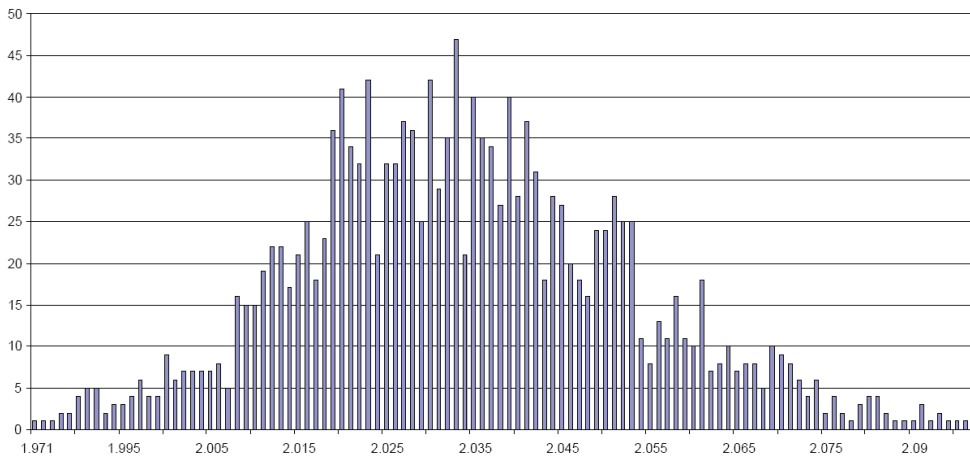
Figure 7 Spectra of wave periods for 12 consequent experimental runs N corresponds to the number of occurrences of the wave period

2.2 Statistical data processing

In the following a short description of the modified ensemble-averaging method is given. The first step was to find the average wave period (2.03 seconds) during the experiments and also all individual wave periods of all waves during the experimental run. Then all the waves were scaled so that they would be with the same length. For instance, if the period was longer (n=2050 points, sampling frequency was 1000 Hz, i.e. 2050 points correspond to the wave period 2.05 seconds), the required amount of points was evenly removed from the period, so that the period would be exactly 2030 points. If the period was shorter than the average, the required amount of points was added to the period. All the added points were given a dropout value and they were disregarded from the analysis. During the same process all very short and long periods with $n\pm30$ points larger or smaller than the average value were removed from the analysis. Finally, the ensemble average velocity was found with the equation

$$\langle u_i(t)\rangle = \begin{cases} \dfrac{1}{N}\displaystyle\sum_{k=0}^{N-1} u_i^*\left(t+kT_m\right)\cdot D_i\left(t+kT_m\right) & N_D \geq 10 \\ 0 & N_D < 10 \end{cases} \qquad 0 \leq t \leq T_m$$

(14)

where $u_i^*(t)$ is the time scaled velocity, T_m is the mean wave period, $D_i(t)$ is the dropout signal and N_D is the actual number of summed values (i.e. points with $D(t)=1$). If the ensemble averaged value is 0, then the measured data were not reliable.

According to the definition (6), the turbulent fluctuations can be calculated as

$$u'_i(t) = u_i(t) - \langle u_i(t)\rangle . \tag{15}$$

Classical ensemble averaging method calculates the turbulent fluctuations as

$$u'_i(t) = \frac{1}{N}\sqrt{\sum_{k=0}^{N-1}\left(u_i\left(t+kT\right)-\langle u_i(t)\rangle\right)^2} \qquad 0 \leq t \leq T$$

(16)

Similar to the averaged velocity, the value of the root-mean square of the turbulent fluctuations were found using a modified ensemble averaging

$$\langle u_i'(t)\rangle = \begin{cases} \dfrac{1}{N}\sqrt{\displaystyle\sum_{k=0}^{N-1}\left(u_i^*\left(t+kT_m\right)-\langle u_i(t)\rangle\right)^2 \cdot D_i\left(t+kT_m\right)} & N_D \geq 10 \\ 0 & N_D < 10 \end{cases} \qquad 0 \leq t \leq T_m$$

(17)

As the LDA system used only two measured components of the velocity, the turbulent kinetic energy was calculated using the method proposed by Stieve and Wind (1982)

$$k(t) = \frac{1,33}{2}\left(u'^2(t) + v'^2(t)\right).$$

$$(18)$$

The beginning of the coordinates is defined on the still water level to the beginning of the surf zone model, where the still water depth begins decreasing (Fig. 8). The measured data are presented in a non-dimensional form: the horizontal axis has a value

$$x_1 = \frac{x - x_b}{h_b} \qquad (19)$$
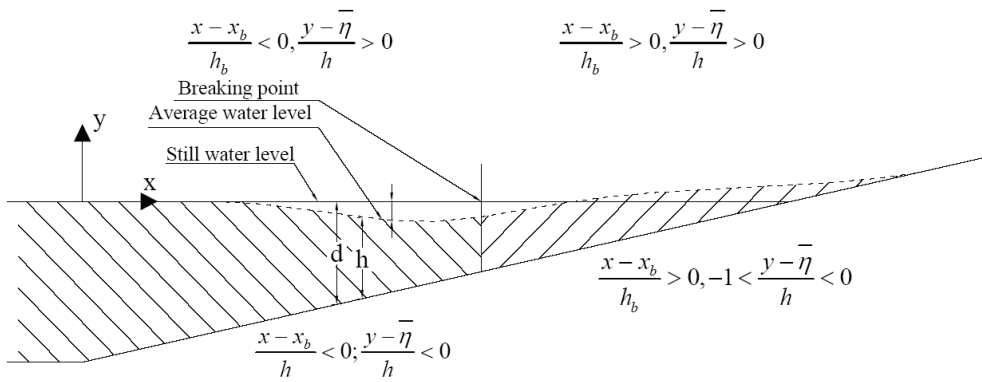
Figure 8 Dimensionless values

This value is 0 if $x = x_b$, defining the breaking point, positive if $x > x_b$ and negative if $x < x_b$.

Vertical axis is given with a value

$$y_1 = \frac{y - \eta}{h}$$

$$(20)$$

This is −1 if $y = -d$ and 0 if $y = \overline{\eta}$. The surface elevation in the case of breaking waves is classically depicted as

$$\eta_1 = \frac{\eta - \overline{\eta}}{h} \qquad (21)$$

The normalization of velocity components and the turbulent kinetic energy is carried out using the local wave phase velocity C:

$$C = \sqrt{gh}, \qquad (22)$$

where g is the acceleration due to gravity and h is average water depth in the current cross-section.

3 The variation of the two-dimensional velocity field during one wave period

3.1 Time series of the measured velocities

The time series usually depicted in the results of experimental investigations are the results directly measured during the experiments. All other data are derived from these.

Figure 9 shows the surface elevation and ensemble averaged horizontal and vertical velocity components at different cross-sections. As measurements were performed in 29 different cross-sections, only three were chosen to be depicted in this thesis. These cross – sections are $(x - x_b)/h_b = -2.36$, $(x - x_b)/h_b = 0.09$ and $(x - x_b)/h_b = 2.17$. From the 29 cross – sections measured, 3 cross-sections were chosen that describe data in the cross – section before breaking, during the initial breaking process and after the breaking had occurred. Vertical axis gives values of non-dimensional surface elevation and velocity. Different lines in the figures represent various measuring locations over the vertical, namely $(y - \bar{\eta})/h = -0.99$, $(y - \bar{\eta})/h = -0.89$, $(y - \bar{\eta})/h = -0.54$, $(y - \bar{\eta})/h = -0.17$ and $(y - \bar{\eta})/h = 0.18$. The explanation of the coordinate system is given above in section 2.2.

The surface elevation is depicted in Fig. 9 (A – C). It can be seen from the figures that the surface elevation in different cross-sections is not constant. In contrast to the inner surf zone measurements by Svendsen (1987) and Chang & Liu (1996), where the value $(\eta - \bar{\eta})/h$ is almost constant, the surface elevation in the outer surf zone changes considerably, especially in the region of initial breaking. Here the maximum surface elevation is equal to the average water depth and minimum surface elevation is 0.15 times the average water depth. This result agrees with the ones by Ting and Kirby (1995). The ratio of wave height to water depth H/h is 1.13, i.e. remarkably larger than the usual ratio described in association with the spilling and weakly plunging breakers ~0.8.

Figure 9 (D – F) gives values of variations in the ensemble-averaged horizontal velocity component during one wave period. It can be noticed that the horizontal component follows the variation of surface elevation and that there is a secondary crest after the velocity maximum. This secondary wave can be explained with a secondary wave generated by the backflow of water from the shoreline. Similar secondary waves have been described also earlier in the works by Ting and Kirby (1995).

Before the wave breaks, the maximum of the horizontal component is equal to ~0.4C in all cross-sections. After the crest this similarity between the cross-sections disappears. The non- dimensional horizontal velocity varies between 0.15C and 0.8C.
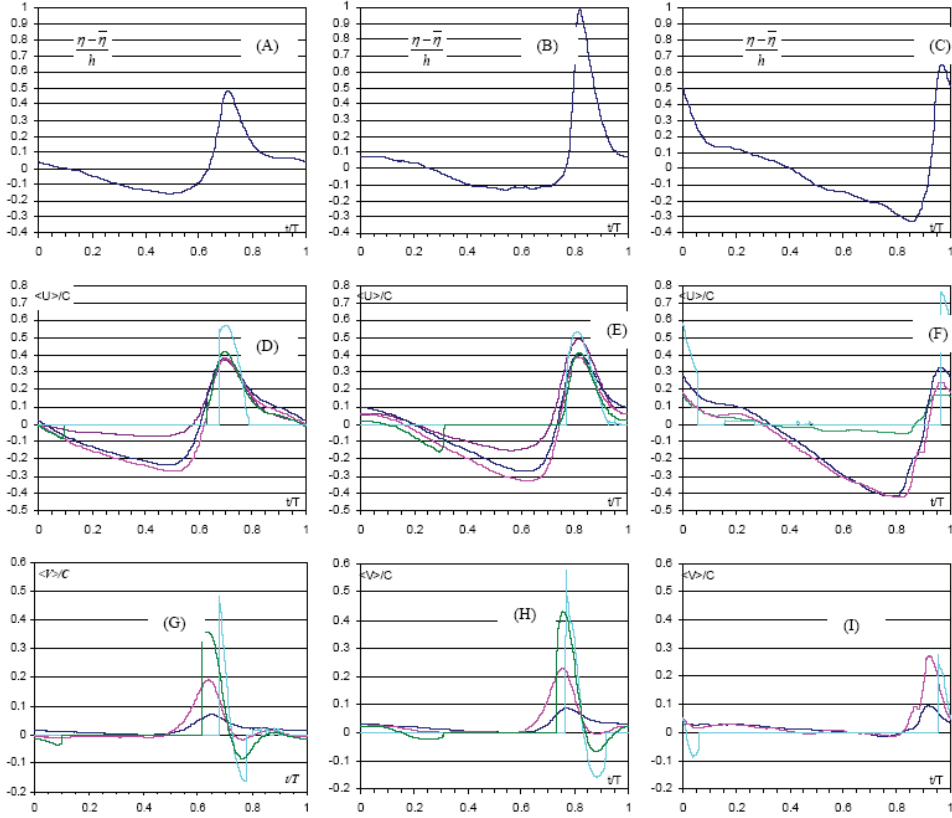
Figure 9 Surface elevation (A-C), horizontal velocity component (D–F) and vertical velocity component (G–I) in cross-sections $x - x_b / h_b = -2.36$ *(left column),* $x - x_b / h_b = 0.09$ *(centre column) and* $x - x_b / h_b = 2.17$ *(right column). at heights* $(y - \bar{\eta}) / h = -0.99$ *, (——)* $(y - \bar{\eta}) / h = -0.89$ *, (——)* $(y - \bar{\eta}) / h = -0.54$ *, (——)* $(y - \bar{\eta}) h = -0.17$ *, (——)* $(y - \bar{\eta}) / h = 0.18$

It can be noted that in the measuring points close to the still water level the value of the horizontal component is zero. As mentioned in the section concerning measurement procedures, this means that at this location there are no reliable data available. In the present case it means that the measuring volume was not formed due to the fact that the laser beams were out of the water in the wave trough. In most articles this data is not presented.

Figure 9 (G – I) gives the variation of the ensemble-averaged vertical velocity component. It can be noticed that the maximum value of the vertical velocity is always reached during the maximum acceleration of the horizontal velocity. The maximum of the vertical component moves along the wave crest, in front of it. This is the location where the backflow from the previous wave and the onshore movement of the new wave meet. It follows that water has

nowhere else to go than upwards. The maximum acceleration of the horizontal velocity is explained with the sudden reversal of the flow.

According to the experimental data, it can be concluded that during the maximum deceleration of the horizontal velocity component, the vertical velocity in the upper layers of the water column achieves its minimum value. This result supports the MAC (Marker and Cell) method Sakai et al (1986), which has been used to model the processes on the coastline. Here all computational elements are marked with so-called markers. These markers move according to the calculated velocity field.

The maximum value of the vertical component of the velocity in the intermediate layers of the water column is ~0.2C before the breaking point, which is in good agreement with earlier investigations of Ting & Kirby (1995). Near the still water level the value is ~0.5 C. After the breaking point during the backflow phase of the wave, the value of the vertical component of the velocity at all layers achieves its close to zero value.

3.2   Velocity variation over the vertical profiles

The measured values of physical quantities over the vertical describe the distribution of the given quantity at different time moments.

Figure 10 depicts the vertical distributions of the horizontal and vertical ensemble-averaged velocities. Similar to Fig. 9, the profiles under investigation are $(x - x_b)/h_b = -2.36$, $(x - x_b)/h_b = 0.09$ and $(x - x_b)/h_b = 2.17$.

The profiles correspond to the profile before breaking, at the breaking point and immediately after breaking. It is easy to notice that there are two types of lines in the figures.

The upper row of figure 10 depicts the variation of the horizontal velocity component at different time moments in the three abovementioned profiles. It can easily be observed that there are two types of lines on the figures. The lines coloured pink, green and dark blue represent the backflow from the beach, the lines coloured black, brown and light blue represent the onflow towards the beach. The flow profiles during backflow resemble the classical steady flow profiles in open channels. During the onflow towards the beach the velocity profiles are remarkably different from the steady open channel flow. The measurements show that during the onflow, the horizontal velocity of the water particles is higher in the near bed zone and in the layers close to the water surface than it is in the intermediate layers. This can be explained with the backflow of water that decelerates the water particles in the intermediate zone to the level that it forms almost a homogeneous flow pattern in the given zone. The Boussinesq types of wave models on the beach make the same assumption Schäffer et al (1993).
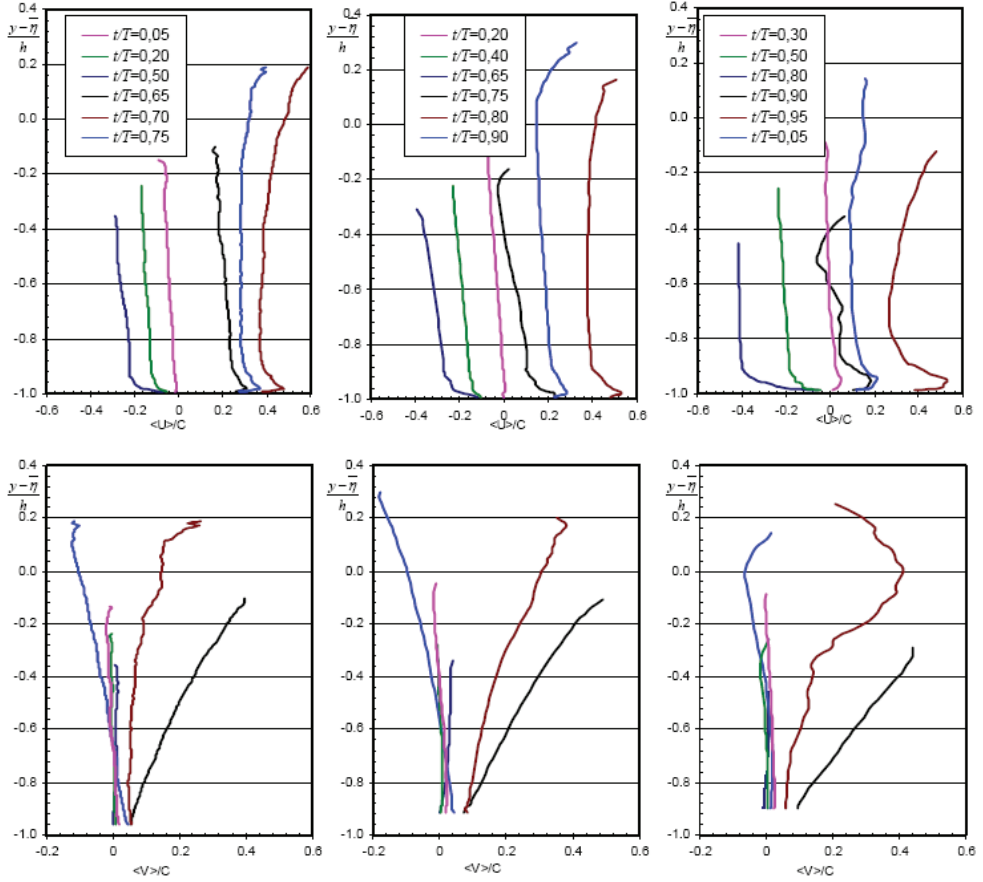
Figure 10 Ensemble-averaged horizontal and vertical velocity profiles. Left column $x - x_b / h_b = -2.36$*, middle column* $x - x_b / h_b = 0.09$ *and right column* $x - x_b / h_b = 2.17$

The ensemble-averaged distributions of the vertical velocity component are shown in Figure 10 (lower row). The colours of lines represent the phases of the wave at the same times as for horizontal velocities. Similarly to the horizontal velocity component, the backflow values of vertical velocity resemble an open channel flow. The value during the backflow is approximately zero. During the wave phases when the flow is directed towards the shore, the value of the vertical velocity changes linearly from zero at the bottom to up to ~ 0.4C above the still water level. This means that under the wave crest water is "pulled" into the crest during wave propagation and the shoaling process (brown and black lines). The light blue line represents the phase of the wave when water is intensively flowing out of the wave crest. This results in an increase of negative (directed towards the bottom) flow velocity. This phenomenon is especially pronounced in the profiles near the breaking point $x - x_b / h_b = 0.09$, where the velocity reaches ~0.2C. At $(x - x_b)/h_b = 2.17$ this value is more than two times smaller. This suggests that the wave has entered the area of wave setup.

29

4 Investigation of the unsteady boundary layer

As there is practically no data of boundary layer flows in waves in the surf zone, most mathematical models describing the flow in the surf zone assume that the flow resembles the unsteady boundary layer flow described by Jensen (1989) and Jensen et al. (1989), although these experiments were carried out in an oscillatory pipe flow. It is clear that the processes associated with inertial forces result in different phenomena in the case of pipe and free boundary flows: in a pipe flow the pressure increases, whereas for free boundary flows the flow depth is increased. This means that although the works by Jensen describe periodical oscillatory flows in pipes well, they fail to describe adequately the boundary layer flow in the surf zone

This part covers the qualitative comparison of the most commonly used formulas described in section 2.1 and the experimental results achieved during the present study Liiv (1995, 1998, 2001).

4.1 Results of the boundary layer investigation

The following results on the experimental investigation of oscillatory flow in the surf zone were obtained during experiments described in the article by Lagemaa & Liiv (2008). The present study was initiated to compare the measured velocity distribution in the boundary layer with the velocity distributions used in the mathematical models.

Figure 11 presents an example of measured time series of the shear velocity $u*$ before processing. The data are from the profile with coordinates $(x - x_b)/h_b = 0.09$. It can be seen that the value of $u*$ fluctuates considerably around its mean value. In Figure 11 only four of the 151 periods that were measured are presented. The data processing smoothened the curve and also removed dropouts that can be seen in the figure between $\omega t = 360$ and 720 degrees. The process of data processing is described in detail in Lagemaa & Liiv (2008).

In order to verify the results presented in Figure 11, a comparison was made with the results obtained by Jensen et al. (1989). They performed the experiments with a Constant Temperature Anemometer (CTA) in an oscillating U – tube. In the case of $Re = 3.4$ x 10^6, the shear velocity was found to be $u^*=0.73$ m/s. In this case with the Reynolds number equal to 3.0 x 10^6, the shear velocity was equal to 0.62 m/s. As variations in the two velocities were small, this result was found to confirm the applicability of the given approach to shear velocity measurements. A comparison of the results was also made with results presented by Arnskov et al (1993). Here the value τ_0 / ρ was calculated. The overall shape of the variation pattern of the value for waves alone case agreed well for both experiments, but as the resolution of the graphs in the article was low, the graphical comparison is unfortunately impossible.

Individual realization of u*
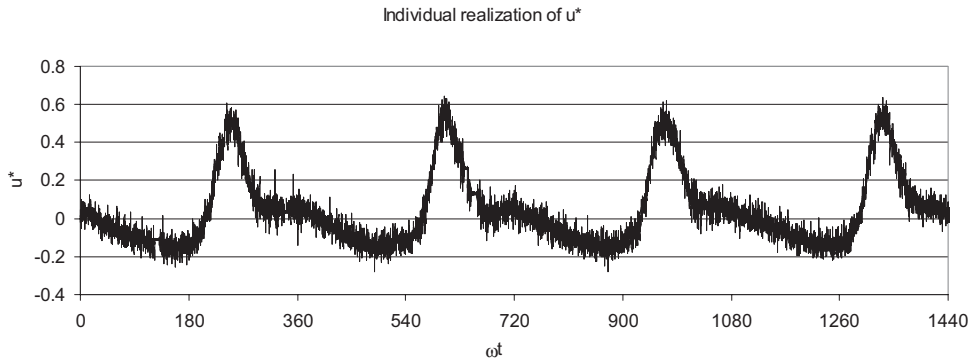
Figure 11 Measured time series of shear velocity before data processing

Figures 12 to 14 present the ensemble-averaged variation of non-dimensional shear velocities and the corresponding surface elevations during one wave period in the same cross-sections as for Fig. 10. The left vertical axis is the shear velocity and the right axis is for surface elevation.
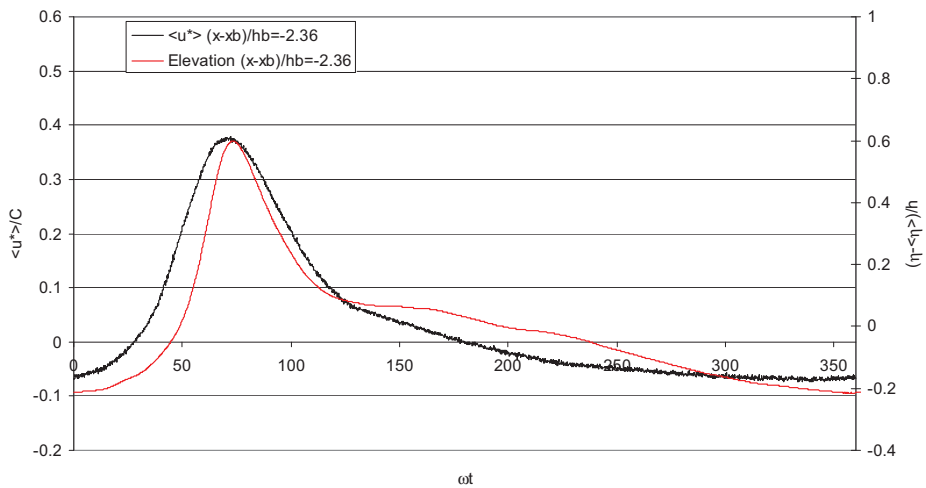
Figure 12 Ensemble-averaged variation of non-dimensional shear velocity and the surface elevation at $(x - x_b)/h_b = -2.36$
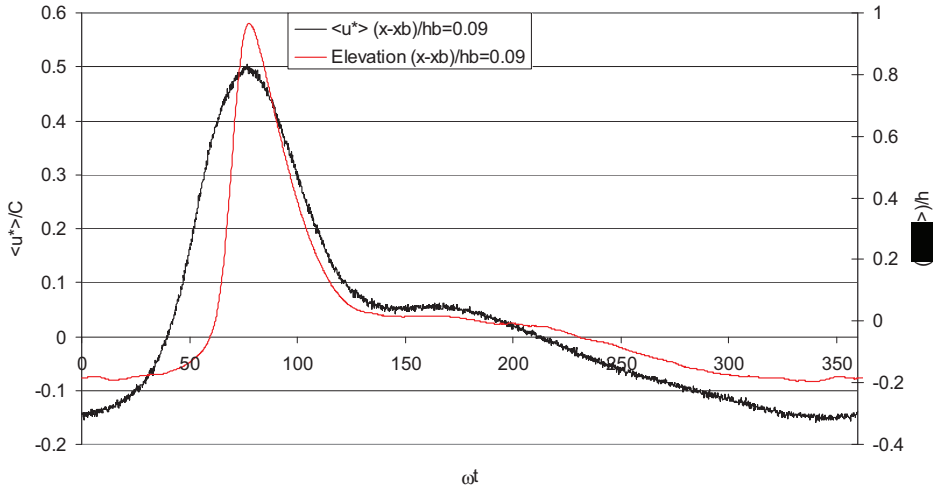
Figure 13 Ensemble averaged variation of non-dimensional shear velocity and the surface elevation at $(x - x_b)/h_b = 0.09$
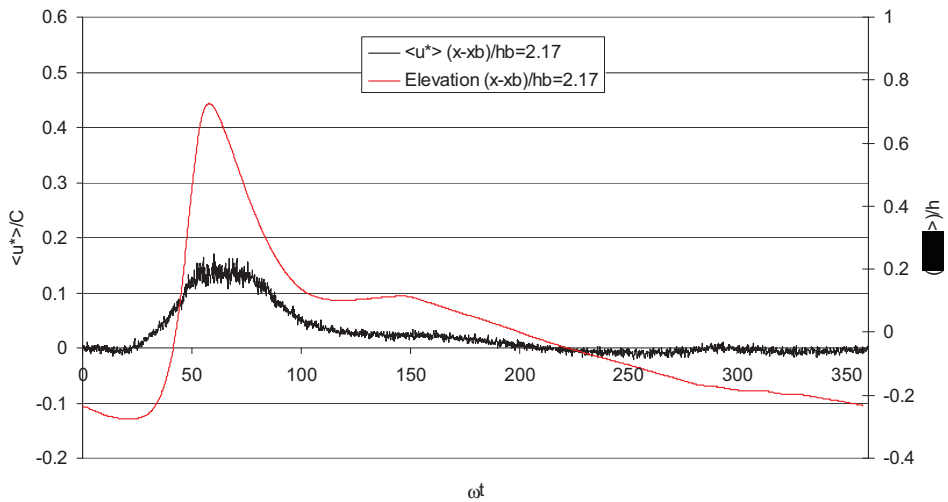
Figure 14 Ensemble averaged variation of non-dimensional shear velocity and the surface elevation at $(x - x_b)/h_b = 2.17$

The most distinctive feature that can be observed in the three figures is that the shear velocity increases towards the breaking point and decreases after breaking.

The analysis of the shear velocity in the boundary layer shows that the results achieved are totally different from the results obtained in the oscillatory flows in pipes by Jensen (1989) and Jensen et al. (1989). This can be explained firstly

with the inclined surface of the experimental setup and secondly with the open boundary on the water surface that allows a closer representation of the natural phenomenon of wave movement.

Figures 15 to 20 present the dimensionless velocity profiles of $u+$ at different phases of the wave breaking. Here $y+$ is the dimensionless distance from the bed and is calculated using $y+ = h \cdot \langle u \rangle / v$ and $u+$ represents the ratio of local velocity to the friction velocity

$$u+ = \langle u(z;t) \rangle / \langle u*(t) \rangle. \tag{24}$$

The choice of arguments on the axis is to make the results comparable with the results by Jensen (1989) presented in Figure 3. Figures 15 and 16 give the variation of $u+$ in the profile with coordinates $(x - x_b)/h_b = -2.36$, Figs. 17 and 18 and Figs. 19 and 20 have coordinates $(x - x_b)/h_b = 0.09$ and $(x - x_b)/h_b = 2.17$, respectively. As mentioned before, the phase 0 degrees also correspond to the wave trough. The same choice of wave phase is also selected in Fig. 3.

Also, as presented in Fig.3, for comparison, all figures have lines that depict a steady flow velocity distribution near the wall. The line is calculated using the following considerations:

- very near the wall is a viscous sub-layer with a linear velocity distribution

$$\frac{u}{u_*} = \frac{u_* y}{v} \tag{25}$$

- at some distance of the boundary we come to the turbulent velocity profile described with

$$\frac{u}{u_*} = 2,5 \ln \frac{u_* y}{v} + 5,5 \tag{26}$$

- between these two zones there is a transition zone

$$3,5 < u_* y / v < 30.$$
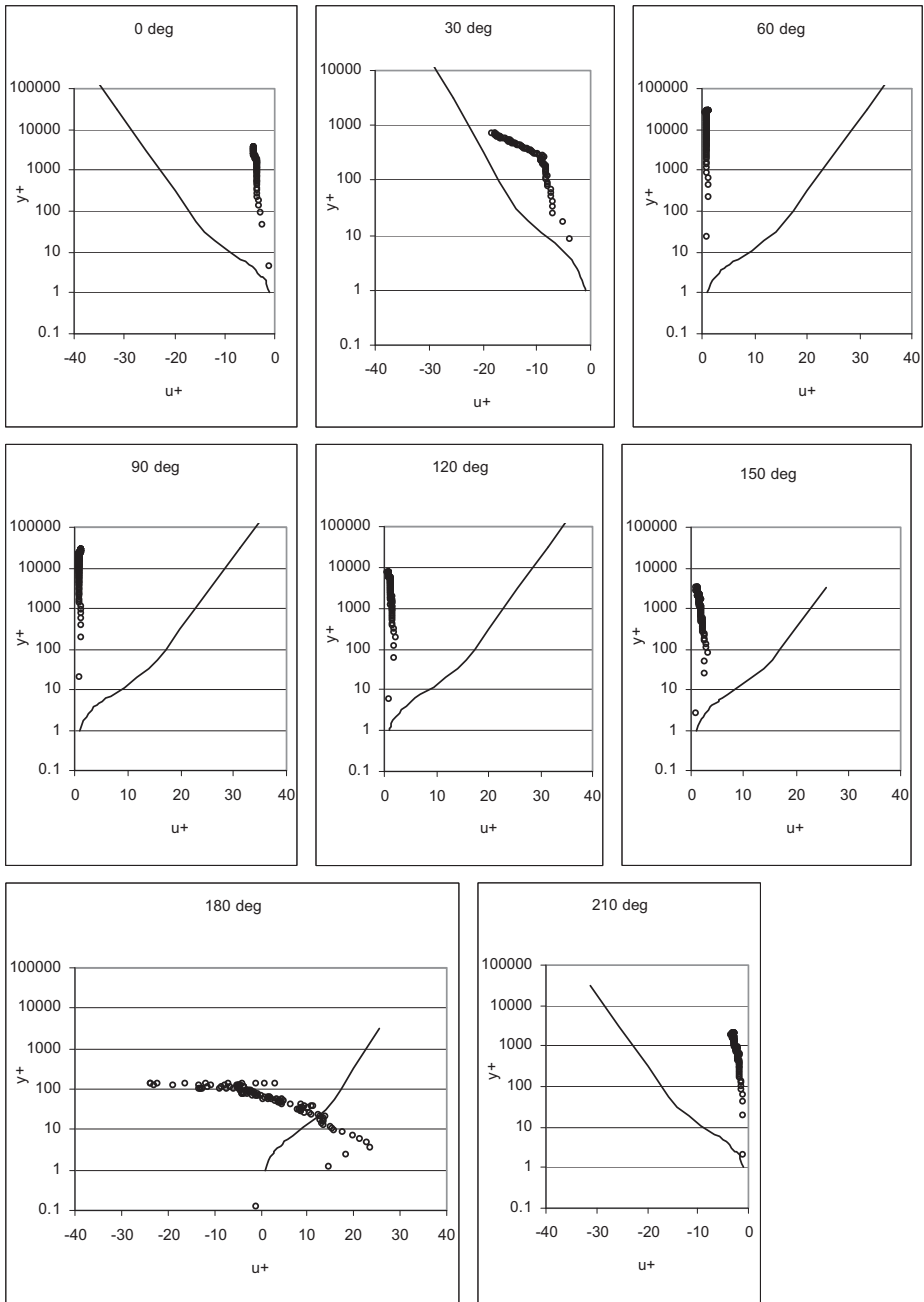
Figure 15 Dimensionless velocity profiles of u+ at different phases of the wave breaking: section $(x - x_b)/h_b = -2.36$
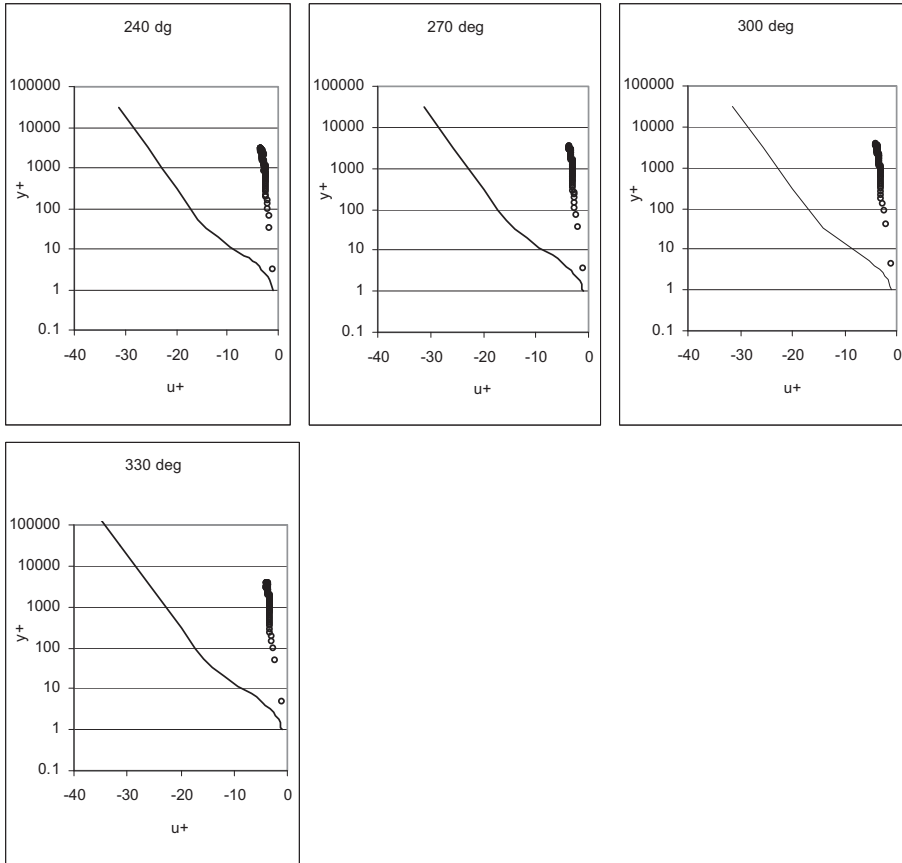
Figure 16 Dimensionless velocity profiles of u+ at different phases of the wave breaking: section $(x - x_b)/h_b = -2.36$

Previous investigations have shown that in the case of stationary flow, the dominant stresses for the flow in the viscous sub-layer are the viscous stresses, whereas in the core region, turbulent stresses prevail.

This pattern in the case of stationary flow is also printed in Figs. 15 to 20 (solid line). Jensen (1989) found that this relationship describes relatively accurately the flow in a U – shaped oscillatory flow tunnel. The results of the investigation are depicted in Figure 3.
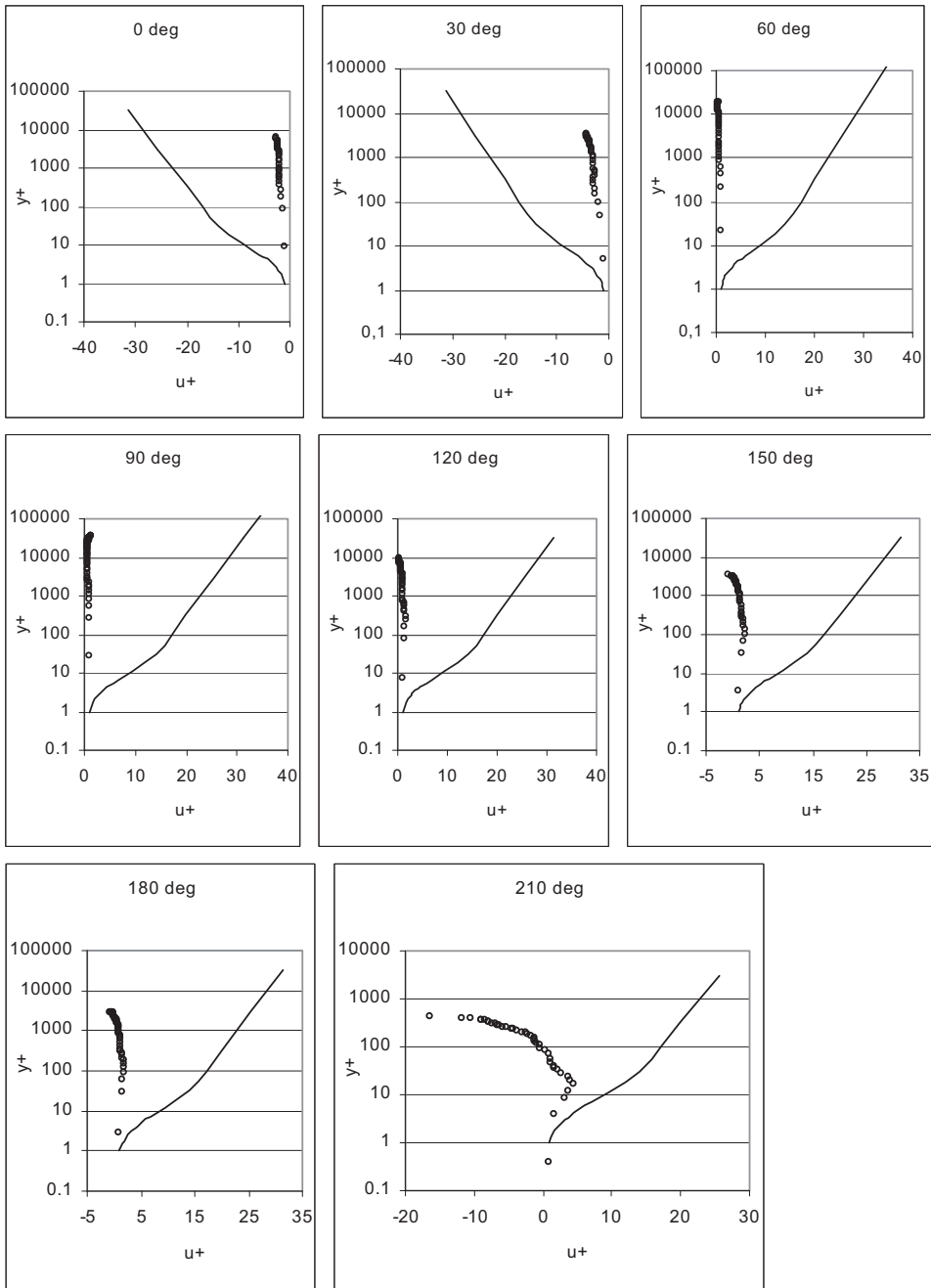
Figure 17 Dimensionless velocity profiles of u+ at different phases of the wave breaking: section $(x - x_b)/h_b = 0.09$
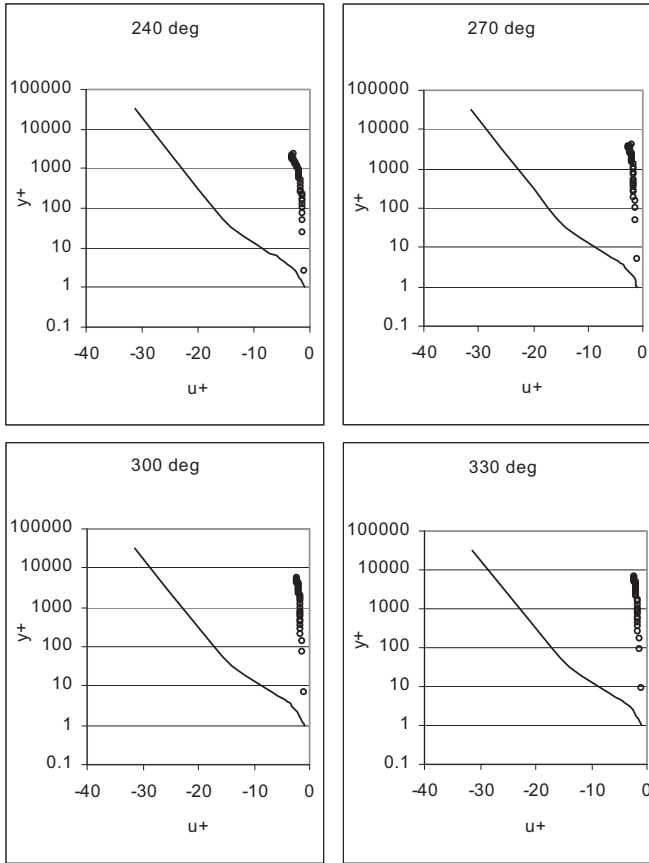
Figure 18 Dimensionless velocity profiles of u+ at different phases of the wave breaking: section $(x - x_b)/h_b = 0.09$

The flow situation in the case of present experimental run was completely different from the flow in a U – tube with a constant cross-sectional area. This investigation deals with a free surface oscillatory flow on the inclined bottom. Moreover, the flow incorporates a relatively rapid change of the cross–sectional area due to wave breaking, and the generation of a two – phase environment (air – water) on the wave crest and after breaking point over the whole cross – sectional area. In addition to the local inertial forces associated with flows in U-tubes with constant cross sections, there are also convective inertial forces. The convective inertia forces are generated in the flow when cross sectional area of the flow changes, as is the case for the free surface flows. Thus the energy balance in case of free surface wave motion is governed by the two mentioned agents, not one as in case of oscillatory water movement in U-tubes.

The profiles of dimensionless velocity u+ Eq. (10) in Figs. 15 to 20 are presented for different phase angles. The angle step is 30 degrees. Depending on the flow direction, the stationary flow profile (Eqs. (11) and (12)) is plotted either on the right (flow towards the shoreline) or on the left (low towards the

deep water) side of the vertical axis. 0 degrees corresponds to the lowest surface elevation in the wave trough. It can be seen from the figures that the flow is directed towards the shore between 60 and 180 degrees. At the breaking point, the flow reversal is somewhat later at 210 degrees. At other phases, the flow is directed towards the deep water. This is a distinct difference between the results of Jensen (1989). His results suggested that the adaption sinusoidal particle movement should be used, resulting in half periods of flow towards the shore and deep water. The data shows that the value of $y^+ = y^+(u^+)$ changes little both for $(x - x_b)/h_b = -2.36$ and $(x - x_b)/h_b = 0.09$. The only exceptions are flow reversals at 30 and 180 degrees for $x - x_b/h_b = -2.36$ as well as 30 and 210 degrees for $(x - x_b)/h_b = 0.09$.

The experimental results prove that the flow reversal starts at the top of the water column and spreads gradually downwards to the bottom. This phenomenon is best illustrated in Fig. 15 at 180 degrees, where the backflow in the upper layers of the water column meets the still shoreward moving flow on the bottom. The velocity profiles are almost uniform in Figs. 15 to 18, except for the wave phases at which the flow reverses. Close inspection of the values of $u+$ reveals that the value varies between the value of 1 and 2 during the flow towards the shoreline and between 1 and 3.5 during the backflow. This suggests that in comparison to the stationary flow situation there are different processes that govern the development of the boundary layer flow under breaking waves.

There are two possible agents that may contribute to the relatively low values of $u+ = \langle u(z;t) \rangle / \langle u*(t) \rangle$ Experiments in pressure pipes Liiv (2004) have shown that during strong local accelerations, the value of $u+$ stays constant over the whole cross-section. The ensemble averaged horizontal accelerations in the case of the present experiment at certain phases of the wave cycle were found to up to 1.3 times the acceleration due to gravity. The measured values of horizontal acceleration were found to be up to 5 times the acceleration due to gravity. This suggests that the acceleration of water particles and the associated local inertia forces keep the dimensionless flow profile nearly uniform. The second agent that contributes to the uniform profile, especially during the flow phases towards the shoreline is strong mixing processes due to the overturning of the wave crest. The water particles with high values of momentum are plunged to the bottom and there they transfer their energy to all the particles.
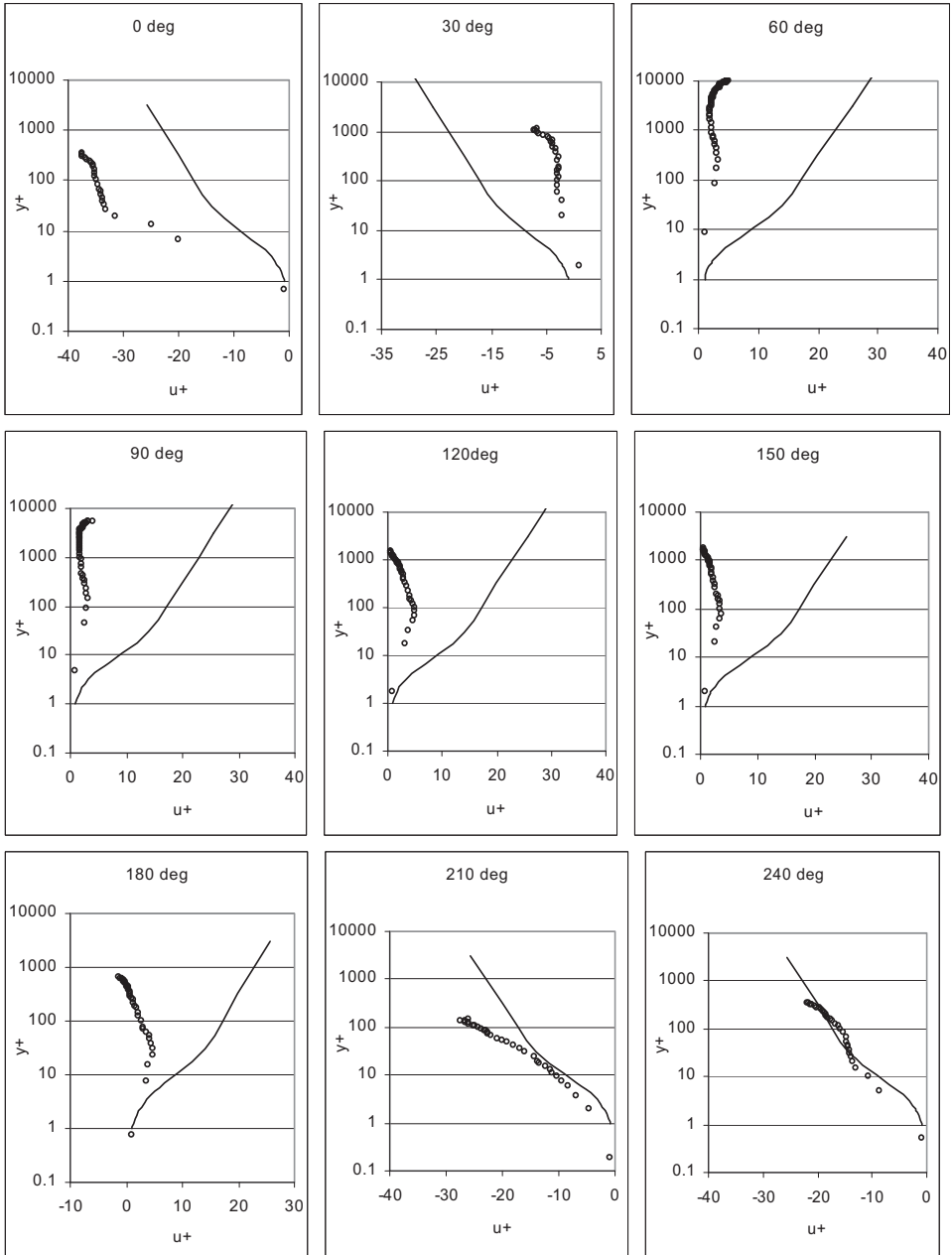
Figure 19 Dimensionless velocity profiles of u+ at different phases of the wave breaking: section $(x - x_b)/h_b = 2.17$
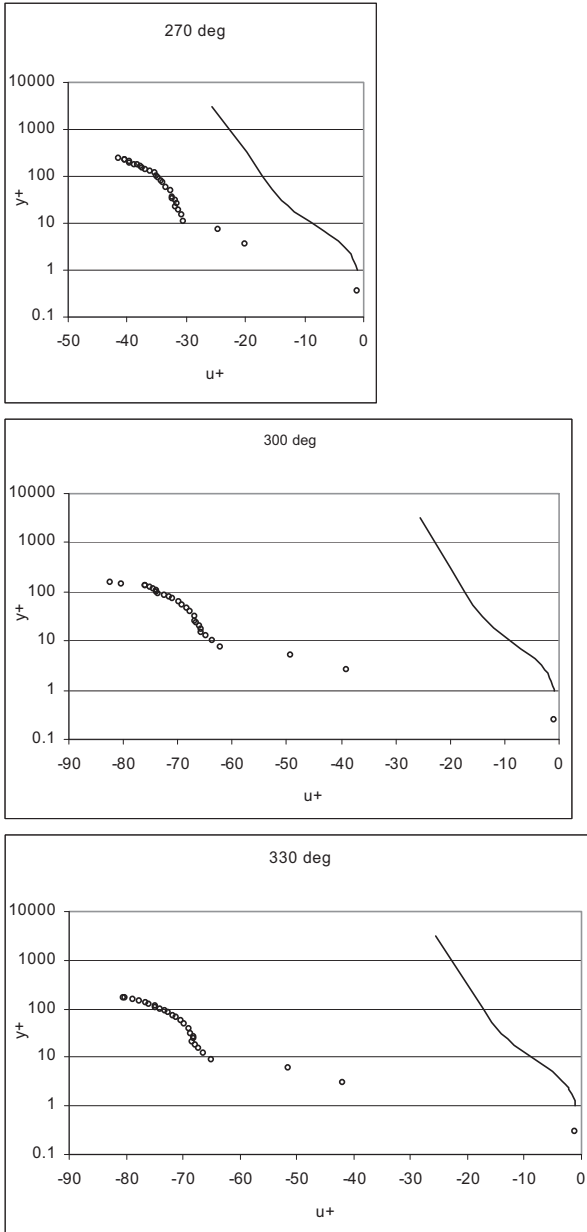
Figure 20 Dimensionless velocity profiles of u+ at different phases of the wave breaking: section $(x - x_b)/h_b = 2.17$

The situation is totally different in the case of the profile that is located after the breaking point at $(x - x_b)/h_b = 2.17$. Although the flow towards and away from the shoreline occurs still at the same wave phases, the behaviour of $u+$ is different from the previous cross–sections. During the flow phases towards the shoreline the dimensionless flow profile is nearly uniform, with the value of $u+$

ranging from 1 to 5. It is quite interesting to follow the mixing process. The area of high value of local velocity in comparison to the friction velocity moves towards the bottom from $y+=10000$ at $\omega t = 60^O$ to $y+=50$ at $\omega t = 180^O$. At the same time the flow in the upper parts of the water column starts reversing.

The behaviour of the flow during the backflow, $\omega t = 210^O$ to 0° suggests that the forces that govern the flow here are different from the ones that dominated the backflow in the previous investigated profiles. First of all it must be noted that at $x - x_b / h_b = 2.17$ the height of the water column in the approaching wave crest is 2.5 times larger than in the wave trough. This brings along the issues of convective accelerations and flow continuity, a problem that was not an issue in the profiles before and during breaking, where the wave crest had a sufficient supply of water in the relatively deep wave trough preceding the wave. The flow behaviour after the flow has reversed at $\omega t = 210^O$ and 240° resembles very much the stationary open channel flow. The same conclusion can also be made when inspecting the rightmost green line in Figure 10. It resembles very much the traditional curve of the open channel flow. The next phases are crucial in the development of the flow in the current profiles. The approaching wave crest at 300 and 330 degrees draws the water particles into the crest generating a strong flow from the relatively shallow wave trough. This phenomenon can be well seen in Figure 20. The ratio $\langle u(z;t)\rangle/\langle u*(t)\rangle$ exceeds the calculated open channel boundary layer velocity distribution value 5 up to 40 times.

5   The variation of turbulent kinetic energy around the breaking point

5.1   Time series of turbulent kinetic energy

As described in Chapter 3, at all measuring points the values of fluctuating components of velocity $u'(t)$ and $v'(t)$ were calculated. Figure 21 presents this result at $(x - x_b)/h_b = -2.26$ and $(y - \overline{\eta})/h = -0.87$.

It can be seen in the Figure 21 that the values of both velocity components and turbulent fluctuations vary on a wide scale in time, but as the aim was to investigate the variation of turbulent kinetic energy, discussions on the variations of the present quantity are beyond the scope of this investigation.

Using Eq. (18), the value of turbulent kinetic energy k in all measuring points was calculated. The time series of dimensionless turbulent kinetic energy at various heights over the bed is presented in Fig. 22. It can be seen that the kinetic energy has two local peaks. These maximums correspond to the local extremes of the vertical component of the velocity and also to the maximums of the acceleration and deceleration of the horizontal velocity component. It is shown that if before breaking the energy levels before and after the wave crest are approximately equal, then as the breaking process develops, the kinetic

energy precedes the wave crest. This is one of the major differences between spilling and plunging breakers. According to Lin & Liu (1998), the energy inside the spilling breaker moves behind the wave crest.
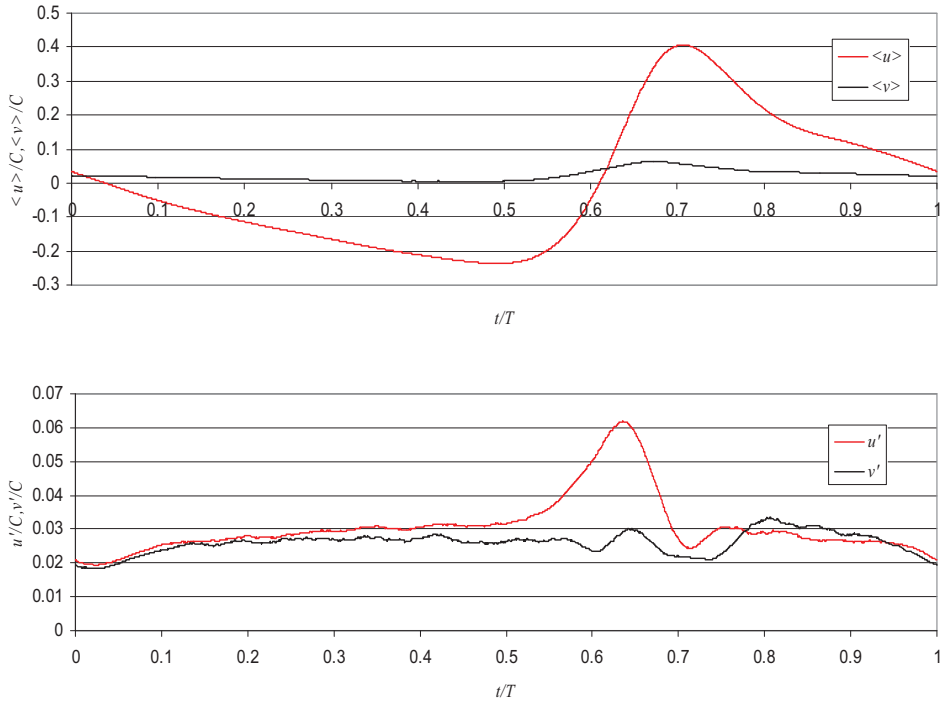
Figure 21 Ensemble-averaged horizontal and vertical components of the local velocity at the point with coordinates $(x - x_b)/h_b = -2.26$ *and* $(y - \bar{\eta})/h = -0.87$ *and the corresponding turbulent ensemble-averaged turbulent fluctuations u' and v'*

Before the breaking, the level of turbulent kinetic energy is low. The energy is generated only in the upper layers of the water column, reaching there the level $\sim 0.015C^2$ under the wave crest. When the breaking is initiated, energy level grows considerably and reaches also the bottom layer. This suggests that the wave front has plunged into the wave crest in front of it. After the breaking point the maximum measured kinetic energy was $\sim 0.65C^2$. It is also interesting to follow the development of the levels of turbulent kinetic energy along the surf zone model. The energy before the wave crest before $(x - x_b)/h_b = -2.36$ and immediately after breaking $(x - x_b)/h_b = 0.09$ has energy levels equal to no more than $\sim 0.001 \ C^2$. In the third cross– section $(x - x_b)/h_b = 2.17$, the level of turbulent kinetic energy before the wave crest has risen nearly five times. In this cross–section the large scale eddies have reached the bottom and the mixing processes have carried the turbulent kinetic energy all over the water column.
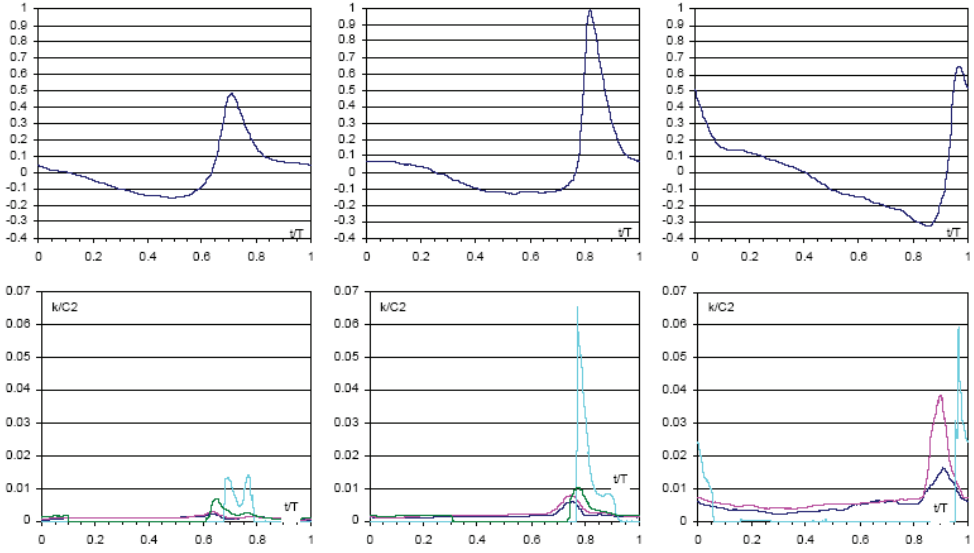
Figure 22 Surface elevation and turbulent kinetic energy in cross-sections $x - x_b / h_b = -2.36$ *(left column),* $x - x_b / h_b = 0.09$ *(centre column) and* $x - x_b / h_b = 2.17$ *(right column). at heights* $(y - \overline{\eta})/h = -0.99$ *, (——)* $(y - \overline{\eta})/h = -0.89$ *, (——)* $(y - \overline{\eta})/h = -0.54$ *, (——)* $(y - \overline{\eta})h = -0.17$ *, (——)* $(y - \overline{\eta})/h = 0.18$

5.2   The variation of turbulent kinetic energy

5.2.1   The variation of turbulent kinetic energy across the surf zone

The measured profiles are close enough to each other to give a qualitative picture of the variation of turbulent kinetic energy over the whole measured area. As mentioned before, the horizontal step between the profiles was 10 mm before the breaking and 30 mm after the breaking point.

Figure 23 gives the distribution of turbulent kinetic energy. It can be seen that before breaking (left column) the level of kinetic energy is low. There is only a slight increase of turbulent kinetic energy in the wave crest (Brown line) In the next figures (middle and right columns) it can be followed how the kinetic energy diffuses towards the bottom layers. This phenomenon becomes first evident under the crest (Brown line) and as the wave progresses also during the backflow phases (Black line).

Figure 24 gives the time-averaged variation of turbulent kinetic energy across the surf zone at different non-dimensional heights above the surf zone model. These values have been obtained during the analysis of turbulent fluctuations using Eq. (18). The analysis of the measured data shows that the level of turbulent kinetic energy is increased as we approach the shore. Figure 24 shows

clearly how after the wave has plunged into the trough, the level of turbulent kinetic energy increases especially on the levels above the still water level.
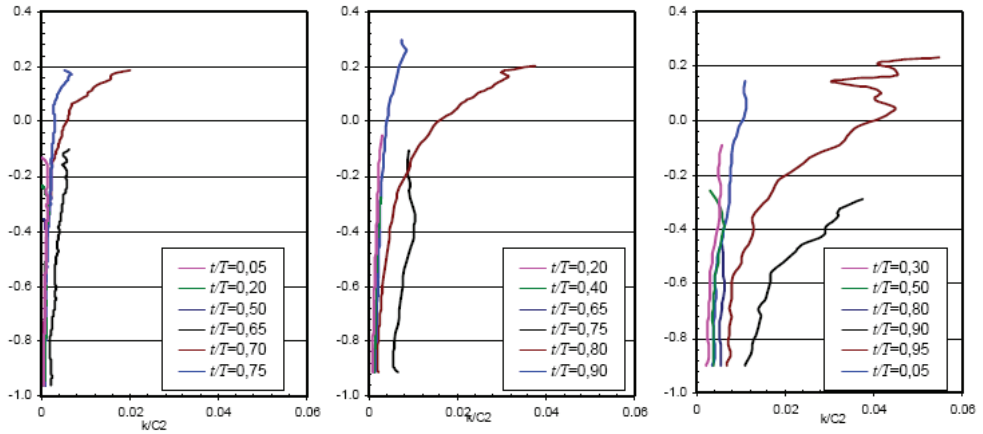
Figure 23 Ensemble-averaged turbulent kinetic energy profiles. Left column $x - x_b / h_b = -2.36$, middle column $x - x_b / h_b = 0.09$ and right column $x - x_b / h_b = 2.17$
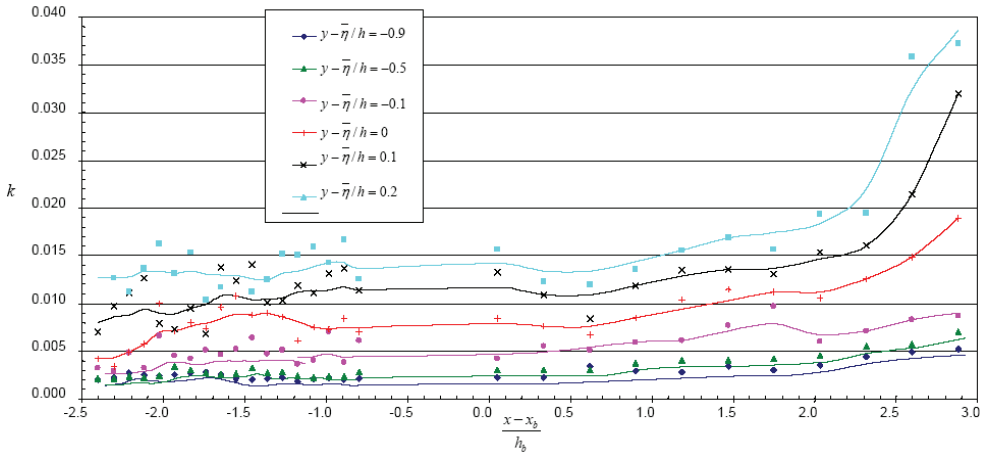
Figure 24 Time-averaged variation of turbulent kinetic energy perpendicular to the coastline at different heights above the bottom

It can be seen that the level of kinetic energy and also turbulent intensity is low until the wave crest plunges. The plunging point is probably characterized with especially high values of turbulent intensity, but due to the high level of air entrainment it is impossible to measure it using the LDA techniques. It has been suggested that the value of turbulent intensity there is more than ten times higher than in other part of the wave.

The development of Particle Image Velocimetry (PIV) methods and computer graphics has led to the usage of field graphs in the description of breaking waves Takikawa et al (1997) and Christensen & Deigaard (2001). The advantage of field graphs over the conventional methods is that it enables one to

follow the qualitative nature of the breaking process. The field graphs in the case of LDA measurements are usually not presented, because of lack of sufficient data. In the case of the present experimental run, the measured data had a sufficiently high spatial resolution to make it possible to present field graphs.

5.2.2 Velocity vector and turbulent kinetic energy fields around the breaking point

Figures 25 to 30 present velocity vector fields and turbulent kinetic energy fields for the measured area under the breaking wave. As the vertical resolution of measurements is very high, only every third point is depicted on the figures. The figures are equipped with the still water level, instantaneous surface profile and the wave flume bottom. The white area between the surface profile, and the coloured kinetic energy plots represent the area, there due to high air entrainment, or lack of laser beams in the water, the measurements did not give reliable data. In order to get a better understanding of the processes involved, the length scale of the vectors in all of the figures is kept the same. Due to this some very low velocities are represented by a vector that has been omitted with the minimal length. These vectors show mainly the direction of the flow.

At $t/T = 0.4 - 0.5$ there is a backflow all over the measuring section. Here the flow resembles very much the flow in open channels. The same could be concluded from the flow profiles in Fig. 10. The first signs of the arrival of the wave crest appear at $t/T = 0.6$. It can be seen as the surface starts to elevate and the magnitude of the vertical component of velocity becomes comparable with the horizontal velocity component. At $t/T = 0.7$ the wave crest has entered the measuring section. At this time moment the process that occurs when the flows towards and from the shore meet can easily be followed. This process eventually results in the increase of the water column in the wave and the breaking of the wave. Also, there is always an area in front of the wave crest where water particles move perpendicular to the wave movement towards the surface. This phenomenon is caused by the collision of the water masses moving towards each other. This movement is more intense near the still water level. The figures depicting $t/T = 0.8$ to 0.9 (figures 29 and 30) shows that the water particle movement in the upper layers of the water column behind the wave crest is directed slightly downwards, suggesting that the decreasing water surface presses water particles down.

A close inspection of the figures of the velocity fields leads to a conclusion that there are great large-scale vortices under the breaking wave with the vertical length scale equal to approximately the water depth and horizontal length scale equal to approximately the wave amplitude. This can more easily be observed if the velocity fields are plotted with finer time step than in Figures 25 to 30.

In addition to the velocity vector plots, the figures 25 to 30 present turbulent kinetic energy fields in the breaking wave. Similarly to the vector plots, the scale of turbulent kinetic energy on all figures is kept the same. The scale is also represented with isolines in the figures. It has to be noticed that in order to show

both very low and high values of turbulent kinetic energy, the scale is not linear. To my knowledge similar graphs have not been reported by other authors.

As it can be seen in the figures describing the turbulent kinetic energy field, the higher values are concentrated in the area under and before the wave crest (cf. $t/T = 0.7$ to 0.9). The shoreward moving wave crest generates more and more energy that through dispersion spreads towards the bottom. At $t/T = 0.7$, when the crest is situated before the breaking point ($x = 2.90$ m), the turbulence generated in the wave crest starts spreading downwards. It reaches the bottom at $t/T = 0.9$.

As shown, the area with the largest values of turbulent kinetic energy occurs in the wave crest, whereas Fig. 22 shows that the generation of the turbulent energy takes place in front of the crest, where the acceleration of the horizontal velocity component is at a maximum. This suggests that energy is drawn from the generation zone and carried along with the wave.

The second area with relatively high turbulent energy is observed in the area behind the wave crest. The level of energy is not high, but noticeable. Figure 2 shows that in this area the horizontal velocity is decelerating. The increase in turbulent fluctuations and hence also turbulent kinetic energy has been observed by other authors Aitsam et al (1990). The third area of generation of turbulence is the bottom boundary layer. As during the present experimental run, smooth model bottom was used, the increase of turbulent energy due to the generation from the bottom boundary layer is not large. In fact, it has been shown by Ting & Kirby (1995) that the generation from the boundary layer even in the case of rough bottoms, is negligible in comparison to the generation from the wave crest. In conclusion, it can be said that turbulent energy is concentrated in the wave crest and that in the rest of the wave there is practically no turbulent energy. Turbulence is generated in front of the wave crest, drawn into and carried in it. Most of the turbulent energy dissipates behind the wave and during the breaking process. The same conclusion was also drawn by Lin & Liu (1998).
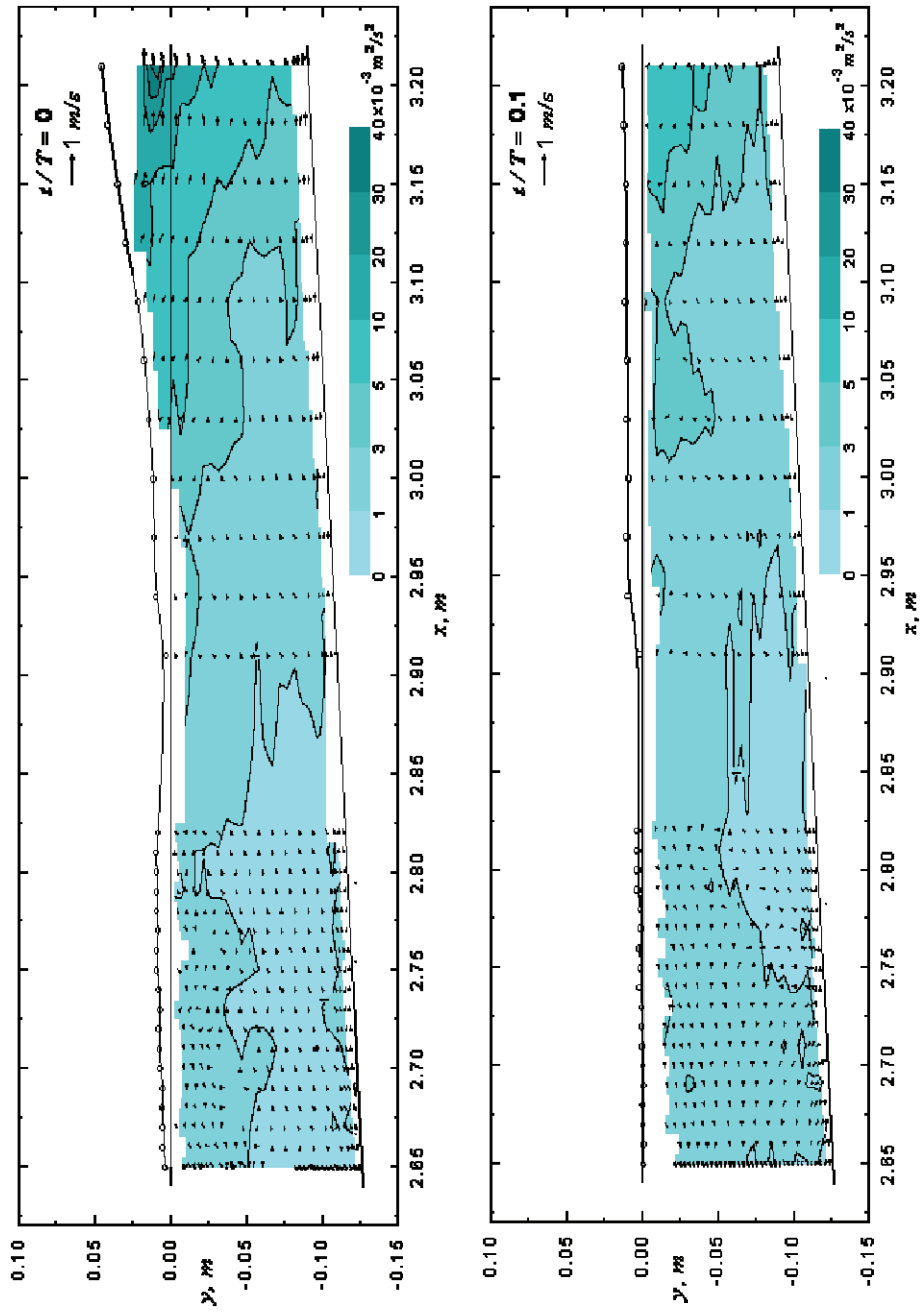
Figure 25 Turbulent kinetic energy and velocity field at t/T=0.0 and t/T = 0.1
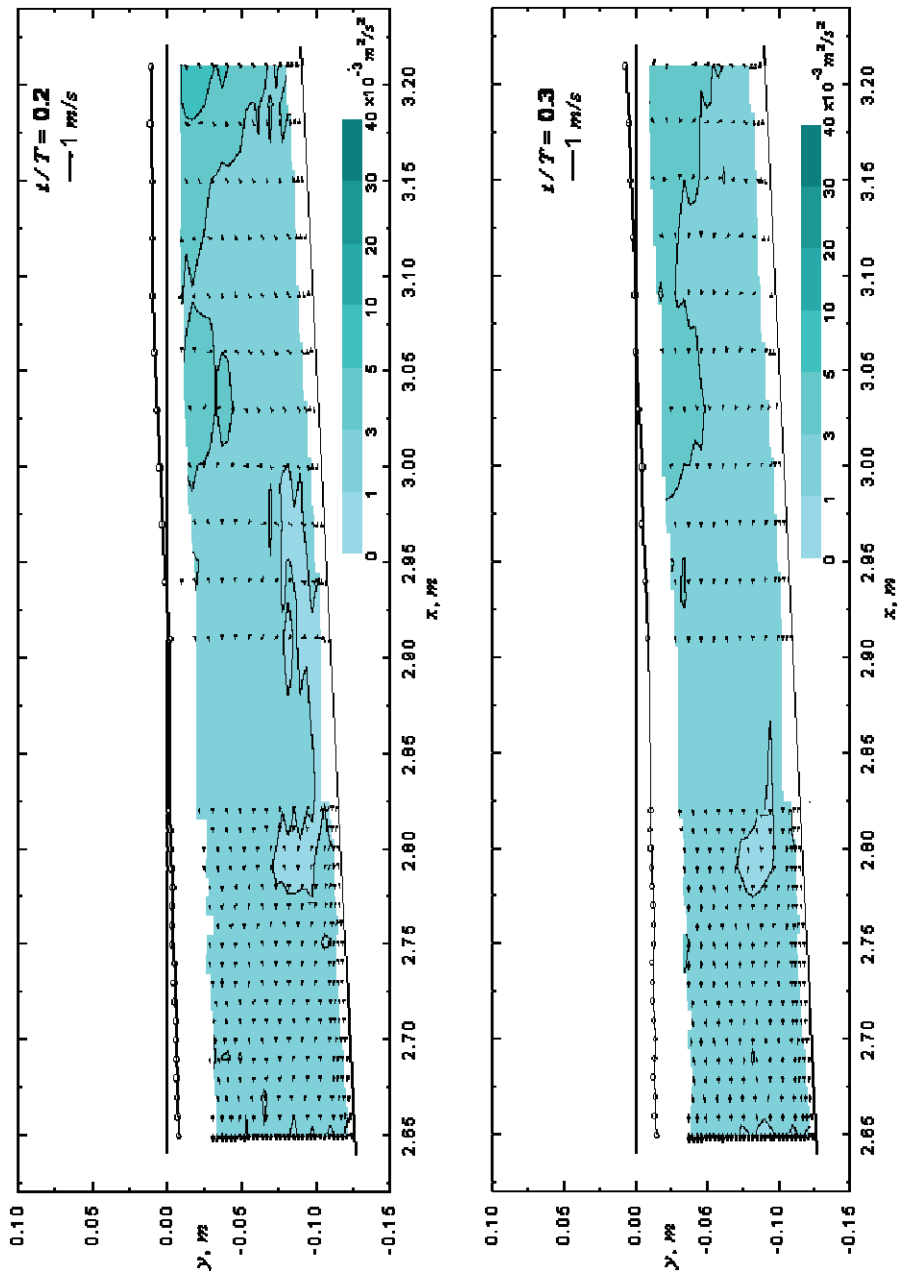
Figure 26 Turbulent kinetic energy and velocity field at t/T=0.2 and t/T = 0.3
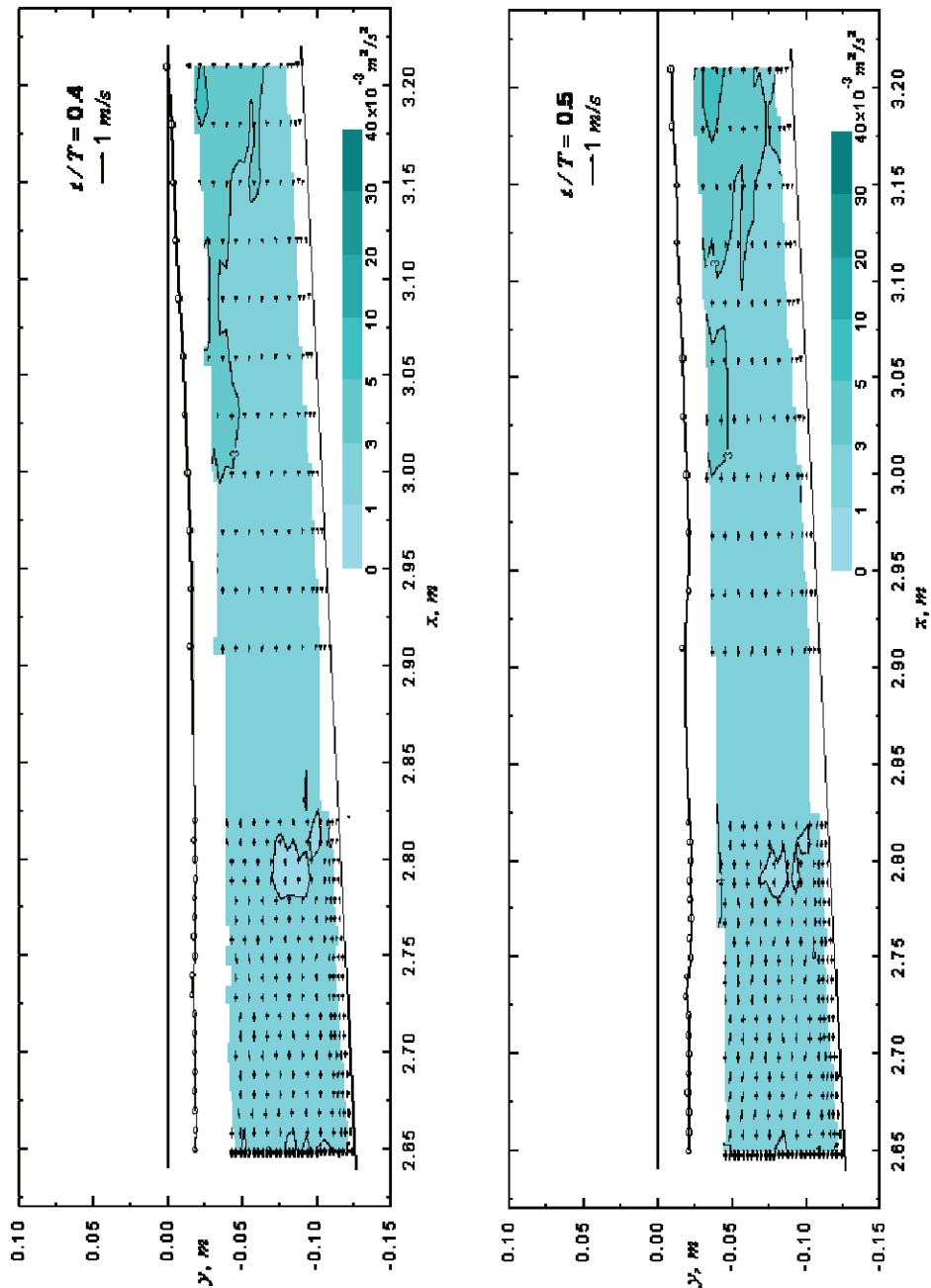
Figure 27 Turbulent kinetic energy and velocity field at t/T=0.4 and t/T = 0.5
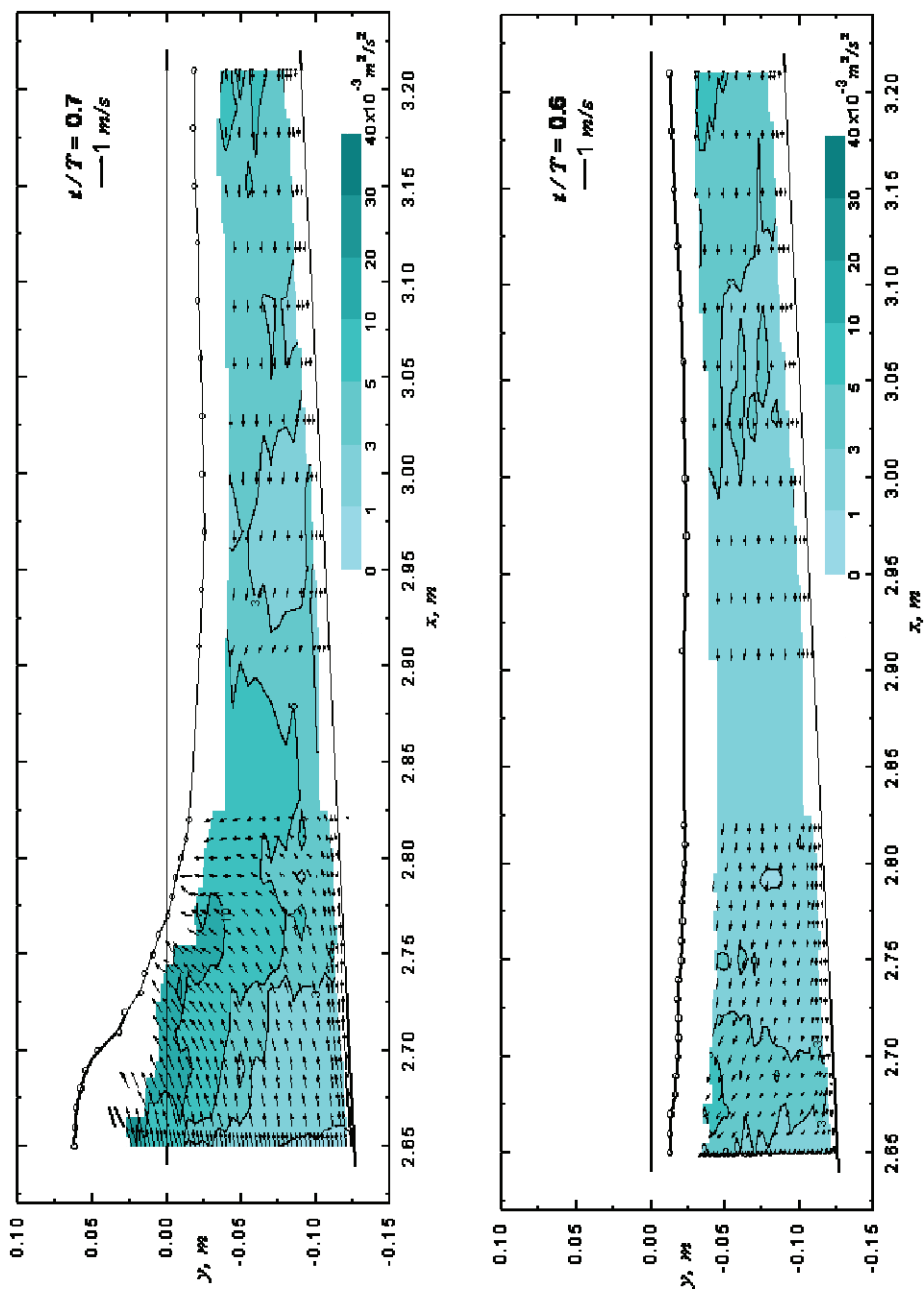
Figure 28 Turbulent kinetic energy and velocity field at t/T=0.6 and t/T = 0.7

50
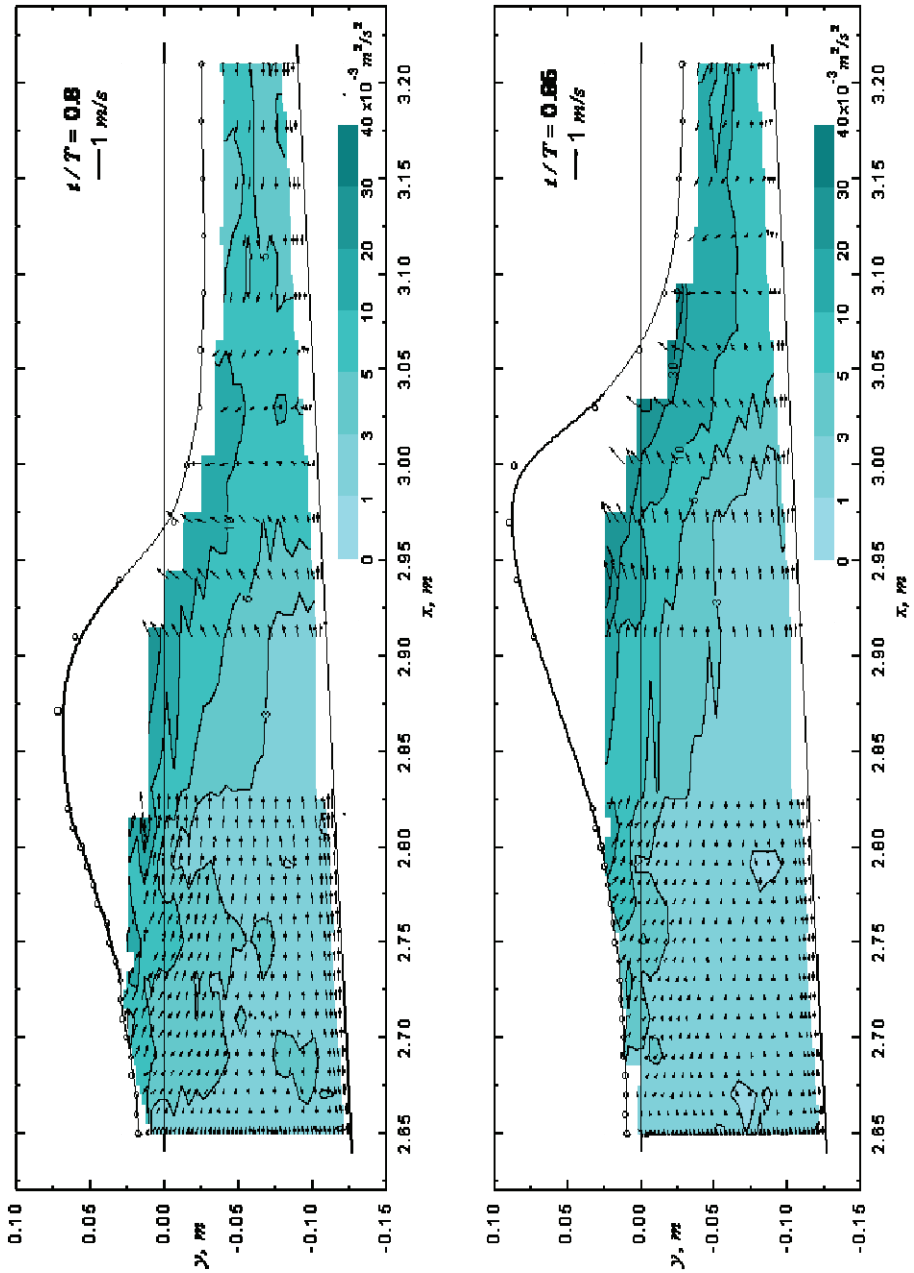
Figure 29 Turbulent kinetic energy and velocity field at t/T=0.8 and t/T = 0.85

51
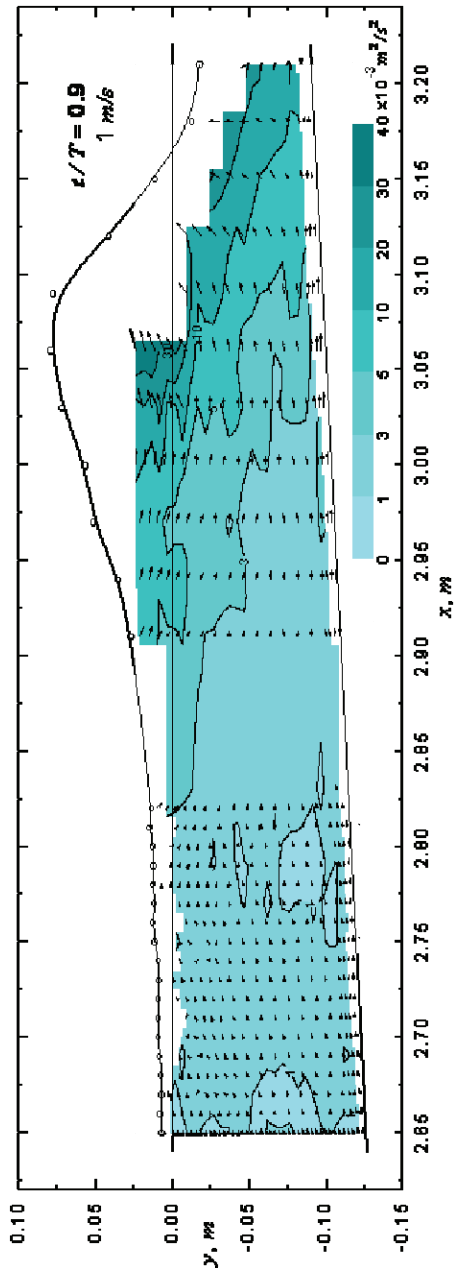
Figure 30 Turbulent kinetic energy and velocity field at t/T=0.9

6 Conclusions

The direct result of the investigations is the physical two-dimensional surf zone model that enables experimental investigation of the velocities and turbulent kinetic energy under the breaking wave during the wave period. The experimental setup allows data to be collected and stored with frequencies that enable ensemble averaging.

The two-dimensional velocity field, the boundary layer flow and the turbulent kinetic energy was recorded in 29 cross-sections before, after and in the breaking point of the generated wave. The total number of measuring points was 1852.

The LDA system was used for the measurement of the non-stationary velocity field inside the boundary layer and the time dependent shear velocity on the bottom of the on the surf-zone model.

The ensemble averaging of the recorded data gave the following results:

- Based on the measured horizontal and vertical fluctuations of the velocities, the turbulent kinetic energy field was calculated.
- The time and space dependent boundary layer velocity profiles were calculated and a comparison has been made with existing data.

It can be concluded that the flow under broken and near breaking waves is completely different from that in the sinusoidal wave theories.

- During wave phases when the flow is directed away from the shoreline, the ensemble- averaged profiles of the horizontal velocity component resemble the profiles of the steady open channel flow, although in several cases the flow is over-accelerated in comparison to the steady open channel flow, as shown in article 2. During the phases when the flow is directed towards the shore, the horizontal velocity of the water particles is higher in the near bed zone and in the layers close to the water surface than in the intermediate layers
- The ensemble-averaged vertical velocity component gains its maximum value simultaneously with the maximum acceleration of the horizontal velocity component. In the upper layers of the water column, behind the wave crest, the vertical component of the velocity is always negative, during backflow phases the value is of the order of zero.

As a result of the experimental investigations, the two-dimensional flow and energy fields were calculated. These allow the following conclusions:

- The turbulent kinetic energy has two local maximums that correspond to the extreme values of the vertical and horizontal accelerations.

- Before the breaking point, the time-averaged turbulent kinetic energy is practically constant. It starts increasing from the breaking point and has a sudden increase immediately before the crest plunges into the preceding trough.
- After the breaking point the maximum value of the turbulent energy is located on the crest from where it spreads all over the water column. This is different from the spilling breaking wave, where the turbulent fluctuations do not reach the bottom.
- There is always an area with water particles with purely vertical velocity travelling in front of the wave crest. This phenomenon is more evident in the area immediately under the still water level.
- The turbulent kinetic energy generated in the crest during the breaking process dissipates immediately after the wave has passed.

The results show that the stationary open channel flow velocity distribution used in most mathematical models fail to describe the flow under the breaking wave although previous investigations have proven that it describes the oscillatory flow in U-shaped flow tunnels relatively well. The dimensionless semi–logarithmic plots of dimensionless velocity distribution $u+ = \langle u(z;t) \rangle / \langle u*(t) \rangle$ plotted as the function of $y^+ = y^+(u^+)$ are completely different from each other.

Further research possibilities

1. The results obtained in the investigation of the boundary layer, suggest that there is a lot to be done in the field of enchasing the existing mathematical models. Prior to that, more experiments, with different wave conditions and beach configurations have to be carried out for generalization of the results.
2. Based on the conclusions of the present study it would be interesting to perform an analysis of the eddy viscosity in time and in space. The results could be compared with the existing models.
3. If the models fail to predict the variation of eddy viscosity, an attempt could be made to find the pattern of the variation and give a mathematical form for it.
4. As it was found, the acceleration of water particles in the wave is occasionally many times the acceleration due to gravity, the determination of the kinetics of solid particles in the flow could be important. It can be suggested that the usual approach to settling in still water does not apply to areas of wave breaking and therefore the determination of dynamic settling velocity could be an issue.

References

Aitsam, A., Daniel, E., Liiv, U., 1990. Investigation of the velocity distribution and shear stresses in decelerated pipe flow, Proc. Estonian Acad. Sci. Phys. Math. 39, pp. 290-295

Arnskov, M. M., Fredsoe, J. and Sumer, B. M., 1993. Bed shear stress measurements over smooth bed in three dimensional wave-current motion, Coastal Eng., 20, pp. 277-316.

Blondeaux, P. & Vittori, G., 1990. Oscillatory flow and sediment motion over a rippled bed, Proc. 22nd Int. Conf. Coastal Eng., Delft, pp. 2186-2199.

Brevik I., 1981. Oscillatory rough turbulent boundary layers, J. Waterway Port Coastal Ocean Div. ASCE, 107, pp. 175-188.

Bryan, K.R.,Black, K.P., Gorman, R.M., 2003. Spectral estimates of dissipation rate within and near the surf zone, J. of Physical Oceanography, pp. 979-993.

Chang, K.-A., Liu, P.L.-F., 1996. Measurements of breaking waves using particle image velocimetry, Proc. 25th Int. Conf. on Coastal Eng., vol. 1. ASCE, Orlando, FL. pp. 527-537.

Chang, K.-A., Liu, P.L.-F., 1999. Experimental investigation of turbulence generated by breaking waves in water of intermediate depth, Phys. Fluids, 11(11), pp. 3339-3400.

Christensen, E. D., Deigaard, R., 2001. Large eddy simulation in breaking waves, Coastal Eng., 42, pp. 53-86.

Cox, D.T., Kobayashi, N., Okayasu, A., 1996. Bottom shear stress on the surf zone, Journal of Geophys. Res., 101(C6), pp. 14337-14348.

Deigaard, R., Mikkelsen, M.B., Fredsoe, J. 1991. Measurements of the bed shear stress in the surf zone, Prog. Rep., vol. 73, ISVA, Tech. Univ. Denmark, Lyngby, pp. 484-497.

Feddersen, Gallagher, E.L.,F., Elgar, S., Guza, R.T., 2003. The drag coefficient, bottom roughness, and wave breaking in the nearshore, Coastal Eng., 48, pp. 189-195.

Feddersen, F., Trowbridge J.H., 2005, The effect of wave breaking on surf-zone turbulence and alongshore currents: a modelling study, J. of Physical Oceanography, 35, pp. 2187-2202.

Feddersen, F., Williams, A. J., 2007. A direct estimation of the Reynolds stress vertical structure in the nearshore, J. of Atmospheric and Oceanic Techn., 24, pp. 102-116.

Fredsoe, J., Andersen, O.H., Silberg, S., 1985. distribution of suspended sediment in large waves. J. of Waterway, Port, Coastal and Ocean Engineering, ASCE, 111(6), pp. 1041-1059

Grant, W.D., & Madsen, O.S., 1979. Combined wave and current interaction with a rough bottom, J. Geophys. Res., 84, pp. 1797-1808.

Grant, W.D.& Madsen, O.S., 1982. Movable bed roughness in unsteady oscillatory flow, J. Geophys. Res., 87, pp. 469-481.

Haydon, T.R., Hann, D.B., Davies, P., 1996. Greated, C.A., Barnes, T.C.D., Turbulence structure in surf zone, Proc. 25th Int. Conf. on Coastal Eng., vol. 1. ASCE, Orlando, FL, pp. 214-220.

Heinloo J., Toompuu A., 2009. A model of average velocity in oscillating turbulent boundary layers, Journal of Hydraulic Research, 47, No. 5, pp. 676–680

Jensen, B.L. 1989. Experimental investigation of turbulent oscillatory boundary layers, Series Paper 45, Institute of Hydrodynamics and Hydraulic Engineering (ISVA), Technical University of Denmark, 157 p.

Jensen, B.L., Sumer B.M., Fredsoe J., 1989. Turbulent oscillatory boundary layers at high Reynolds numbers, J. Fluid Mech., 206, pp. 265-297.

Jonsson, I.G. & Carlsen, N.A., 1976. Experimental and theoretical investigations in an oscillatory turbulent boundary layer, J. Hydraulic Res., 14, pp. 45-60

Jonsson, I.G., 1996. Wave boundary layers and friction factors, Proc. 10th Int. Conf. Coastal Eng., Tokyo, pp. 127-148.

Kaijura, K., 1968. A model of the bottom boundary layer in water waves, Bulletin Earthquake Research Institute, 46, pp. 75-123.

Kalkanis, G., 1957. Turbulent flow near an oscillating wall, Beach Erosion Board, Tech. Memo 97, 47 p.

Kalkanis, G.,1964. Transportation of bed material due to wave action, U S Army C E R C, Tech Memo 2, 39 p.

Krstic, R.V., Fernando, H.J.S., 2001. The nature of rough-wall oscillatory boundary layers, J. Hydraulic Res., 39 (6), pp. 655-666.

Liiv T., Lagemaa P., 2008. The variation of the velocity and turbulent kinetic energy field in the wave in the vicinity of the breaking point, Estonian Journal of Engineering, 2008,14, 1, 42-64.

Liiv, T., 1995. An experimental investigation of the breaking wave characteristics in coastal regions, Int. Conf. on Coastal and Port Eng. in Developing Countries, Proc. of the COPEDEC IV, Rio de Janiero, vol. 3, pp. 2334-2343.

Liiv, T., 2001. Investigation of turbulence in a plunging breaker wave, Proc. Estonian Acad. Sci. Eng., 7/1, pp. 58-78.

Liiv, U., Liiv, T., 1998. Shear investigations of the breaking waves in the flume, Proc. 3rd Int. Conf. on Hydro-Science and Eng. Brandenburg University of Technology at Cottbus, Germany, Aug. 31 – Sept. 3, CD-ROM, 12 p.

Liiv. U., 2004. Unsteady pipe flow transition to turbulence under constant acceleration, In Proc.10th Asian Congress of Fluid Mechanics. Sri Lanka, CD-ROM, 7 p.

Lin, P., Liu P.L.F., 1998. A numerical study of breaking waves in surf zone, J. Fluid Mech., 359, pp. 239-264.

Lin, P. and Liu, P. L.-F., 1998. Turbulence transport, vorticity dynamics and solute mixing under plunging breaking waves in surf zone, J. Geophys. Res., 103, No C8, pp. 15677-15694.

Liu, P. C. and Babanin, A.V., 2004. Using wavelet spectrum analysis to resolve breaking events in the wind wave time series, Annales Geophysicae, 22, pp. 3335-3345.

Nadaoka, K., Kondoh, T., 1982. Laboratory measurements of velocity field in the surf zone by LDV, Coastal Eng. Jpn., 25, pp. 125-146.

Nielsen, P. 1985. On the structure of oscillatory boundary layers, Coastal Engineering, 9, pp. 261-276.

Nielsen, P. 2005. Coastal bottom boundary layers and sediment transport, World Scientific, New Jersey, London, 324 p.

Pedersen, C., Deigaard, R., Sutherland, J., 1998. Measurements of the vertical correlation in turbulence under broken waves, Coastal Eng., 35, pp. 231-249.

Petti, M., Longo, S. 2001. Turbulence experiments in swash zone, Coastal Eng., 43, pp. 1-24.

Rafik A., 2001. Time-Dependnt Eddy Viscosity Models for Wave boundary Layers, Proc. Of 27th Int. Conf. on Coastal Eng. Sydney, Australia, pp.1268-1281

Rodi, W., 1980. Turbulence models and their application in hydraulics, International Association for Hydraulic Research, Delft, 115 p.

Rogers, B. D. and Dalrymple R. A., 2004. SPH Modeling of breaking waves, 29th Int. Conf. Coastal Eng., pp. 1147-1157.

Sakai, T., Mizutani, T., Tanaka, H., Tada, Y. 1986. Vortex formation in plunging breakers, Proc. of the Int. Conf. on Coastal Eng. ASCE, vol. 1., Taipei, Taiwan, pp. 711-723.

Schäffer, H.A., Madsen, P.A., Deigaard, R. 1993. A Boussinesq model for waves breaking in shallow water, Coastal Eng., 20, pp. 185-202.

Sealth, J. F. A., 1982. The suspension of sand by waves, J. Hydraulic Res., 20 (5), pp. 439-452.

Sealth, J. F. A., 1987. Turbulent oscillatory flow over rough beds, J. Fluid Mech., 182, pp. 369-409.

Sealth, J. F. A., 1991. Velocities and shear stresses in wave-current flows, J. Geophys. Res., 96 C8, pp. 15237-14244.

Shin, S., 2004. Determination of the shear velocities, the bottom roughness and friction factors, Publications of the Oregon State University, Swash Zone Turbulence Group, Report 2, 15 p

Stieve, M.J.F. 1980. Velocity and pressure field of spilling breaker, Proc.17th Int. Conf. Coastal Eng. pp. 574-566

Stieve, M.J.F., Wind, H.G. 1982. A study of radiation stress and set-up in the nearshore region, Coastal Eng., 6, pp. 1-25.

Svendsen , I.A., Hansen, J.B. 1976. Determination up to breaking of periodic waves on a beach, Proc. 16th Coastal Eng. Conf., Hamburg, pp. 477-496.

Stansell, P., 2002. Experimental investigation of wave breaking criteria based on wave phase speeds, J. Physical Oceanography, 32, No. 5, pp. 1269-1283.

Svendsen, I.A. 1987. Analysis of surf zone turbulence, J. Geophys. Res., 92(C5), pp. 5115-5124.

Takikawa, K., Yamada, F., Matsumoto, K. 1997. Internal characteristics and numerical analysis of plunging breaker on a slope, Coastal Eng. 31, pp. 143-161.

Ting, F. C. K., Kirby, J.T. 1994. Observation of undertow and turbulence in a laboratory surf zone, Coastal Eng., 24, pp. 51-80

Ting, F.C.K., Kirby, J.T.1995. Dynamics of surf zone turbulence in a strong plunging breaker, Coastal Eng., 24, pp. 177-204.

Ting, F. C. K., Kirby, J.T. 1996. Dynamics of surf-zone turbulence in spilling breaker, Coastal Eng., 27, pp. 131-160.

Trowbridge, J., Madsen, O.S., 1984. Turbulent wave boundary layers I. Model formulation and first order solution, J. Geophys. Res., 89 (C5), pp. 7989-7997

Trowbridge, J.H., Agrawal, Y.C., 1995. Glimpses of wave boundary layer, J. of Geophys. Res., 100 (C10), pp. 20729-20743.

Xiuying Xing, M.E., 2004. Wave bottom boundary layer physics and bed load sediment transport in nearshore, Master of Science Degree Thesis, The Ohio State Univ., 83 p.

Experimental Analysis of Boundary Layer Dynamics in Plunging Breaking Wave

Abstract

An extensive experimental run has been carried out in the wave flume to investigate the boundary layer behaviour under a plunging breaking in the surf zone. Two dimensional Laser Doppler Anemometer was used to investigate such key phenomena as unsteady boundary layer, turbulent kinetic energy and Reynolds stresses. The results of the investigation were compared with the most widely used terms in the mathematical models describing processes in the surf zone. The results on the boundary layer show that there is a considerable difference between the measured values and ones commonly used in the models to calculate unsteady boundary layers. The measured values of turbulent kinetic energy were found to be comparable with the works published so far.

Sukelduva murdlaine piirikihi dünaamika eksperimentaalne analüüs

Kokkuvõte

Tallinna Tehnikaülikooli Hüdromehaanika teadus- ja katselaboratooriumis on uuritud kahemõõtmelisi kiiruste välju, mis tekivad sukelduva murdumise korral laine levikul sileda põhjaga katserennis. Kiiruste välja mõõtmiseks laine põhja piirikihi ja laineoru taseme vahel kasutati laser-Doppleri anemomeetrit. Mõõdetud andmete põhjal on määratud turbulentne kineetiline energia ja Reynoldsi pinged. Töö eesmärgiks oli uurida voolamist laine piirikihis. Tulemusi võrreldi laialt kasutatavate mudelitega, mis arvutavad voolamist laine piirikihis. Võrdlus näitab, et katsete käigus saadud mittestatsionaarsed piirikihi voolamise profiilid ei ühti algandmetega, mida kasutatakse mudelites tänapäeval. Mõõdetud turbulentse kineetilise energia väärtused on võrreldavad tulemustega, mis on saadud teiste autorite poolt.

Curriculum vitae

1. Personal data

Name	Toomas Liiv
Date and place of birth	05.04.1969, Tallinn

2. Contact information

Address	Ehitajate tee 5, 19086, Tallinn
Phone	(+372) 620 25 51
e-mail	toomas@corson.ee

3. Education

Educational institution	Graduation	Education (field of study/degree)
Royal Institute of Technology, Stockholm	2000	Water Engineering/ Licentiate of technology
Tallinn University of Technology, Tallinn	1987	Water Engineering/ engineer

4. Language skills

Language	Level
Estonian	Mother tongue
English	Fluent
Finnish	Average
Russian	Average
Swedish	Reading
Danish	Reading

5. Special Courses

Period	Educational organization
2001	Danish Technical University
1998	Swiss Federal Institute of Technology

6. Professional Employment

Period	Organization	Position
1987 – 2010	Tallinn University of Technology	Researcher

| 2010 - …….. | Tallinn University of Technology | Assistant |
| 1996 – …….. | Corson LLC | Member of the board |

7. Scientific work

Articles:

Liiv, T., Lagemaa, P. (2008). The variation of the velocity and turbulent kinetic energy field in the wave in the vicinity of the breaking point; pp. 42–64. Estonian Journal of Engineering, 14, 42 - 64.

Liiv, T. (2007). An experimental investigation of oscillatory boundary layer around the breaking point. Proceedings of the Estonian Academy of Sciences. Engineering, 13, 215 - 233.

Liiv, T. (2003). Numerical Models in the Design of Saaremaa Deep Harbour. *In: Proceedings of XXX IAHR Congress: The XXX International Association of Hydraulic Engineering and Research (IAHR) Congress; Thessaloniki (Greece), August 24th-29th 2003.* , 2003, 147 - 154.

Liiv, T.; Liiv, U. (2001). Saaremaa deep harbour layout design and computer simulation of wave climate and sand transport. Proceedings of the Estonian Academy of Sciences. Engineering, 7, 174 - 192.

Liiv, T. (2001). Investigation of turbulence in a plunging breaking wave. Proceedings of the Estonian Academy of Sciences. Engineering, 7, 58 - 77.

Liiv T., (1995) An Experimental Investigation of the Breaking Wave Characteristics in Coastal Region. International Conference on Coastal and Port Engineering in Developing Countries, Proceedings of the COPEDEC IV, Rio de Janeiro, Brazil; 1995; 1995, 3, 2334-2343.

Liiv T., Liiv U., 1998. Shear Investigations of the Breaking Waves in the Flume. Proceedings of the 3rd International Conference on Hydro-Science and Engineering; Cottbus/Berlin, Germany; CD-ROM, 12 p.

Liiv T., Liiv U., 1999. Laboratory Study of the Breaking Wave Characteristics; Proceedings of the XXVIII IAHR Congress 22-27 August, Graz, Austria, CD-ROM

Liiv T., 2001. The effect of bottom roughness on the flow quantities under plunging breaking wave motion, 29th Annual Congress of the International-Association-of-Hydraulic-Engineering-and-Research (IAHR)**,** Hydraulics for Maritime Engineering, Theme E, Proceedings pp 313-319

Liiv T., 2005. The Effect of Bottom Roughness on the Flow Structure under Wave Breaking Condition in the Surf Zone. Transactions of the Conference Dedicated to the 100th Birthday prof. R.R. Chugajev; SPbGTY Nautšno-tehnitšeskie vedomosti; Sankt Petreburg, 19-25. (In Russian).

Supervision of master's degree thesis:

Aurika Männik, Master's Degree, 2010, Turbulentse viskoossusteguri muutumine laine murdumisel (The Variation of Turbulent Viscosity During Wave Breaking), Tallinn University of Technology , Faculty of Civil Engineering, Department of Mechanics, Chair of Fluid and Aeromechanics

Merike Viigisalu, Master's Degree, 2010, Mere hüdrodünaamiliste protsesside modelleerimine ja keskkonnamõju strateegiline hindamine Tallinna lahte planeeritavate tehissaarte näitel (The modelling of hydrodynamic processes and strategic environmental assessment vased on the example of artificial islands planned into the bay of Tallinn), Tallinn University of Technology , Faculty of Civil Engineering, Department of Environmental Engineering

Nelly Oldekop, Master's Degree, 2008, Sulundseina tehnoloogiad sadamaehituses ja kasutatavate materjalide analüüs (The sheet piling technologies in harbour construction and the analysis of the materials in use),Tallinn University of Technology , Faculty of Civil Engineering, Department of Mechanics

Maarja Mitt, Master's Degree, 2007, Environmental impact assessment for the road of Nooda in Kakumäe (Environmental impact assessment for the road of Nooda in Kakumäe), Tallinn University of Technology , Faculty of Civil Engineering, Department of Environmental Engineering , Chair of Environmental Protection

Priidik Lagemaa, Master's Degree, 2005, Sukelduva murdlaine eksperimentaalne uurimine välimises rannaalas (Experimental Investigation of Plunging Breaking Waves in Outer Surf Zone), Tallinn University of Technology , Faculty of Civil Engineering, Department of Mechanics

8. Defended theses

Thesis for the Licentiate of technology: Experimental investigation of the Breaking Waves using LDA System

9. Main areas of scientific work

Coastal zone sediment transport processes caused by breaking waves

Mechanics of Fluid-Structure Interaction

Elulookirjeldus

1. Isikuandmed

Ees- ja perekonnanimi	Toomas Liiv
Sünniaeg ja –koht	05.04.1969, Tallinn

2. Kontaktandmed

Aadress	Ehitajate tee 5, 19086, Tallinn
Telefon	(+372) 620 25 51
e-post	toomas@corson.ee

3. Hariduskäik

Õppeasutus	Lõpetamise aeg	Haridus (eriala/kraad)
Kuninglik Tehnikakõrgkool, Stockholm	2000	Vesiehitus/ tehnikalitsensiaat
Tallinna Tehnikaülikool, Tallinn	1987	Veevarustus ja kanalisatsioon/ ehitusinsener

4. Keelteoskus

Keel	Tase
Eesti keel	Emakeel
Inglise keel	Kõrgtase
Soome keel	Kesktase
Vene keel	Kesktase
Rootsi keel	Lugemisoskus
Taani keel	Lugemisoskus

5. Täiendusõpe

Õppimise aeg	Täiendusõppe läbiviija nimetus
2001	Taani Tehnikaülikool
1998	Šveitsi Föderaalne Tehnikainstituut

6. Teenistuskäik

Töötamise aeg	Tööandja nimetus	Ametikoht
1987 – käesoleva ajani	Tallinna Tehnikaülikool	Lepinguline töötaja
1996 – käesoleva ajani	Corson OÜ	Juhataja

7. Teadustegevus

Teadustegevuse nimekiri on toodud Ingliskeelse elulookirjelduse punktis 7.

8. Kaitstud lõputööd

Litsensiaadi väitekiri: An Experimental investigation of the Breaking Waves using LDA System

9. Teadustöö põhisuunad

Kaldajoone murdlainetusest tekkiva uhtlainete transpordiprotsesside uurimine

Vedeliku ja konstruktsiooni koostoime mehaanika

INVESTIGATION OF TURBULENCE
IN A PLUNGING BREAKING WAVE

Toomas LIIV

Institute of Mechanics, Tallinn Technical University, Ehitajate tee 5, 19086 Tallinn, Estonia; toomas@corson.ee

Abstract. The velocity field created by a plunging breaking wave on a smooth bottom with slope 1 : 17 was studied experimentally in a wave flume. Laser Doppler anemometry was used to investigate the flow field above the bottom boundary and below the trough level of the wave. Turbulence intensities, Reynolds stresses, and turbulent kinetic energy were examined. The results show that large-scale motions dominate in turbulence under the plunging breaker. The flow has characteristic features of an outer surf zone. It is found that turbulent quantities in the zone close to the bottom depend on the nature of the flow acceleration. During the deceleration phase, all turbulent quantities reach their maximum values. In the layers close to the wave trough, turbulent quantities depend on the wave parameters. Turbulent kinetic energy reaches its maximum value under the wave crest and decreases rapidly to a constant value under the wave trough. Turbulence is generated on the surface during the breaking process and it diffuses towards the bottom. The energy level first decreases downward and then increases again close to the bottom due to the bottom boundary layer turbulence. Kinetic energy is transported landward in the upper layers of the flow and seaward near the bottom.

1. INTRODUCTION

Plunging is the most dramatic wave breaking phenomenon in which the wave curls over and looses a considerable amount of energy in one big splash. Breaking is of a complex nature, the physics of which is not yet well understood. At the breaking point, the front face of the wave becomes vertical and begins to curl forward. A jet from the overturning wave front plunges into the wave trough in front of it and a violent transition of the wave begins. This process entraps considerable amount of air which bursts into small bubbles. The breaking process generates turbulence and vorticity which cause mixing of solutes and sediment in the surf zone. Most of the previous studies have been concerned with experiments

rather than with theoretical analysis of the breaking process. Experiments are still necessary as they help us to obtain a better understanding of the breaking process. Furthermore, it would be possible to extend the theory of this type of waves. The following review aims to give a short "state of the art" knowledge on the subject.

In the past decade, a progress has been made in modelling the breaking process in spilling type breaking waves, the most common approach being solving the model based on the equation of kinetic energy transportation [1]. For the spilling breakers, the results are satisfactory, but for plunging breakers the approach seems to be inadequate. The model does not take into account the convection of turbulence by wave-induced flows that are important in plunging breakers. Takikawa et al. [2] used the Reynolds transport equation and Lin and Liu [3] used the $k - \varepsilon$ equation. The results obtained using these equations are not satisfactory. This is due to the complexity of the phenomena of breaking and due to the lack of knowledge about the plunging breakers.

The turbulent fluctuations in the Reynolds equation are represented by the Reynolds stress tensor $\rho < u'v' >$. This can be modelled using Reynolds stress transport model that consists of six partial differential equations [4]. To solve this model is time consuming and computationally expensive. A common approach is to use simpler methods to determine the Reynolds stresses [3]. However, these equations require empirical coefficients that can only be determined by experiments.

Until the beginning of 1980s the measurement of velocities inside breaking waves was associated with difficulties due to the lack of adequate instrumentation. Developments in Laser Doppler technology have made it possible to make velocity measurements with good accuracy and reliability. During the past two decades, a lot of work has been done on breaking waves. Some of the more detailed studies include works by Peregrine and Svendsen [5], Stieve [6], and Battjes and Sakai [7].

Peregrine and Svendsen [5] investigated spilling breakers using visualization techniques. The authors proposed a model of the flow field for the steady and quasi-steady breaking flows such as hydraulic jumps, bores, and spilling breakers. They concluded from visual observations that the turbulent flow, immediately following the breaking of the wave, resembles a turbulent mixing layer. In the model, the region of turbulent flow, following breaking, is assumed to spread downstream and towards the bottom similarly to a mixing layer. At some distance downstream, the upper region of the wave becomes affected by gravity whereas for waves in shallow water the lower region becomes affected by the bottom boundary. Still further downstream there is a wake or decay region.

Stieve [6] used LDA to measure the velocities of the breaking waves in the surf zone on a model with a slope of 1 : 40. The study was restricted to the spilling type of breaking waves. The main conclusion was that the existing linear and cnoidal wave theories do not predict the velocity field in the breaking waves. Stieve also found a wake type flow in the region behind the crest.

Battjes and Sakai [7,8] measured the velocity field in a steady standing breaker, generated behind a wing that was inserted into a uniform channel flow. The mean flow, turbulent intensities, and the Reynolds stresses were analysed in comparison with turbulent shear layer and turbulent wake theories. The authors concluded that the whole velocity field resembles turbulent wakes rather than turbulent shear layer.

Flick et al. [9] measured the velocity in the surf zone on a slope using a hot film anemometer. They investigated the variation of the turbulent intensity due to the breaker type of the waves. It was found that the correlation between surface elevation and bottom velocity is lower under a plunging breaker than under a spilling breaking wave. They concluded that turbulent fluctuations are more important in plunging than in spilling waves.

Nadaoka et al. [10] found that the velocity field within the surf zone is clearly divided into two zones: a transition zone and a bore establishment zone. The velocity field within the latter zone consists of an upper layer and a bottom layer. The upper layer is characterized by large scale eddies associated with small scale turbulence and entrained air bubbles, whereas the bottom layer is characterized by the existence of small scale turbulence originated from the upper layer and the bottom boundary layer. They also concluded that turbulence is an important factor in suspending sediment and transporting it around in the surf zone.

Sakai et al. [11] found that the turbulent intensity varies more in the case of a transient breaker between spilling and plunging than in the case of a spilling breaker. In the latter case, the turbulent intensity is not damped so much as the waves propagate in the surf zone. They found that the turbulent intensity is larger in the upper part of the wave than near the bottom. The main conclusion was that the turbulent wave theory does not give a reasonable answer to the variation of Reynolds stress in the surf zone and more investigations are needed. Later, Sakai et al. [12] found that the magnitude of the Reynolds stress term in the on-offshore momentum equation during one wave period is small compared with the local acceleration and convection terms.

Hattori and Aono [13] suggested that the type of turbulence structure associated with spilling and plunging breakers is characterized by the differences of turbulent intensity distributions in the inner regions, by the slopes of the velocity spectrum tails, and by the generation mechanism of bottom boundary layer generated turbulence. From flow visualization it was concluded that the turbulence generated in the bottom boundary layer has a coherent structure similar to turbulent spots found in turbulent shear flows. Such large turbulence structures are stretched vertically during the passage of the wave crest and reach the free surface behind the crest of breaking waves. It was concluded from the statistical analysis that regions of large turbulent intensity exist near the plunging point of the wave. The turbulence motion transfers wave energy shoreward.

Tada et al. [14] discussed the phase variation of surf zone turbulence by using existing data. The data was compared with analytical solutions, especially applying the one equation model of the turbulent kinetic energy transportation.

They concluded that the single equation model overestimates the production and dissipation terms of turbulent kinetic energy. It was found that it is necessary to refine the product term to predict more accurately the phase variation of turbulent intensity during one wave period.

In 1994, Ting and Kirby [15] studied undertow and turbulence in spilling and plunging breakers. They found that despite the similarities in wave profiles in the bore region, the characteristics of turbulence and undertow are different in spilling and plunging breakers.

Ting and Kirby [16] studied experimentally the region below the trough level and above the bottom boundary layer under the spilling breaker. They suggested that the length and the velocity scales of the large eddies are determined by the rate of the energy transfer from the organized wave induced motion to the turbulent motion, and the size of the surface roller. Turbulent flow is well developed in the inner surf zone. The velocity spectrum has an inertial subrange with a slope –5/3. They suggested that diffusion plays the most important role in turbulence transport.

The present study deals with the dynamics of the surf zone turbulence generated by a plunging breaker on the plane beach. The breaking wave characteristics were measured by the use of a two-dimensional LDA system. Experimental results confirm that there are zones with accelerations and decelerations inside the breaking waves. The flow shows characteristics of the outer surf zone so that the turbulence generated on the surface does not affect the bottom boundary. During the acceleration period the values of turbulent intensities and Reynolds stresses decrease. The influence of acceleration on values of kinetic energy and its transport will be discussed.

2. EXPERIMENTAL SETUP AND PROCEDURES

The experiments were carried out in a wave flume situated in the Hydraulics Laboratory of Tallinn Technical University. The flume was 0.6 m wide, 0.6 m deep, and 22 m long. The flume walls were made of glass on both sides. The waves were generated in the constant depth section of the flume, which was 13 m long. The still water depth in the constant depth section of the flume was kept at 0.3 m throughout the experiments. Figure 1 shows the experimental setup. Waves were generated using a flap type wave generator that enabled to generate both regular and irregular waves. A computer was used to produce signals for generating regular sinusoidal waves controlled by the generator.

The waves broke on a hydraulically smooth surf zone model made of vinyl plates. The setup had a slope of 1:17. Velocity distribution was measured in the breaking waves using a two-component Argon-ion LDA with an output power of 5 W. The measuring system is based on a two-dimensional tracker which operates in forward scatter fringe mode. The two velocity components were measured simultaneously. The flow velocity data was collected with a sampling
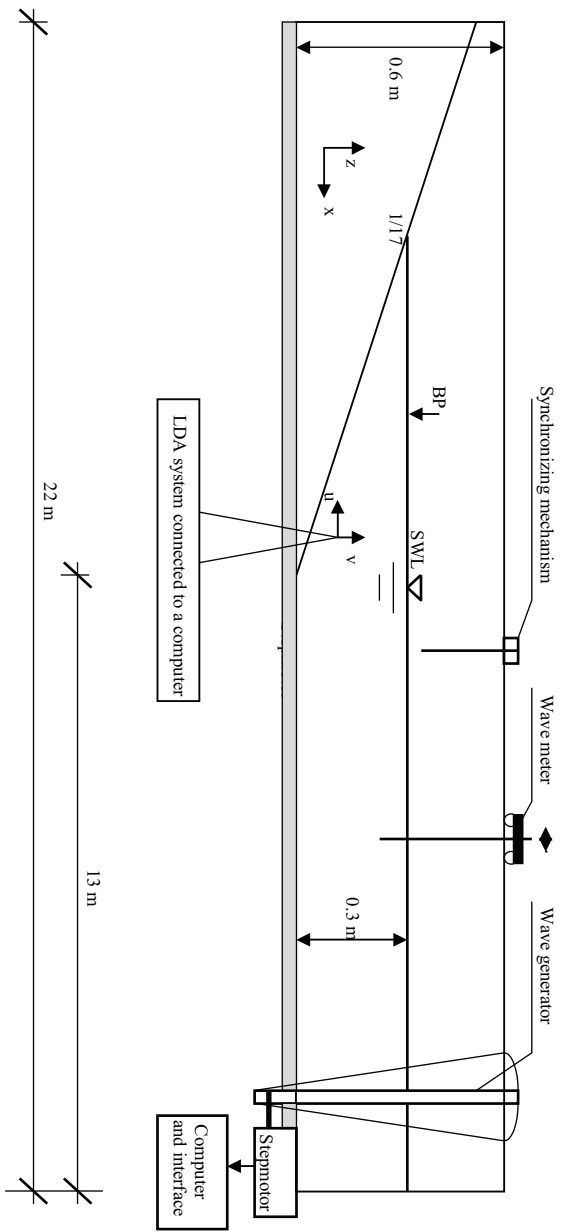
Fig. 1. Sketch of the experimental setup, side view.

frequency of 1000 Hz during 150 wave periods. The experiments carried out by other researchers have shown that in order to resolve the processes inside breaking waves, the minimum suitable frequency is 100 Hz and the appropriate number of successive waves for an ensemble average is approximately 100. In the preliminary tests performed, the effect of the increase of wave periods in the ensemble was studied. The results proved that if the number of wave periods was increased from 66 to 150, the fluctuations in the ensemble-averaged velocities decreased up to 5%, giving smoother ensemble-averaged velocity profile.

The water was seeded with irodin particles to reduce the drop-out rate of the Doppler signal. Sometimes during the experiments, entrained air bubbles blocked the laser beams. This results in signal drop-outs when no signal is recorded. During the signal drop-out the frequency tracker keeps the output voltage the same as the voltage just before the drop-out. This is called track and hold operation. To find if the signal drops out or not, a so-called drop-out signal is recorded simultaneously with the output of regular channels.

Three sets of experiments were carried out with different wave characteristics given in Table 1. Velocity profiles were measured along the flume centerline at five different sections (Table 2). Horizontal and vertical velocities were measured at various heights above the flume floor in each section at 5 mm intervals. The origin of the co-ordinate system was at the bottom of the surf zone model at the first section.

Table 1. Test conditions (h_b and H_b are still water depth and wave height at the breaking point, respectively, H_0/L_0 is deep water wave steepness)

Run	T, s	h_b, m	H_b, m	H_0/L_0	x_b, m
1	0.91	0.115	~0.081	0.023	0.08
2	1.62	0.123	~0.087	0.017	~0
3	2.00	0.131	~0.092	0.012	−0.06

Table 2. Location of measurement points and still water depths

	Number of the section				
	1	2	3	4	5
x, m	0	0.115	0.265	0.38	0.495
H, m	0.115	0.107	0.098	0.092	0.084

The breaking point of the wave was determined by visual observation at the point where the creation of air bubbles and the overturning of the wave crest began. In all runs, breaking points were established approximately at 1.6–1.8 m from the shoreline. It corresponds to the vicinity of the first profile. The breaker was of the plunging type.

In order to obtain during experiments a reliable representation of the wave structure, the measurements were synchronized. The synchronizing mechanism was made of a pair of electrodes and was situated in the deep-water section of the flume above the still water level. The electrodes were connected to the computer through an interface. When the front face of the wave crest reached the electrodes, it gave an impulse to the computer which started the measurements.

Conductivity probes were used to measure wave height variation. The system uses two low resistance probes and measures the actual conductance of the changing volume of the water. The probes are simple to operate and if used in fresh water they give correct wave height variations [17]. The probes were operated using the same program as for the laser measurements and the measurements were taken simultaneously with the velocity measurements along the same profiles. Furthermore, the wave height in the constant depth section of the flume was measured.

Systematic and random errors of the measured velocities were estimated from the instrument specifications and reproducibility tests. The main cause of errors in LDA measurements is the misalignment of the LDA system and non-optimal size of the optical probe. The experimental studies were preceded by a series of calibration and reproducibility tests. The results indicated that the relative standard error in velocity measurements did not exceed 8%.

Regular sinusoidal waves produced by the computer are

$$\xi = e_1 \sin \omega t + e_2 \sin(2\omega t + \beta_2), \tag{1}$$

where ξ is the motion of the wave generator flap, $\omega = 2\pi/T$ is the wave frequency, and β_2 is the angle between the two components of flap motion. The waves were not totally free from the second harmonic components. The reason for these components is that the rigid flap of the generator could not exactly produce the variation of the particle motion, which corresponded to a progressive wave of constant form [18]. However, the amplitude of the second harmonic wave components was always less than 3%. This is important because the waves in the constant depth part of the wave flume represent the initial conditions for the shoaling process.

Statistical analysis of the velocity components in the breaking region showed that the velocity data had a nonstationary random character. Breaking wave motion can be described as a fluctuating quantity with a quasi-periodic character. Breaking motion is the sum of a purely periodic component and a fluctuating component and can be treated as an ensemble over the wave period

$$U_i = (\langle u \rangle + u'), \quad V_i = (\langle v \rangle + v'), \tag{2}$$

where U_i and V_i are the measured instantaneous velocities, $\langle u \rangle$ and $\langle v \rangle$ are the periodic components, and u' and v' are the fluctuating parts. The periodic component is obtained by averaging the signals at a fixed phase of the reference signal (the command signal of the wave generator).

The fluctuating component of the velocity is formed by the turbulence fluctuations of the breaking process and will therefore be considered as turbulent intensity components. Turbulence was defined as the deviation of the original velocity from the periodic velocity:

$$u' = U_i - \langle u \rangle, \quad v' = V_i - \langle v \rangle. \tag{3}$$

The cross product of u' and v' was calculated at every 0.001 s. This cross product multiplied by density with a negative sign is the instantaneous Reynolds stress. In the present study, Reynolds stresses are defined as an ensemble-average instantaneous Reynolds stress at a fixed phase of the reference signal (the command signal of the wave generator).

The Reynolds stress equations can be used to estimate the acceleration of fluid particles. A simplified set of equations can be obtained by ignoring the spanwise derivatives of the velocity. The equation in the streamwise direction x is given by

$$\frac{\partial u}{\partial t} + u \frac{\partial u}{\partial x} + v \frac{\partial u}{\partial z} = -\frac{1}{\rho} \frac{\partial}{\partial x} \left(p - \rho \langle u'^2 \rangle \right) + \frac{1}{\rho} \frac{\partial}{\partial z} \left(-\rho \langle u'v' \rangle \right). \tag{4}$$

Equation (4) is a common form used by analysing problems in coastal engineering. The first and the third term on the left side refer to the local acceleration and convective acceleration, respectively. It is important to study the relevance of each term in Eq. (4). This can be done by estimating the magnitude of each term using experimental data. Sakai et al. [12] established that the local acceleration term was several orders of magnitude larger than other terms in the equation. The actual order depended on time. The difference was greatest under the wave crest. One conclusion was that the acceleration of fluid particles can be approximated by the local acceleration. In the present study, acceleration refers to this quantity, i.e., $\partial u / \partial t$ and $\partial v / \partial t$ are taken as the derivatives of velocity.

To study the turbulence characteristics and energy cascade processes in a breaking wave, velocity spectrum analysis was carried out. According to the definition of the turbulence, the wave-inducted and turbulent velocity spectra components are statistically independent from each other. The spectrum was computed using the FFT method.

3. RESULTS

The experimental results are presented in Figs. 2 to 6. All velocity values are normalized using the local phase velocity $C = \sqrt{gh}$ where h is the local still water depth and g is the acceleration of gravity; wave period is 2.00 s.

Figure 2 presents the ensemble-averaged horizontal and vertical velocities at various heights above the flume bottom. Figure 2 correspond to the point where the shoaling wave has just broken. Local still water depth is 0.115 m and wave height is 0.095 m. Horizontal velocities are approximately $0.35C$ under the crest
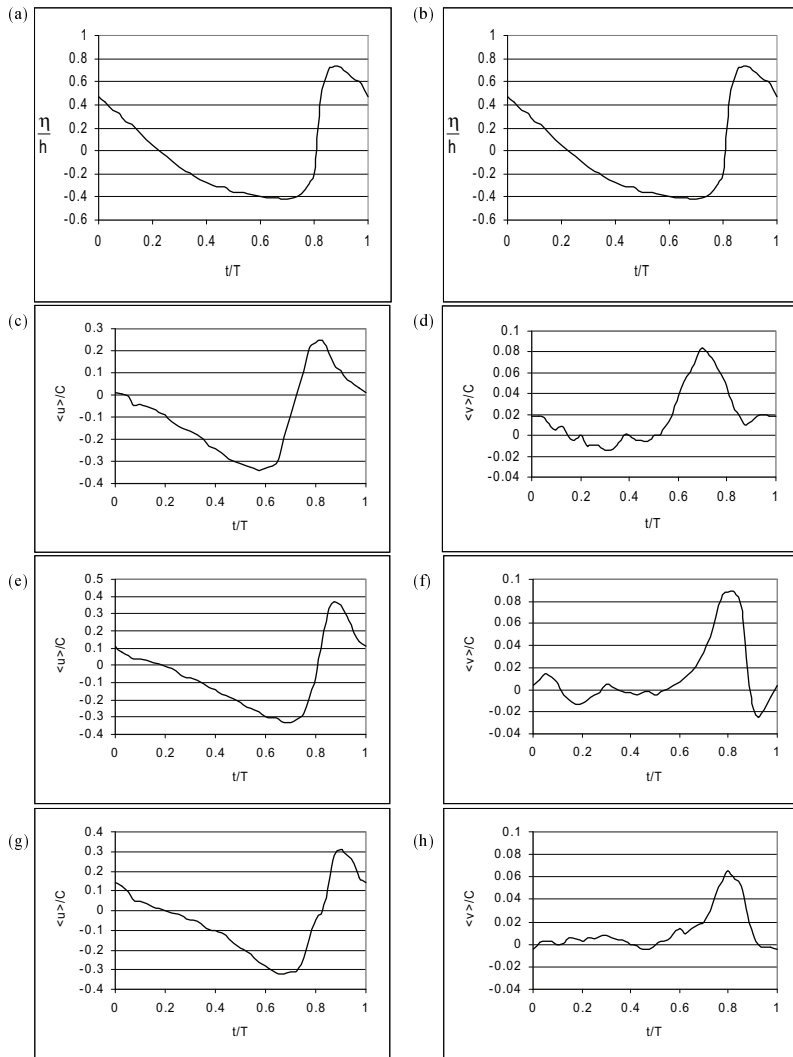
Fig. 2. Ensemble-averaged horizontal (left) and vertical (right) velocities at different locations above the surf zone bed: (a), (b) wave profiles; (c), (d) $z/h = 0.522$; (e), (f) $z/h = 0.352$; (g), (h) $z/h = 0.131$.
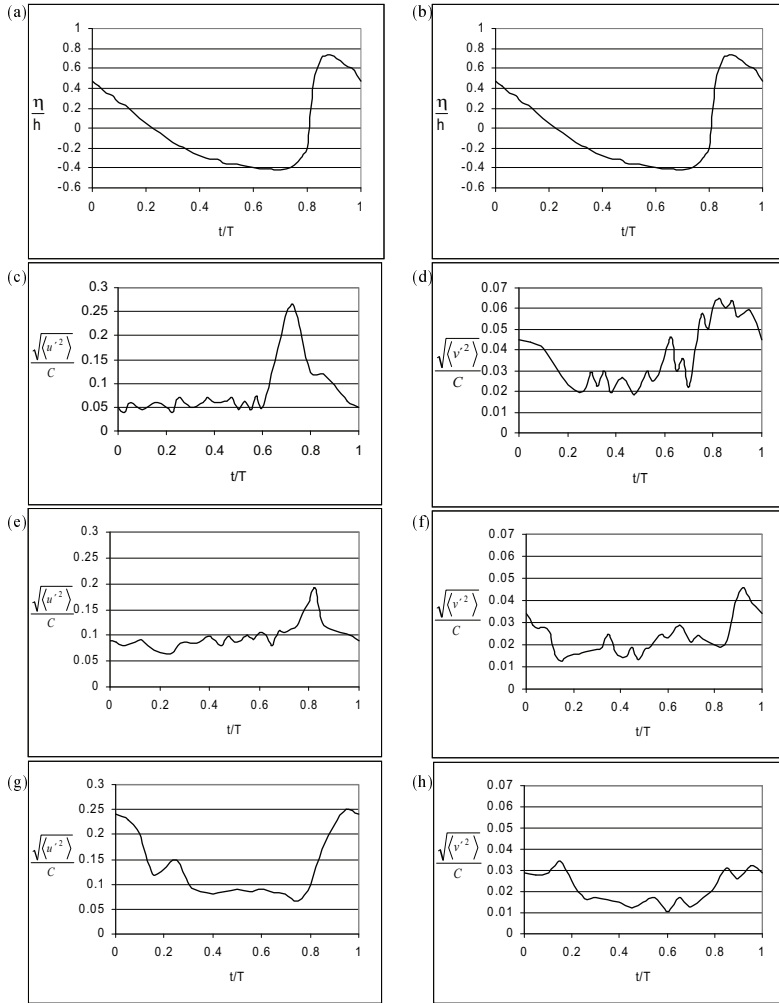
Fig. 3. Ensemble-averaged horizontal (left) and vertical (right) turbulent intensities: (a), (b) wave profile; (c), (d) $z/h = 0.525$; (e), (f) $z/h = 0.352$; (g), (h) $z/h = 0.131$.
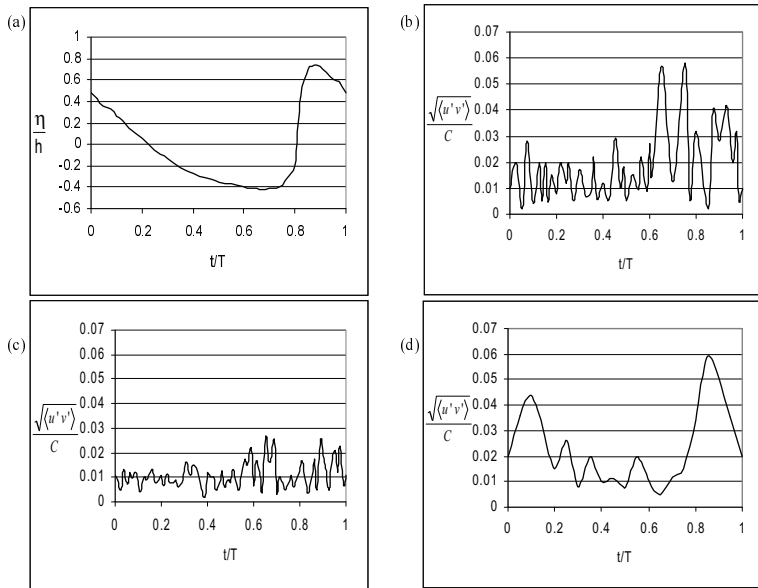
Fig. 4. Ensemble-averaged Reynolds stress plots at different locations above the surf zone bed: (a) – wave profile; (b) $z/h = 0.525$; (c) $z/h = 0.352$; (d) $z/h = 0.131$.
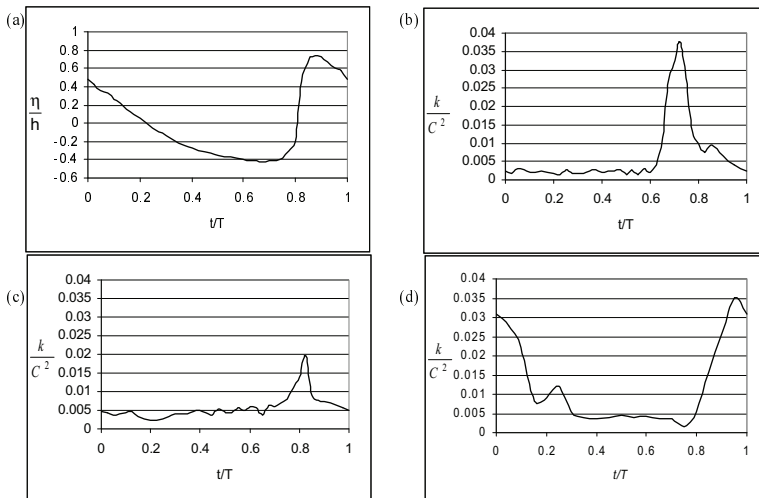
Fig. 5. Ensemble-averaged turbulent kinetic energy at different locations above the surf zone bed: (a) – wave profile; (b) $z/h = 0.525$; (c) $z/h = 0.352$; (d) $z/h = 0.131$.
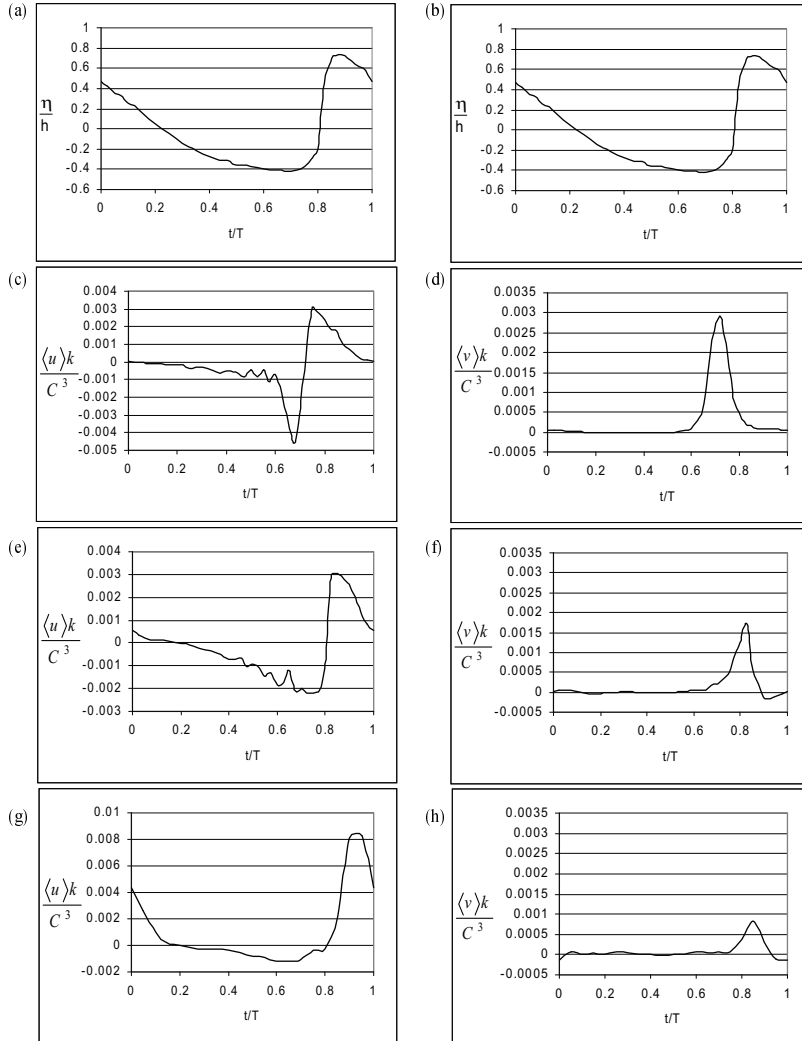
Fig. 6. Ensemble-averaged horizontal (left) and vertical (right) energy fluxes: (a), (b) wave profile; (c), (d) *z*/*h* = 0.522; (e), (f) *z*/*h* = 0.352; (g), (h) *z*/*h* = 0.131.

and $-0.3C$ under the trough. The maximum vertical velocity is approximately $0.08C$ under the wave crest. This value decreases towards the bottom. Comparing the values of horizontal and vertical velocities, it can be seen that the maximum of the vertical velocity component is reached approximately at the same time as the maximum of the horizontal velocity component.

Figure 3 presents ensemble-averaged turbulent intensities for the same locations as in Fig. 2. It can be seen from the figures that turbulence intensity varies significantly during a wave cycle. It is highest during the overturning phase of the wave. There is also a time lag between the occurrence of the maximums in horizontal intensities. In the upper layers of the flow, the peak value of the intensity is under the wave crest and the peak is delayed towards the bottom. Figure 4 plots the dimensionless Reynolds stresses at the same locations as in previous figures. The Reynolds stresses show the same trend as turbulent intensities, maximum for these values occurs when the wave crest has passed the measuring point. Close to the bottom boundary, the graph representing the Reynolds stresses is smoother. This indicates that the turbulent processes near the bottom are less violent than near the free surface boundary.

The phase-averaged kinetic energy is presented in Fig. 5. As only two components of the velocity were measured, the kinetic energy was calculated as $k = (1.33/2)\langle u'^2 + v'^2 \rangle$, according to Stieve and Wind [19]. It is seen that the turbulent kinetic energy is highest in the overturning wave front and it decays rapidly after passage of the wave front.

The ensemble-averaged horizontal and vertical energy fluxes $\langle u \rangle k$ and $\langle v \rangle k$ are presented in Fig. 6. Energy flux was transported shoreward in a zone near the bottom boundary layer and shoreward and offshoreward in the upper part of the water column depending on the wave phase.

4. DISCUSSION

Measured velocities were analysed to study the influence of flow acceleration on the flow structure within the wave. Several examples are presented in Fig. 2. It can be seen from these examples that the acceleration of the water particles in horizontal and vertical directions varies over the depth and time. The variation is partly due to the pressure field acting in the breaking wave that varies in time and space during a wave cycle. The common feature for the horizontal velocity component is the existence of one accelerating region with positive gradient and one deceleration region with negative gradient (Figs. 2c, e, and g). At the end of the deceleration period of the horizontal velocity component, at $t/T = 0.55$, the vertical velocity component changes its sign. The change in sign indicates a change in direction of the large scale eddies. All turbulent quantities, generated during the breaking process of the wave, change when the acceleration changes

its sign. The increase in values of the vertical turbulent intensity component starts before the end of the deceleration period of the horizontal velocity component.

The results obtained from the calculation of the Reynolds stresses in the present study are in good agreement with the results of Sakai et al. [12] for the plunging breaker. They measured the flow velocities of the breaking waves on a bed with a slope of $1:20$, with a wave period of 1.82 s. According to the results, Reynolds stresses reach maximum value when the ensemble-averaged flow decreases. Results obtained from experimental investigations indicate that the Reynolds stresses behave like the turbulent intensities. Figure 4d shows the time variation of non-dimensional Reynolds stresses at a relative depth of 0.131. It can be noticed that during the deceleration period, the value of Reynolds stresses is constant. The rise in the value starts at the beginning of the acceleration period, at $t/T = 0.75$. The maximum value is achieved at $t/T = 0.83$, i.e., at the end of the acceleration phase of the horizontal velocity component.

Comparing values of turbulent quantities in different locations above the surf zone bed, it can be noticed that the peak values of these quantities do not occur at the same time. The peak values are delayed as the bottom is approached. The delay between the maximum values of turbulent intensities and Reynolds stresses are presented in Figs. 3 and 4. Near the trough level at $z/h = 0.525$ the deceleration of the horizontal velocity (Fig. 2c) starts at $t/T = 0.82$ and continues until $t/T = 0.6$. The deceleration of the vertical velocity component starts at $t/T = 0.7$ and ends at $t/T = 0.85$. At $t/T = 0.6$ the rise in the value of the turbulent horizontal intensity starts and it reaches its maximum value at around $t/T = 0.75$. When the maximum acceleration of the horizontal velocity component is reached (at $t/T = 0.72$), the horizontal intensity starts decreasing. During the deceleration period, the horizontal intensity remains almost constant. At $t/T = 0.6$, the first peak in vertical turbulent intensity (Fig. 3d) occurs. The second peak is at $t/T = 0.84$ that corresponds to the phase of the wave where both velocity components are decelerating. The Reynolds stresses (Fig. 4b) at $z/h = 0.525$ show the same trend as the turbulent intensity components. There are two peak values, one at $t/T = 0.6$ and the other at $t/T = 0.75$. In the region close to the bottom, at $z/h = 0.131$ (Figs. 2g and 2h), the velocity profile is different from the upper layers. In points close to the trough level, the horizontal component of velocity reaches its maximum value earlier than in the zone close to the bottom (Fig. 2c). The delay between the levels $z/h = 0.131$ and $z/h = 0.525$ is approximately 0.1 wave periods. This delay can be explained with the speed of the turbulent mixing processes from the free surface towards the bottom. The turbulent intensities in the region near the bottom (Figs. 3g and 3h) show also that these quantities depend on the sign of acceleration. During the accelerating phase of the wave the turbulent fluctuations are pressed down, whereas the intensity of the horizontal component undergoes a rapid rise when

the deceleration phase of the wave starts. Previous investigations with U-tubes in turbulent oscillatory flows have indicated that acceleration damps the turbulent fluctuations and therefore in areas of high accelerations the lowest values of the turbulent intensities can be measured. Deceleration and transition periods are characterized with high values of turbulent intensities. In the region close to the bottom, at $z/h = 0.131$, the flow behaves as a turbulent oscillatory flow, i.e., maximum intensities occur during the deceleration period. For the regions near the trough level the value of turbulent horizontal intensity rises during acceleration phase of the horizontal velocity component. The peak value of horizontal turbulent intensity at the level $z/h = 0.525$ occurs during the plunging phase of the wave. Wave breaking generates an extra source of turbulence near the free surface, that increases the turbulence intensity level. The fact that the layers near the bottom are not affected by the wave generated turbulence is a characteristic feature of the outer surf zone region described already by Peregrin and Svendsen [5]. Figures 3c, 3e, and 3g show that the level of turbulence intensity decreases when moving from the surface towards the bottom. In the vicinity of the bottom, the level rises again. This suggests that there is a contribution of turbulence from the bottom boundary layer.

Hattori and Aono [13] investigated the plunging wave spectrum. These investigations indicate that the power law of the spectra depends on the horizontal and vertical co-ordinate. Their measurements showed that for the horizontal velocity component the spectrum at high frequencies gives a slope between –2 and –3. The present study confirms these findings. In the layers close to the free surface, the turbulent velocity spectrum gives slopes –2 for horizontal (Fig. 7a) and –5/3 for vertical (Fig. 7b) velocities. Near the bottom boundary layer, the horizontal turbulent velocity spectrum (Fig. 7c) gives slope –5/3, and vertical –1.2 (Fig. 7d). Flows having spectrum with the slope –5/3 correspond to the inertial subrange, which means that the Reynolds number is very large. The value of the Reynolds number, necessary for an inertial subrange to exist, has order 10^5 [20]. In the present case the Reynolds number is 1.55×10^5. Figure 7c agrees also with the results by Ting and Kirby [16] who found that the slope of the spectrum for both the horizontal and the vertical component of velocity was equal to –5/3. The value was found not to depend on the location of the measuring point inside the breaking wave.

The horizontal turbulent velocity spectra with a slope –5/3 (Fig. 7c) shows that the situation in the layers close to the bottom is similar to the turbulent shear flows where turbulence is produced by the bottom shear stress. According to [20], if a spectrum in an inertia subrange has a slope –5/3, the energy cascade processes inside the flow are present. Turbulent energy is transferred from large scale eddies to smaller scales. At $z/h = 0.525$ the horizontal turbulent velocity spectrum has a slope –2. It is known that slopes of –5/3 and –2 in turbulence spectra at high frequencies correspond respectively to highly and slowly convective flows.
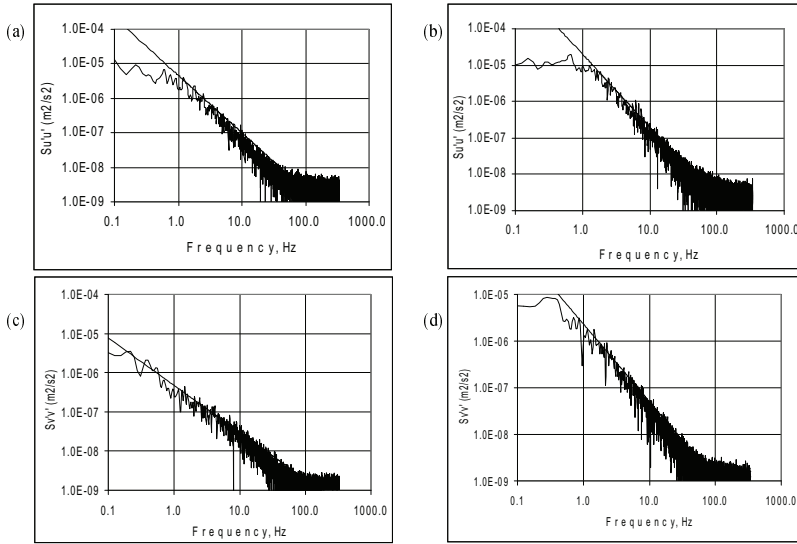
Fig. 7. Velocity spectra: (a), (c) $z/h = 0.131$; (b), (d) $z/h = 0.525$.

It can be concluded from the slopes of the spectra that energy, inserted into the flow during the plunging phase of the wave, is not dissipated near the free surface. It seems that most of the energy is carried away from the surface by large scale eddies. Energy is dissipated in the layers close to the bottom. It can be seen from the graphs presented in Fig. 5 that energy level at $z/h = 0.525$ under the wave trough is approximately two times smaller than at levels $z/h = 0.352$ and $z/h = 0.131$. This also suggests that energy is transported from the surface towards the bottom. Ting and Kirby [16] assumed that if the value of the slope for high frequencies is higher than –5/3, the turbulence cannot attain a fully developed state. These phenomena can be related to the location of the measuring point, i.e., close to the trough of the wave, the flow is dominated by large scale eddies.

The main source of turbulence under the breaking waves is the injection of turbulence at the free surface during the breaking phase. The turbulence characteristics vary with time and space. The source of turbulence moves with wave crests and turbulent energy is dissipated as the wave progresses. It can be concluded that the energy cascade processes cannot attain a fully developed state in the upper layers in the surf zone.

The results of [15] about the velocity field and turbulence in the plunging breaker show that for all the measured values the maximums of these quantities occur approximately at the same time. The authors concluded that reason for the

73

phenomena is strong vertical mixing. The results of the present study do not agree with these findings. It seems that all depicted turbulent quantities depend strongly on the phase of acceleration of the corresponding velocity component. Figures 8a and b compare the results of the present study with the results obtained in [21]. Both figures correspond to the breaking region near the trough level. The results of [21] show that the kinetic energy is maximum when the horizontal velocity component reaches its highest value. However, the values presented in Fig. 8a show that the peak value of the kinetic energy is reached approximately when the flow starts to accelerate. On the levels close to the bottom boundary, no change in the relation between velocity and kinetic energy was found in [21]. Results of the present study indicate that the maximum of the turbulent kinetic energy in the zone close to the bottom is reached when the flow decelerates (Figs. 2g and 5d). This result seems reasonable as the variation of the turbulent kinetic energy in the surf zone is closely related to the change in the values of turbulent intensities. For two-dimensional case the relation is $k = (1.33/2)\langle u'^2 + v'^2 \rangle$. But as discussed earlier, turbulent intensities depend on
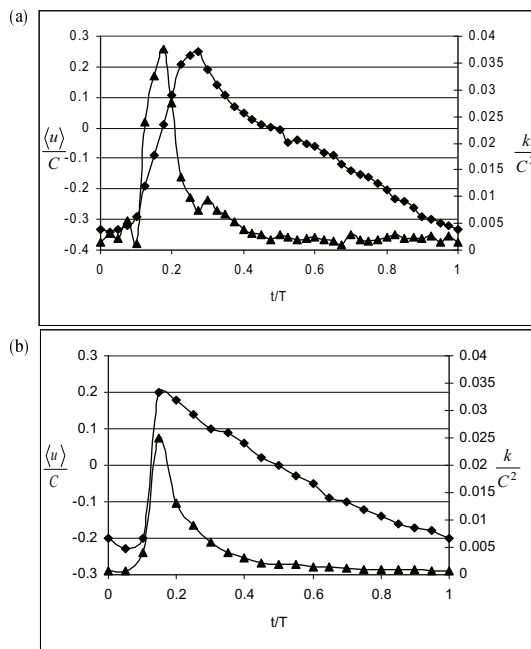
Fig. 8. Ensemble-averaged horizontal velocity ($\blacklozenge$) and kinetic energy ($\blacktriangle$): (a) – results of the present study; (b) – results by Ting and Kirby [21].

the sign of the time derivative of the corresponding velocity component. Data presented in Fig. 3 also suggest that the intensity of the vertical component of velocity depends on both velocity components.

It can be concluded from Fig. 5 that turbulence levels under the breaking wave are high and that the vertical gradients of the kinetic energy are small, except under the overturning wave front at $t/T = 0.7$ (Fig. 5b). The foregoing results show that the turbulent mixing process is strong inside the breaking wave. The energy inserted from the bottom boundary layer can compensate for the energy loss due to dissipation from the top layers to the bottom. The fact that vertical mixing is strong indicates the presence of large-scale turbulent eddies. Svendsen et al. [22] suggested that the main part of production of turbulent kinetic energy takes place in the surface roller and spreading of turbulence is mainly due to convection.

Figure 5 shows that turbulent energy is highest in front of and under the wave crest and it declines after its passage. Turbulence also decreases downward, which indicates that energy is dissipated while convecting downward. This implies that turbulent production in the zone under the trough level and above the bottom boundary layer is small. The energy level increases again near the bottom. This result indicates that most of the turbulent energy production takes place in the surface roller and in the bottom boundary layer. This result agrees with findings by Nadaoka and Kondoh [23]. They measured the velocities in the plunging breaking waves on a surf zone model with a slope $1:20$. They took measurements in and outside the surf zone. According to their results, the main source of turbulence outside the surf zone is the bottom-generated turbulence. This is a typical situation for flat wall turbulence. Inside the surf zone, the main source of production of turbulence is located on the free surface. The turbulence generated on the surface diffuses towards the bottom. The present results show that most of the turbulence is generated when the wave breaks.

In the area near the trough level, at $z/h = 0.525$, the energy flux is directed both shoreward (Fig. 6c) and upward (Fig. 6d) under the wave front. The horizontal flux changes its sign at the instant of plunging. The horizontal gradients under the wave are large. It suggests that advection plays an important role in the distribution of turbulence. It takes about 0.2 wave periods for the energy, containing large scale eddies, to reach the level $z/h = 0.131$. At $t/T = 0.9$, there is a strong current directed offshoreward. The current is so strong that the vertical upward directed energy flux is one order of magnitude smaller than on the levels $z/h = 0.352$ and 0.525. In [21] it was found that the energy flux is directed towards the shore over the whole depth in the surf zone. In the present study the shoreward energy flux in the area near the trough level is approximately two times stronger than that obtained in [21].

The disagreement with the results of [21] can be due to differences in the wave characteristics. In [21], the experiments were performed on a much gentler slope ($1:35$) compared to the present study ($1:17$). The wave period and the ratio of wave height to the water depth was also different. They used waves with

5 s periods with $H/h = 1.24$. These should be compared with 2 s and 0.72 used in the present study. One possible explanation is that with increasing H/h the interaction of the wave with the bottom boundary layer becomes stronger. This implies that the energy transfer increases and the mixing processes become more effective. The latter imposes a damping effect on the turbulent fluctuations.

5. CONCLUSIONS

Two components of the velocity inside a plunging breaking wave were measured with a LDA. Measurements were made at different locations inside the surf zone between the bottom boundary layer and the trough level. Turbulent intensities, Reynolds stresses, turbulent kinetic energy, and energy flux were analysed. The main conclusions of the study are the following.

1. The variation of turbulent intensities and Reynolds stresses during one wave period is significant. This is because turbulence is inserted into the system unevenly and when the wave breaks the turbulence level is high. Turbulence decays rapidly after passage of the wave crest.

2. Turbulent quantities depend on the local value and sign of acceleration.

3. Turbulent kinetic energy varies strongly during one wave cycle; it is highest right before and under the wave crest and decreases rapidly in the wave trough. Most of the energy is produced at the instant when the wave breaks. The energy level decreases towards the bottom.

4. The energy flux in the plunging breaking wave is directed shoreward and changes its direction when the wave plunges into the wave trough. There is a strong shoreward energy flux in the zone near the bottom.

5. Increasing value of H/h causes an increase in turbulent mixing, which imposes an additional source of damping the turbulent fluctuations.

ACKNOWLEDGEMENT

REFERENCES

1. Deigaard, R., Fredsoe, J., and Hedegaard, I. B. Suspended sediment in the surf zone. *J. Water-way Port Ocean Eng. ASCE*, 1986, **112**, 115–128.
2. Takikawa, K., Yamada, F., and Matsumoto, K. Internal characteristics and numerical analysis of plunging breaker on a slope. *Coastal Eng.*, 1997, **31**, 143–161.
3. Lin, P. and Liu, P. L.-F. Turbulent transport, vorticity dynamics and solute mixing under plunging breaking waves in surf zone. *J. Geophys. Res.*, 1998, **103**, 15677–15649.
4. Speziale, C. G., Sarkar, S., and Gatski, T. B. Modelling the pressure strain correlation of turbulence: An invariant dynamical systems approach. *J. Fluid Mech.*, 1991, **227**, 245–272.

76

5. Peregrine, D. H. and Svendsen, I. A. Spilling breakers, bores, hydraulic jumps. In *Proc. 16th Coastal Engineering Conference*, 1978, 540–550.

6. Stieve, M. J. F. Velocity and pressure field of spilling breakers. In *Proc. 17th Coastal Engineering Conference*, 1980, 547–566.

7. Battjes, J. A. and Sakai, T. Velocity field in a steady breaker. In *Proc. 17th Coastal Engineering Conference*, 1980, 499–511.

8. Battjes, J. A. and Sakai, T. Velocity field in a steady breaker. *J. Fluid Mech.*, 1981, **111**, 421–437.

9. Flick, R. E., Guza, A., and Inman, C. Elevation and velocity measurements of laboratory shoaling waves. *J. Geophys. Res.*, 1981, **86**, 4149–4160.

10. Nadaoka, K., Hino, M., and Koyano, Y. Structure of turbulent flow under breaking waves in the surf zone. *J. Fluid Mech.*, 1989, **204**, 359–387.

11. Sakai, T., Inada, Y., and Sandanbata, I. Turbulence generated by wave breaking on the beach. In *Proc. 18th Coastal Engineering Conference*, 1982, 3–21.

12. Sakai, T., Sandanbata, I., and Uchida, M. Reynolds stress in the surf zone. In *Proc. 20th Coastal Engineering Conference*, 1984, 42–53.

13. Hattori, M. and Aono, T. Experimental study on turbulence structures under breaking waves. *Coastal Eng. in Japan*, 1985, **28**, 97–116.

14. Tada, Y., Sakai, T., and Obana, E. Variation of surf zone turbulence in a wave period. In *Proc. 22nd Coastal Engineering Conference*, 1990, 716–728.

15. Ting, F. C. K. and Kirby, J. T. Observation of undertow and turbulence in a laboratory surf zone. *Coastal Eng.*, 1994, **24**, 51–80.

16. Ting, F. C. K. and Kirby, J. T. Dynamics of surf-zone turbulence in a spilling breaker. *Coastal Eng.*, 1996, **27**, 131–160.

17. Shepherd, I. E. Wave measurement methods in laboratory experiments. In *Proc. 3rd International Symposium on Ocean Wave Measurement and Analyses*, 1997.

18. Buhr Hansen, J. and Svendsen, I. A. Laboratory generation of waves of constant form. In *Proc. 14th Coastal Engineering Conference*, 1974, 321–339.

19. Stieve, M. J. F. and Wind, H. J. A study of radiation stress and set-up in the surf zone. *Coastal Eng.*, 1982, **6**, 1–25.

20. Tennekes, H. and Lumely, J. L. *A First Course in Turbulence.* MIT Press, 1972.

21. Ting, F. C. K. and Kirby, J. T. Dynamics of the surf zone turbulence in a strong plunging breaker. *Coastal Eng.*, 1995, **24**, 177–204.

22. Svendsen, I. A., Madsen, P. Å., and Buhr Hansen, J. Wave characteristics in the surf zone. In *Proc. 16th Coastal Engineering Conference*, 1978, 520–539.

23. Nadaoka, K. and Kondoh, T. Laboratory measurements of velocity field structure in the surf zone by LDV. *Coastal Eng. in Japan*, 1982, **25**, 125–145.

LAINE TURBULENTSI UURIMINE SUKELDUVA MURDUMISE KORRAL

Toomas LIIV

Eksperimentaalselt on uuritud kahedimensioonilisi kiiruste välju, mis tekivad sukelduva murdumise korral laine levikul sileda põhjaga katserennis (põhja kalle 1 : 17). Kiiruste välja mõõtmiseks laine põhja piirikihi ja laineoru taseme vahel kasutati laser-Doppleri anemomeetrit. Vaadeldi selliseid lainet iseloomustavaid suurusi nagu turbulentsi intensiivsus, Reynoldsi pinged ja turbulentse kineetilise energia muutumine laine perioodi jooksul. Uuringu tulemusel selgus, et sukelduva murdlaine puhul domineerivad suure amplituudiga turbulentsed struktuurid.

Põhja läheduses sõltuvad ülaltoodud turbulentsi karakteristikud voolu kiirendusest. Voolu aeglustuvas faasis saavutavad turbulentsi karakteristikud maksimaalse väärtuse. Turbulentne kineetiline energia jõuab maksimumväärtuseni laineharja all ja väheneb kiiresti konstantse väärtuseni laineoru all. Turbulents genereeritakse pinnakihis laine murdumise käigus ja see levib difusiooni teel põhja suunas. Samas suunas väheneb ka lokaalse energia tase, kasvades uuesti põhja läheduses tingituna põhja piirikihi turbulentsist. Laine kineetiline energia on suunatud ranna poole laine ülemistes kihtides ja mere poole alumistes kihtides.

Paper II
Toomas Liiv, 2007

An Experimental Investigation of the Oscillatory Boundary
Layer around the Breaking Point

Proceedings of the Estonian Academy of Sciences, Engineering,
13/3, 12pp. 215-233.

An experimental investigation of the oscillatory boundary layer around the breaking point

Toomas Liiv

Tallinn University of Technology, Ehitajate tee 5, 19086 Tallinn, Estonia; toomas@corson.ee

Abstract. The article describes experimental investigation of the turbulent oscillatory boundary layer in the vicinity of the wave breaking point. Measurements were carried out on the inclined bottom in 29 cross-sections, of which 3 are investigated in the current paper. These cross-sections are chosen so that they include the breaking point. The semi-logarithmic plots of dimensionless velocity profiles were plotted on the basis of laser Doppler anemometer measurements. The velocity distributions in breaking waves are essentially different from those observed in steady flows or in oscillatory flows in rectangular *U*-tubes.

Key words: oscillatory flow, breaking wave, boundary layer, velocity distribution.

1. INTRODUCTION

One of the most interesting problems, associated with the modelling of oscillatory flows, is the description of the boundary layer flow field and shear stress during the wave period. Different authors have proposed various empirical solutions and performed numerous experiments that in many cases involve uniform flow over a horizontal bottom. One has to distinguish boundary layers in flows with a variation of the water depth due to the bottom change from the case with the horizontal bottom.

Today there are several quasi-stationary models that describe processes in the boundary layer in case of oscillatory flow over horizontal bottom. These models can roughly be divided into three groups.

The simplest model assumes that the velocity distribution in the boundary layer is logarithmic during the whole period of oscillation, while the boundary layer thickness varies. Viability of these models depends on the roughness of the bottom. The first of these classical models was presented in [1].

The second type of models [2–6] assumes that the flow distribution during the horizontal oscillatory flow resembles the flow distribution in a laminar oscillatory flow. These models are derived to describe the harmonic component of the flow. The velocity distribution in this case is approximated as

$$u(z,t) = A\omega[1 - D_1(z)]e^{i\omega t}, \tag{1}$$

where

$$D_1(z) = \exp\left[-(1+i)\frac{z}{\sqrt{2\nu/\omega}}\right]. \tag{2}$$

Here $u(z,t)$ is the variation of the velocity over the vertical coordinate z at time t, A is the amplitude of motion, ω is frequency, $D_1(z)$ is the velocity defect function for smooth laminar flow and ν is kinematic viscosity. Stokes length, δ_S, for the turbulent flow both for rough and smooth boundaries, is expressed through

$$\delta_S = \sqrt{2\nu/\omega}, \tag{3}$$

which describes the vertical scale of the velocity distribution.

The velocity defect function D_1 can be expressed as

$$D_1 = \exp[-(1+i)(z/z_1)^p]. \tag{4}$$

The parameters z_1 and p are tabulated and depend on the relative roughness and Reynolds number. When the relative roughness is greater than about 0.01, Eq. (1) together with Eq. (4) describe well both turbulent and transitional boundary layers [7].

The third type of models to solve the boundary layer problems are eddy viscosity based models together with the equation of motion

$$\rho\frac{\partial u}{\partial t} = -\frac{\partial p}{\partial x} + \frac{\partial \tau}{\partial z}, \tag{5}$$

where p is pressure, ρ is density, x is horizontal coordinate and τ is the shear stress.

When vertical accelerations are neglible in comparison with the acceleration of gravity and due to that the shear stresses vanish outside the boundary layer, Eq. (5) can be written as

$$\rho\frac{\partial}{\partial t}(u - u_\infty) = \frac{\partial \tau}{\partial z}. \tag{6}$$

Here u_∞ is the velocity infinitely far away from the boundary. Assuming that eddy viscosity ν_t depends only on z, but not on t, shear stresses can be expressed as $\tau = \nu_t(\partial u/\partial z)$ and Eq. (6) can be rewritten as

$$\frac{\partial}{\partial t}(u - u_\infty) = \frac{\partial}{\partial z}\left(v_t \frac{\partial u}{\partial z}\right).\tag{7}$$

Different type of eddy viscosity models have been developed in [8] assuming a three-layer eddy viscosity distribution. But Kajura's model [8] is based on the information, obtained from the steady boundary layer investigations. Simplifying this model and abandoning the inner layer, we obtain the Grant and Madsen model [9,10]

$$v_t = ku^*z, \qquad 0 < z < \infty.\tag{8}$$

Here $k \cong 0.4$ is the von Karman coefficient and u^* is the shear velocity.

All mathematical models of coastal processes need some parameters that allow us to describe the velocity distribution in the boundary layer during the breaking process. Using eddy viscosity models, the velocity distribution in the oscillatory boundary layer was mathematically derived in [8–10]. Brevik [11] proposed another model to determine the two-layer eddy viscosity distribution. He simplified the model by omitting the inner layer. Rodi [12] considers all possible eddy viscosity schemes, including the k–ε scheme, for solving turbulent boundary layer problems. Christensen and Deigaard [13] calculated the flow fields, large eddies and turbulent kinetic energy fields of plunging and spilling breakers.

A model that takes into account also the time dependence of eddy viscosity is described in [14]. Only a few of such models are satisfactory in predicting the magnitude and phase of the simple velocity $u(z, t)$ in case of the horizontal bottom.

The models that describe the processes on the inclined bottom usually also take into account the generation of bottom ripples that are responsible for the generation of vorticity in the bottom boundary layer. Already in 1982, several numerical methods for rounded ripple profiles were published [15,16], which describe shear stress on the wall adequately. Blondeaux and Vittori [17] have presented different methods of vorticity generation and prediction of suspended sediment around these vortices. Different types of eddy viscosity models have been used to describe oscillatory flow on the inclined bottom [18]. Feddersen et al. [19] measured the shear coefficient, bottom roughness and wave breaking on the ocean beach. Wave breaking on the natural beach and its boundary layer has also been investigated [20].

Theoretical results [14] agree well with the measurements [21] of the near bottom velocity in an oscillating water tunnel. Jensen et al. [7,22] measured the turbulent boundary layer in an oscillatory water tunnel at large Reynolds numbers studying smooth and rough bottoms. Flush mounted hot film sensors were used for direct measurements of the bottom velocities.

All mathematical models that describe bottom boundary layer flows use data obtained in oscillatory flows in pressure pipes [21]. Investigation of the flow structure and boundary layer in free surface flows started with the introduction of the laser Doppler anemometer (LDA) technology. First papers were published in

the 1980s [23]. Both vertical and horizontal coordinates of the velocity were measured.

Most of the models of the oscillatory boundary layer make assumptions, based on experimental investigations [21]. Experiments have shown that the velocity infinitely far away from the solid boundary, u_∞, varies sinusoidally in time and the shear stress $\tau(0,t)$ follows the same trend with a slight phase shift (Fig. 1). This phase shift is initiated by the hydrodynamic processes in the wave. The same phase lag was also noticed in [24].

The velocity profiles for different values of ωt that correspond to Fig. 1 are presented in Fig. 2.
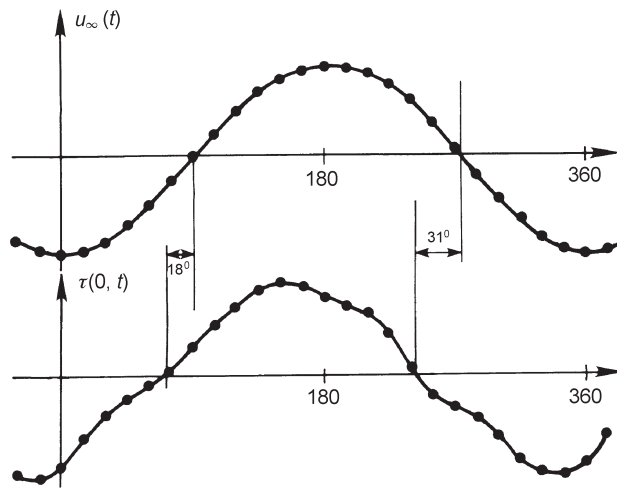
Fig. 1. Time variations of the bed shear stress $\tau(0,t)$ for rough turbulent flow over relatively small roughness elements [1]; horizontal axes present ωt.
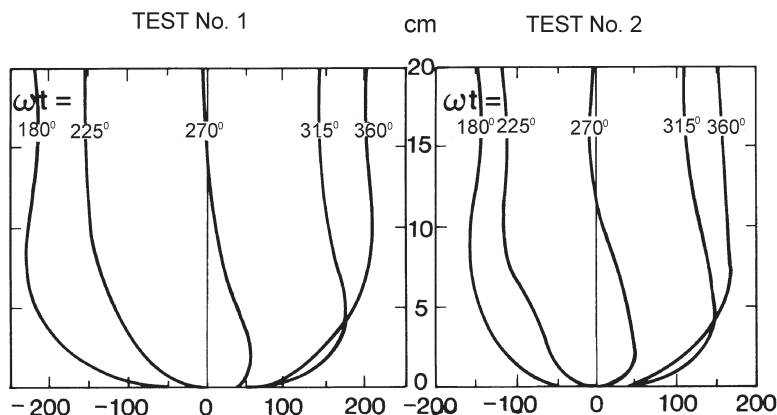
Fig. 2. Instantaneous velocities $u(z,t)$ plotted against elevation from top of the roughness elements. Numbers on the curves refer to the phase ωt of the free stream velocity $A\omega \sin \omega t$ [1].

218

Figure 1 shows that the velocity near the bed turns back before the free stream velocity. The maximum value of the velocity is not on the free surface, but near the bottom, at the level of about ¼ of the stream height.

Most models that calculate the time-dependent flow velocity distribution in the boundary layer use the non-dimensional velocity profiles derived in [7,22]. These experiments were conducted in a U-tube with rectangular cross-section. The free stream velocity changes according to the pattern $A\omega\sin\omega t$. Figure 3 shows the semilog arithmic plot of the mean velocity distribution. The orbital amplitude over the boundary layer was $A = 3.1\,\text{m}$ and the oscillation period $T = 9.72\,\text{s}$. The dimensionless distance y^+ from the bed and the dimensionless velocity u^+ were calculated as

$$y^+ = \frac{z}{\nu}, \qquad u^+ = \frac{\langle u(z,t)\rangle}{\langle u^*(t)\rangle}, \tag{9}$$

where $\langle\cdot\rangle$ is the ensemble average.
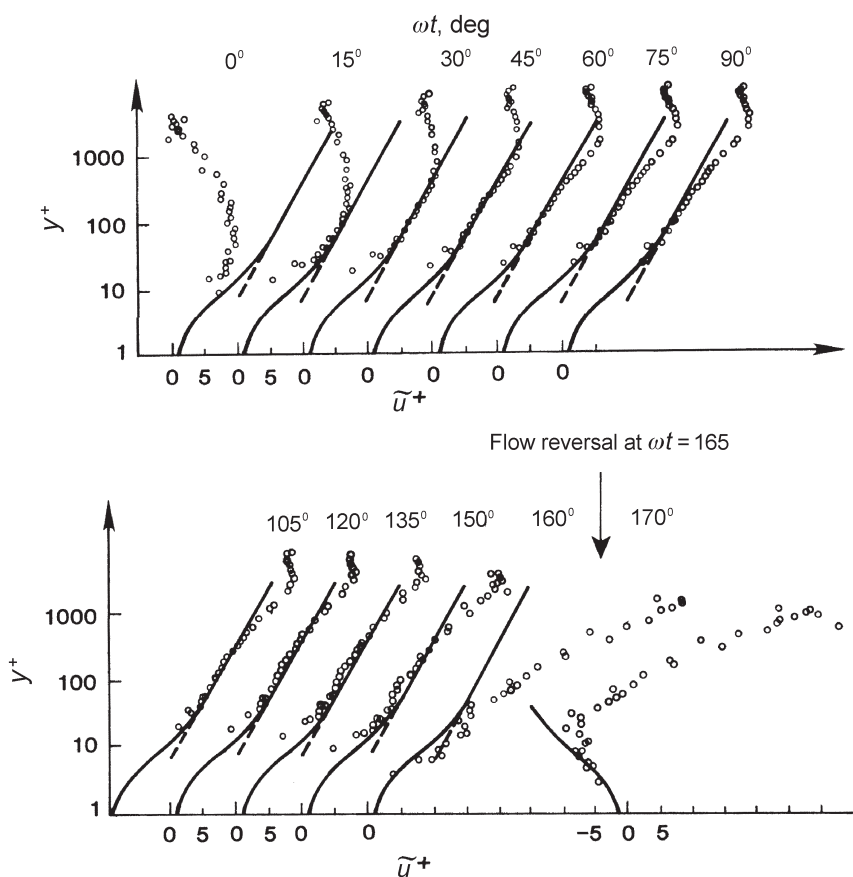
Fig. 3. Dimensionless velocity profiles for smooth turbulent oscillatory flows at different phases of the free stream velocity $A\omega\sin\omega t$ (after [7]).

As the flow is in the boundary layer on the smooth flat surface, these values do not change along the flow.

Here and below u^+ tends to the logarithmic distribution

$$u^+ = (1/k)\ln y^+ + 5 \tag{10}$$

at large values of y^+.

Many experimental works are dedicated to the determination of oscillatory velocity distribution, both for two- and three-dimensional flows and for smooth and rough boundaries, for example [25–32]. Here it is suitable also to mention that systematic investigations of the oscillatory boundary layer flow around the breaking point have been performed and therefore the basis for boundary layer calculations is taken from [6].

Cox et al. [33] investigated shear stresses, measured in the wave flume on the inclined bottom profile. Krstic and Fernando [34] investigated the effect of artificial roughness on the bottom boundary layer. Bryan et al. [35] used Sontek Acoustic Velocimeter to measure wave energy and energy dissipation in the breaking waves on the coast of New Zealand.

The aim of the present article is qualitative comparison of the above described models with experimental results, obtained in the wave flume of the Tallinn University of Technology [36–38].

2. RESULTS ON THE OSCILLATORY BOUNDARY LAYER

The following results on experimental investigation of oscillatory flow were obtained during experiments, described in [24]. The goal was to compare the measured velocity distribution in the boundary layer with velocity distributions, used in mathematical models. The experiments were carried out in a wave flume with a surf zone of a constant slope of 1 to 17. The aim of the investigation was to get an insight into the flow structure and different hydrodynamic processes in the vicinity of the wave breaking point. The velocity field inside the breaking waves was measured with the two-component argon-ion laser Doppler anemometer with an output power of 1.3 W. Forward scatter mode was used throughout the experiments. As the LDA system allows measurement only at one point, the measurements were repeated over the vertical for all 29 profiles and 1852 measuring points. The total number of wave cycles, sampled at each measuring point, was 151. The data processing procedures and main results of investigations are described in [24]. The main attention in the study was focused on the determination of the velocity field inside the breaking wave, especially in the area close to the bottom of the surf zone, where data was collected with the vertical step of 1 mm. The closest measuring point to the bottom was considered to show the bottom shear velocity. The reasoning behind this assumption is that the laser beams, measuring the horizontal velocity component, enter the flume under an angle (Fig. 4). Thus it was possible to project the measuring volume to

the very bottom of the flume. It can also be said that the height of the first measuring point above the bottom is equal to half of the shorter half-axis of the measuring volume. The dimensions of the measuring volume can be calculated as

$$\delta_x = \frac{4F\lambda}{\pi ED_L \cos\dfrac{\theta}{2}}, \quad \delta_z = \frac{4F\lambda}{\pi ED_L \sin\dfrac{\theta}{2}}, \tag{11}$$

where δ_x and δ_z are the lengths of the shorter and longer axis of the measuring volume, respectively, λ is the wavelength of the laser beam, and other notations are shown in Fig. 4. This gives the value of the shorter half-axis 0.12 mm, which gives the same precision as the precision of mounting the hot film probe. The horizontal velocity, measured closest to the bottom, was taken to be the shear velocity u^*.

In order to evaluate the values of the shear velocity, measured in the described way, calibration calculations were made using the method proposed in [39]. This method permits the evaluation of the values of the shear velocity in case of shallow water wave action. The analysis showed that the results achieved were satisfactory and the coincidence of the measurement data with existing information was good.

Figure 5 presents experimentally obtained dimensionless velocity profiles for smooth turbulent oscillatory flow at different wave phases. Only three profiles of the 29 measured ones are presented. In Fig. 5 and further the following notations are used: $\bar{\eta}$ is the average surface elevation, $<U>$ is the ensemble-averaged horizontal velocity, C is the wave phase velocity, x_b is the horizontal coordinate of the breaking point, y_b is the water depth at the breaking point and h_b is the average water depth at the breaking point. The profiles correspond to the profile before breaking, at the breaking point and immediately after breaking. The value of ωt is chosen so that $\omega t = 0$ in the wave trough.

The lines coloured pink, green and dark blue represent the backflow from the beach and the lines coloured black, brown and light blue represent the onflow towards the beach. The flow profiles during backflow resemble the classical steady flow profiles in open channels. During onflow towards the beach the velocity profiles are remarkably different from the steady open channel flow. The measurements show that, during the onflow, the horizontal velocity of the water particles is larger in the near-bed zone and in the layers close to the water surface than in the intermediate layers. This can be explained with the backflow of water that decelerates the water particles in the intermediate zone to the level that it forms almost a homogeneous flow pattern in the given zone.

Figure 6 presents an example of measured time series of the shear velocity u^* before processing; only four of the measured 151 periods are presented. The data is from a profile with coordinates $(x-x_b)/h_b = 0.09$. It can be seen that the value of u^* fluctuates considerably around its mean value. The data processing smoothened the curve and also got rid of drop-outs between $\omega t = 360$ and $\omega t = 720$ deg. Data processing is described in detail in [24].

In order to verify the results presented in Fig. 6, a comparison was made with the results obtained by Jensen et al. [22] with constant temperature anemometer (CTA) in an oscillating U-tube. In case of the Reynolds number $Re = 3.4 \times 10^6$, the shear velocity was found to be $u^* = 0.73$ m/s. For the present case with $Re = 3.0 \times 10^6$, the shear velocity was 0.62 m/s. Since the two velocities are close to each other, this result confirms that the given approach to measuring the shear velocity is adequate. A comparison of the values of τ_0/ρ was also made with the results presented in [28]. The overall shapes of τ_0/ρ agreed well for both experiments, but as the resolution of the graphs in [28] was low, an exact comparison was not possible.

Figures 7 to 9 present the ensemble-averaged variation of non-dimensional shear velocities and the corresponding surface elevations during one wave period in the same cross-sections as in Fig. 5.

The most distinctive feature is that both the shear velocity and the wave height increase towards the breaking point and decrease after breaking.

The analysis of the shear velocity in the boundary layer shows that the obtained results substantially differ from the results obtained in the oscillatory pressure tube [7,22]. This can be explained firstly with the inclined surface of the used experimental setup and secondly with the open boundary on the water surface that allows more adequate representation wave movement.

Figures 10 to 15 present profiles of the dimensionless velocity u^+ at different phases of the wave breaking; $y^+ = h\langle u\rangle/v$ is the dimensionless distance from bed and u^+ is the ratio of local velocity to the friction velocity (see Eq. (9)).

The scale of the axes was selected so that the results are comparable with the results of [7], presented in Fig. 3. As mentioned before, the phase 0 corresponds to the wave trough. The same choice of the wave phase was also used in Fig. 3.

In Figs. 10 to 15, steady flow velocity distributions near the wall are shown for comparison. They are calculated as follows. It is assumed that very near to the wall there is a viscous sublayer with linear velocity distribution

$$\frac{u}{u_*} = \frac{u^* y}{v}. \tag{12}$$

At some distance from the boundary the turbulent velocity profile is described as

$$\frac{u}{u_*} = 2.5\ln\frac{u^* y}{v} + 5.5. \tag{13}$$

Between these two zones there is a transition zone, where

$$3.5 < u^* y/v < 30. \tag{14}$$

Previous investigations have shown that in case of a stationary flow, the dominant stresses for the flow in the viscous sublayer are viscous stresses, whereas in the core region turbulent stresses prevail.
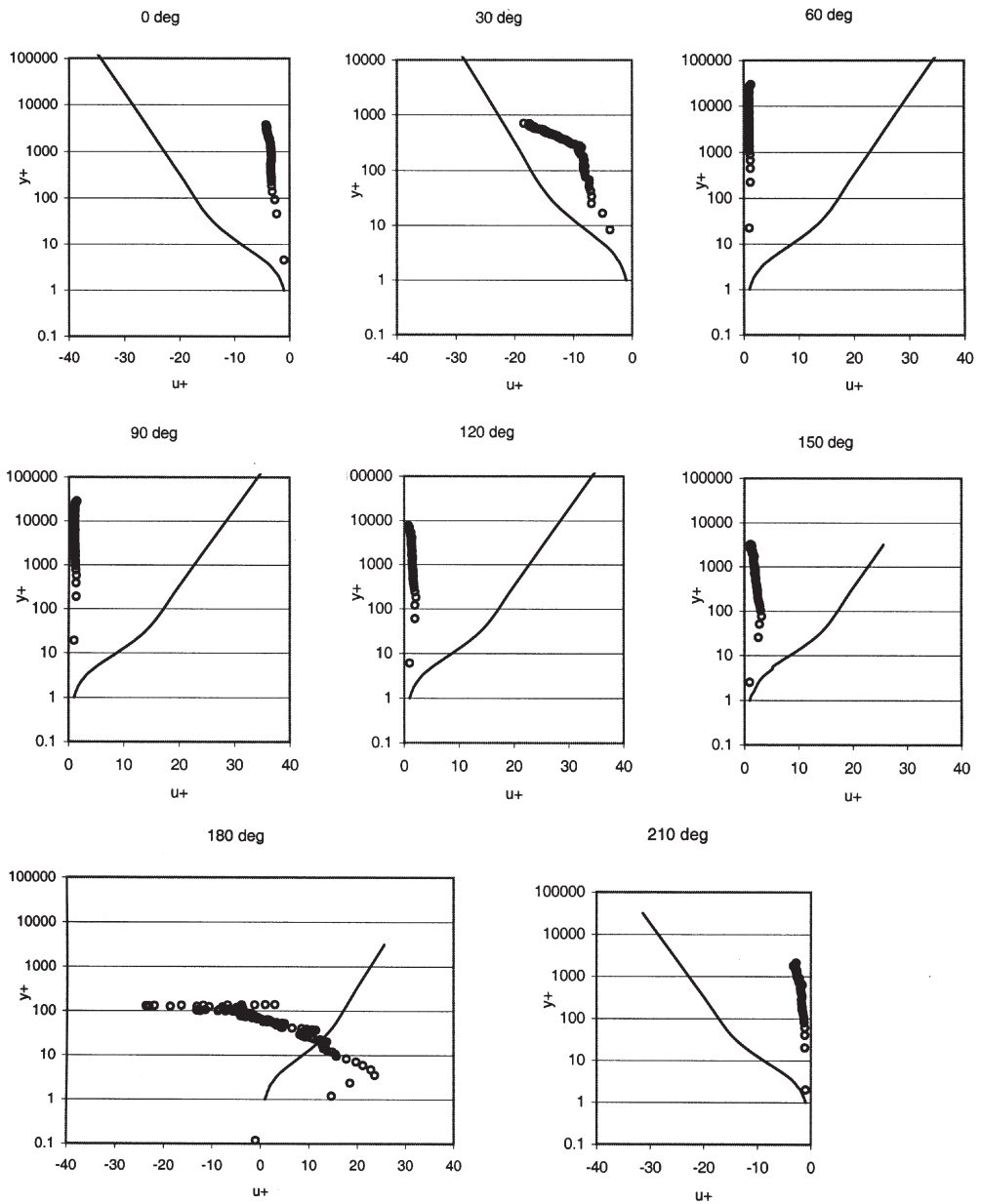
Fig. 10. Dimensionless velocity profiles of $u+$ at different phases of the wave breaking, section $(x - x_b)/h_b = -2.36$; circles show experimental points, solid line indicates the calculated velocity profile in the assumption of the stationary flow.
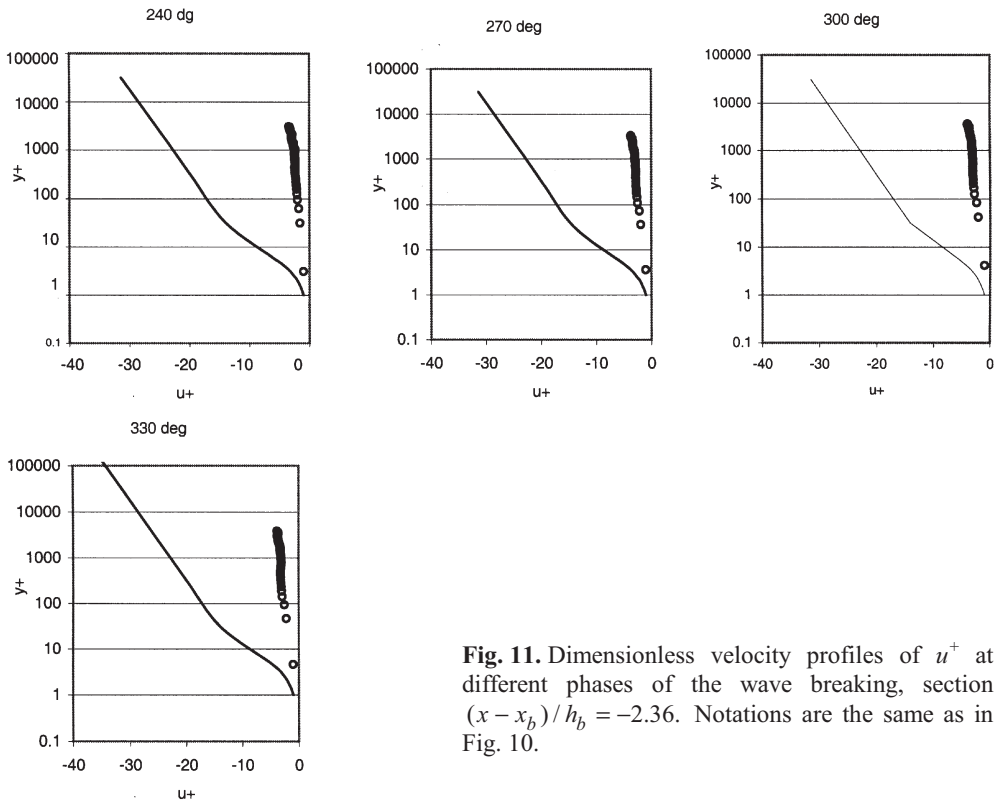
Fig. 11. Dimensionless velocity profiles of u^+ at different phases of the wave breaking, section $(x - x_b)/h_b = -2.36$. Notations are the same as in Fig. 10.

The flow situation in the present experimental run was completely different from the flow in a U-tube with a constant cross-sectional area. The present investigation considers oscillatory flow with a free surface on the inclined bottom. Besides, the flow incorporates relatively rapid change of the cross-sectional area of the flow due to wave breaking, and the generation of two-phase environment (air–water) on the wave crest and after the breaking point over the whole cross-sectional area. In addition to the local inertial forces, the flow is influenced by convective inertial forces.

The profiles of the dimensionless velocity u^+ (Eq. (9)) in Figs. 10 to 15 are presented for different phase angles with a step of 30 deg. Depending on the flow direction, the stationary flow profile (Eqs. (12) and (13)) is plotted either on the right (flow towards the coast) or on the left (flow towards the deep water) side of the vertical axis. Again the value of 0 deg corresponds to the lowest surface elevation in the wave trough. It can be seen from the figures that flow is directed towards the shore between 60 and 180 deg. At the breaking point the flow reversal is somewhat later, at 210 deg. At other phases the flow is directed towards the deep water. The data shows that the value of $y^+ = y^+(u^+)$ changes only a little both for $(x - x_b)/h_b = -2.36$ and $(x - x_b)/h_b = 0.09$. The only exceptions are flow reversals at 15 and 90 deg for $(x - x_b)/h_b = -2.36$ and also at 15 and 105 deg for $(x - x_b)/h_b = 0.09$.
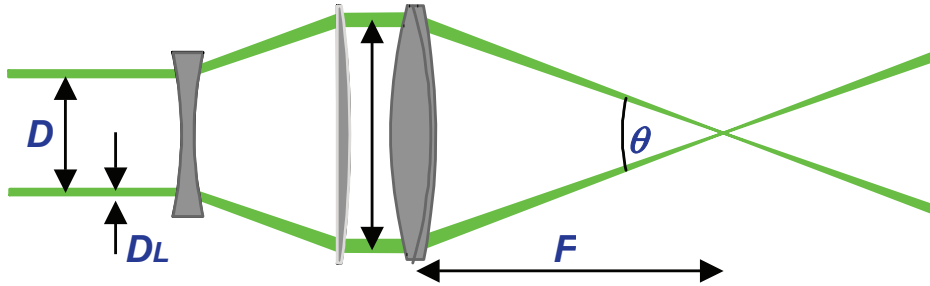
Fig. 4. Measurement scheme.

(a)   (b)   (c)
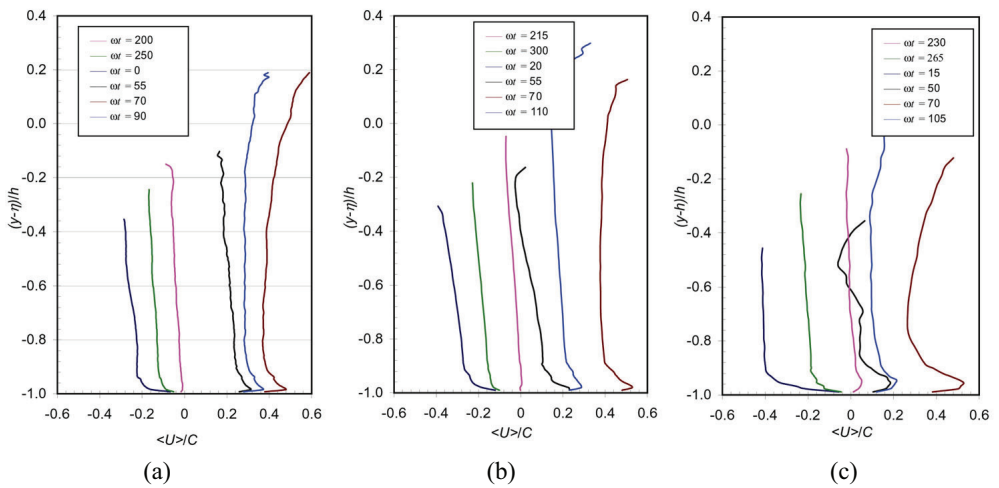
Fig. 5. Dimensionless velocity profiles at different wave phases: (a) – $(x - x_b)/h_b = -2.36$; (b) – $(x - x_b)/h_b = 0.09$; (c) – $(x - x_b)/h_b = 2.17$.
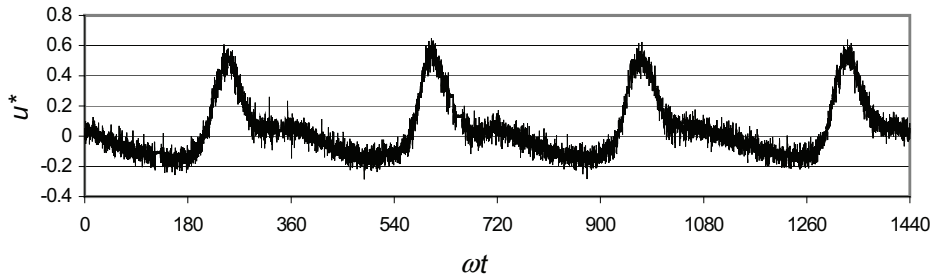
Fig. 6. Measured time series of the shear velocity before data processing.
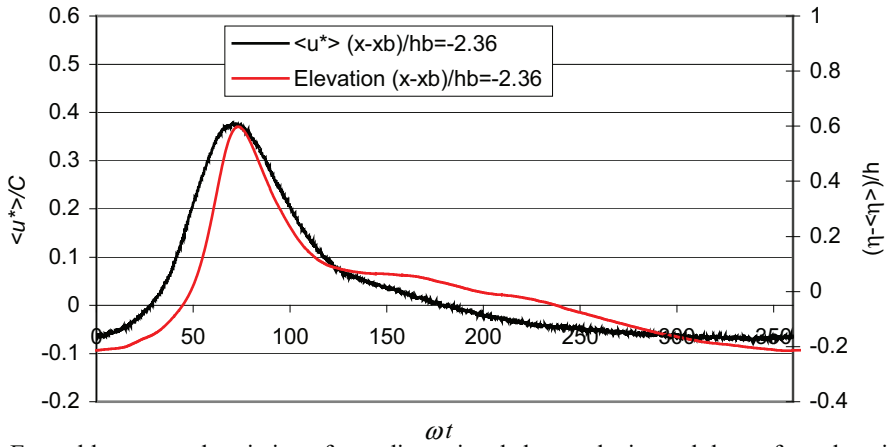
Fig. 7. Ensemble-averaged variation of non-dimensional shear velocity and the surface elevation at $(x - x_b)/h_b = -2.36$.
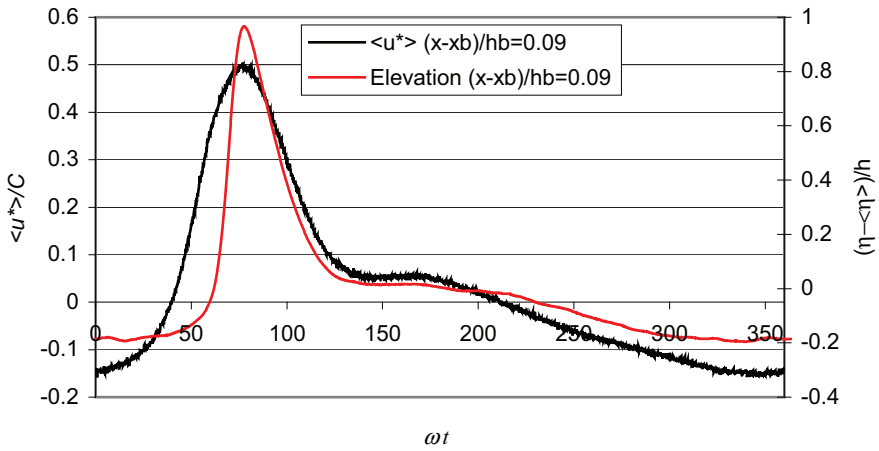
Fig. 8. Ensemble-averaged variation of non-dimensional shear velocity and the surface elevation at $(x - x_b)/h_b = 0.09$.
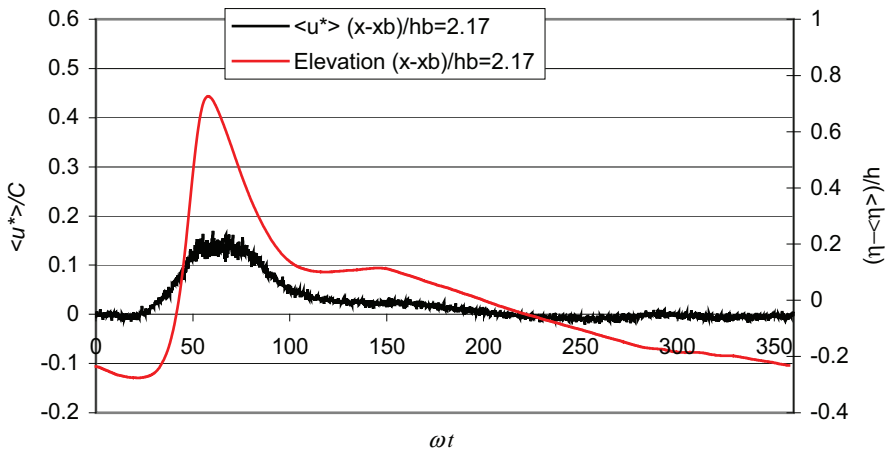
Fig. 9. Ensemble averaged variation of non-dimensional shear velocity and the surface elevation at $(x - x_b)/h_b = 2.17$.
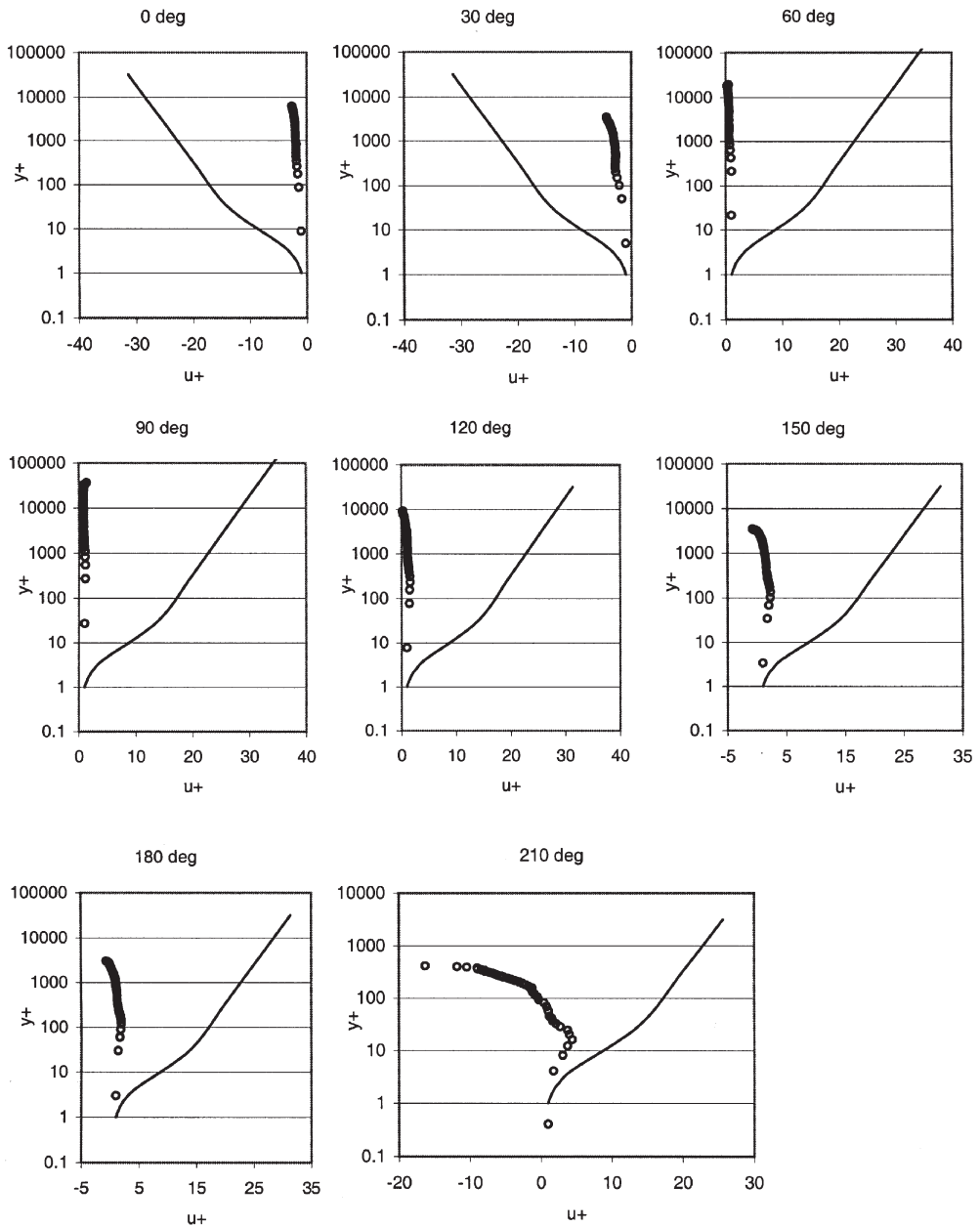
Fig. 12. Dimensionless velocity profiles of $u+$ at different phases of the wave breaking, section $(x - x_b)/h_b = 0.09$. Notations are the same as in Fig. 10.

The experimental results prove that the flow reversal starts at the top of the water column and spreads gradually downwards to the bottom. This phenomenon is best illustrated in Fig. 10 at 90 deg, where the onflow in the wave crest meets the backflow on the bottom. The velocity profiles are almost uniform in Figs. 10 to 13, except for the wave phases at which the flow reverses. Close inspection of

227
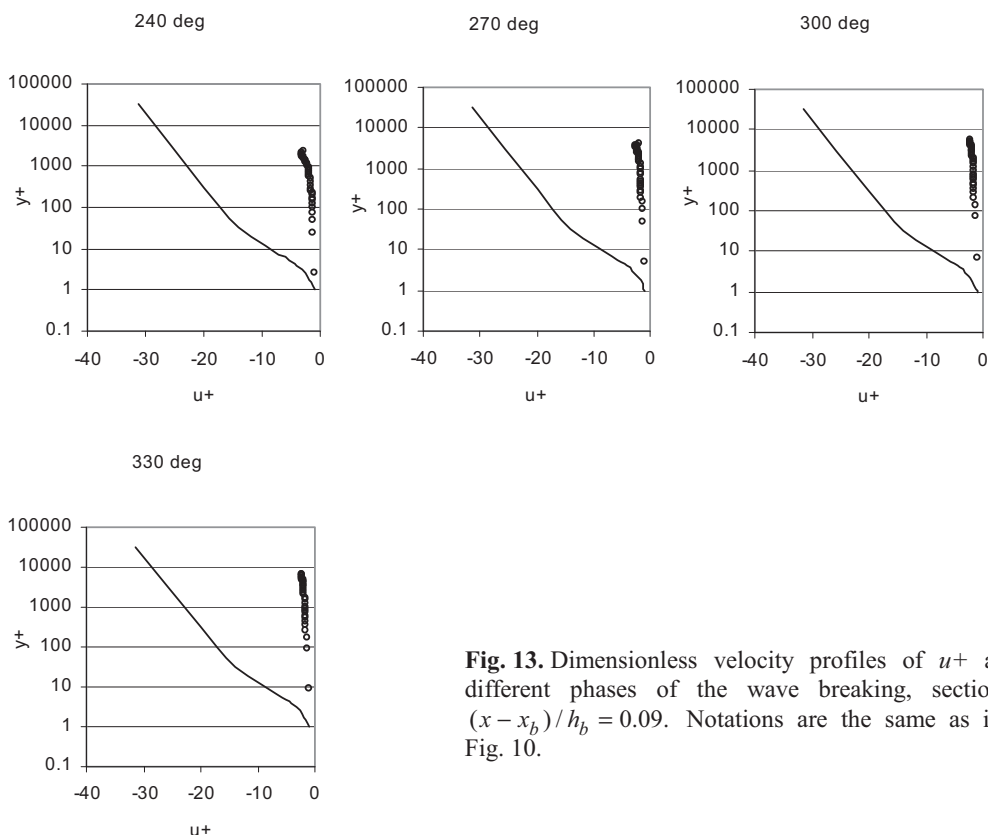
Fig. 13. Dimensionless velocity profiles of $u+$ at different phases of the wave breaking, section $(x - x_b)/h_b = 0.09$. Notations are the same as in Fig. 10.

the values of u^+ reveals that it varies between 1 and 2 during the flow towards the shoreline and between 1 and 3.5 during backflow. This suggests that in comparison with the stationary flow, different processes govern the development of the boundary layer flow under breaking waves.

There are two possible agents that may contribute to almost uniform profiles of u^+. Experiments in pressure pipes [40] have shown that during strong local accelerations, the value of u^+ stays constant over the whole cross-section. The ensemble-averaged horizontal accelerations in the present experiment at certain phases of the wave cycle were found to be up to 1.3 times the acceleration due to gravity. This suggests that the acceleration of water particles and the associated local inertia forces keep the dimensionless flow profile uniform. The second agent that contributes to the uniform profile, especially during the flow phases towards the shoreline, is strong mixing processes due to the overturning of the wave crest. The water particles with high values of the momentum are plunged to the bottom and there they transfer their energy to all the particles.

228
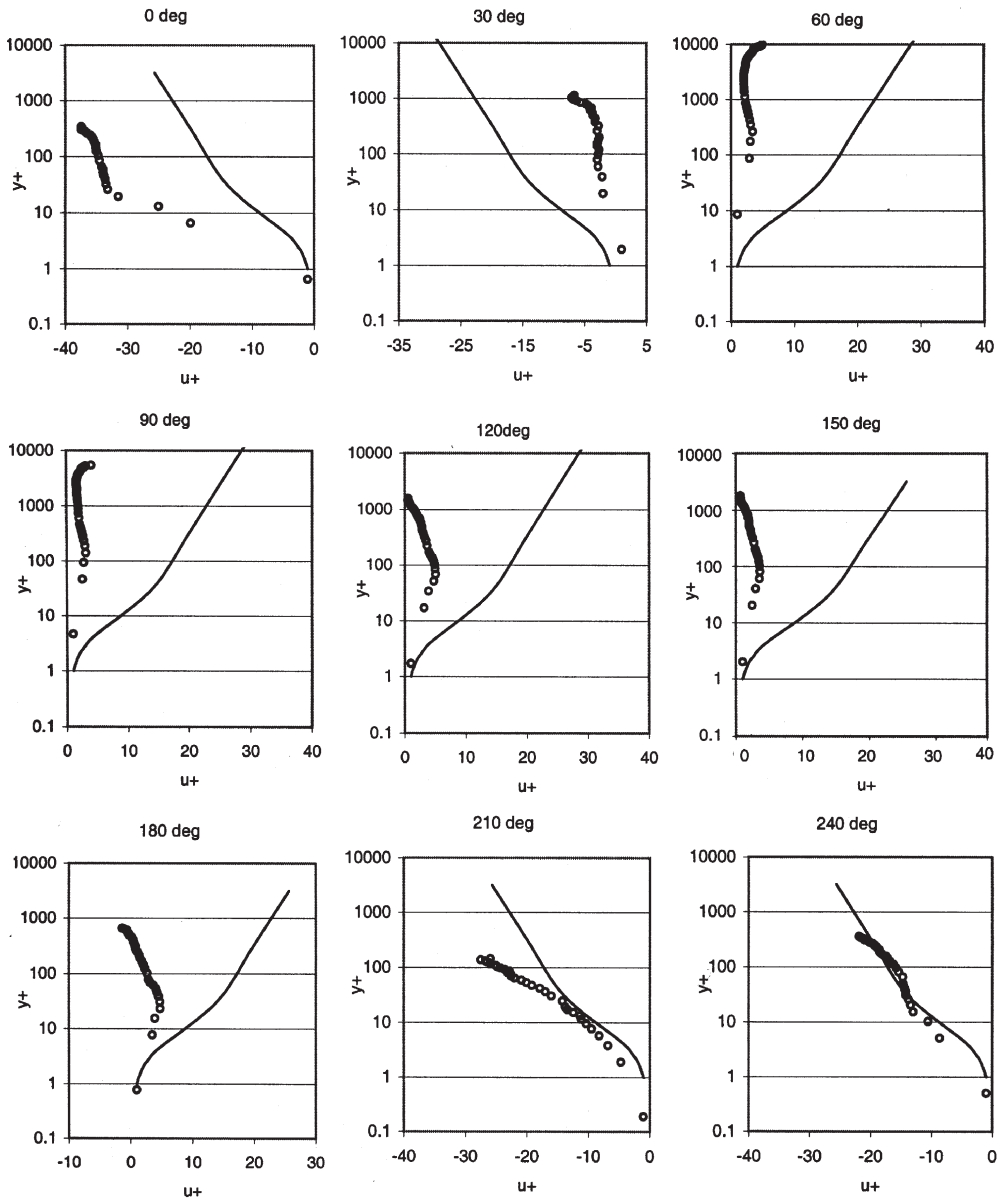
Fig. 14. Dimensionless velocity profiles of $u+$ at different phases of the wave breaking, section $(x - x_b)/h_b = 2.17$. Notations are the same as in Fig. 10.
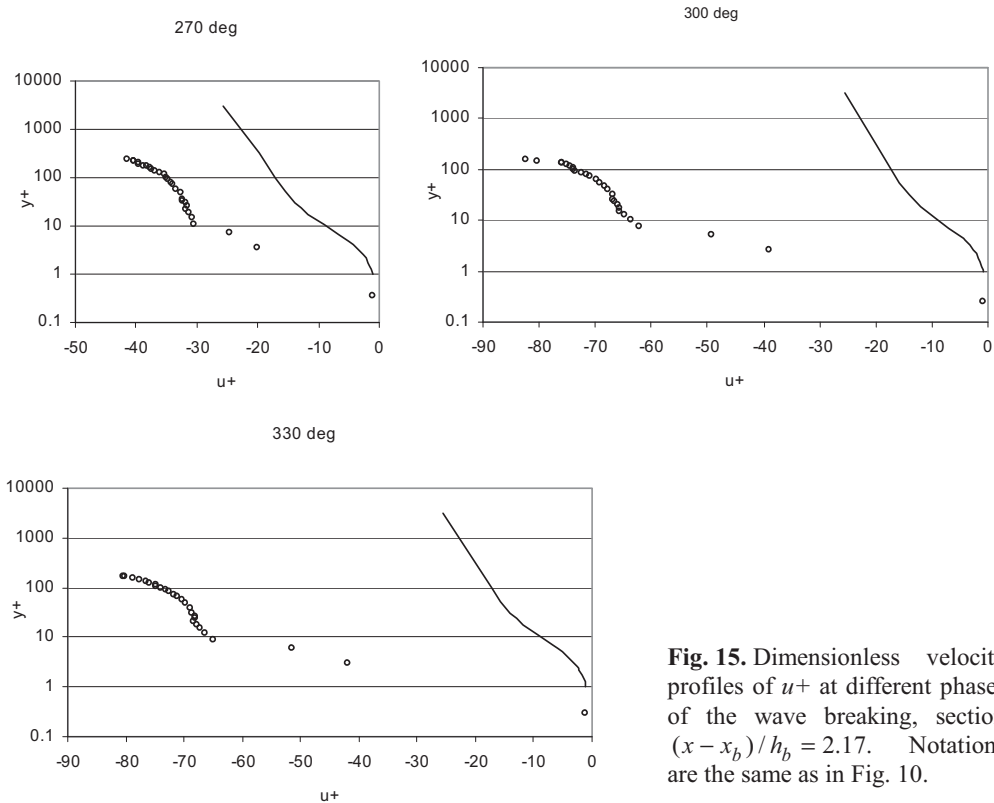
Fig. 15. Dimensionless velocity profiles of $u+$ at different phases of the wave breaking, section $(x - x_b)/h_b = 2.17$. Notations are the same as in Fig. 10.

The situation is totally different in case of the profile after the breaking point at $(x - x_b)/h_b = 2.17$ (Figs. 14 and 15). Although the flow towards and away from the shoreline occurs still at the same wave phases, the behaviour of u^+ is different from the previous cross-sections. During the flow phases towards the shoreline, the dimensionless flow profile is nearly uniform, with the value of u^+ ranging from 1 to 5. It is quite interesting to follow the mixing process. The area of the high value of local velocity in comparison to the friction velocity moves towards the bottom from $y^+ = 10\,000$ at $\omega t = 60°$ to $y^+ = 50$ at $\omega t = 180°$.

The behaviour of the flow during backflow, with ωt varying from 210° to 0°, suggest that the forces, which govern the flow here, are different from the ones that dominated the backflow in the previous investigated profiles. First of all, it must be noted that at $(x - x_b)/h_b = 2.17$ the height of the water column in the approaching wave crest is 2.5 times larger than in the wave trough. This brings along the issues of convective accelerations and flow continuity. These problems were not an issue in the profiles before and during breaking, where the wave crest had a sufficient supply of water in the relatively deep wave trough preceding the wave. The flow behaviour after the flow has reversed at $\omega t = 210°$, resembles very much the stationary open channel flow. The same conclusion can also be made by observing in Fig. 5a the rightmost green line. It resembles very

much the analogous curve for the open channel flow. The next phases are crucial in the development of flow in the current profiles. The approaching wave crest draws the water particles into the crest, generating a strong flow from the relatively shallow wave trough. This phenomenon can be well seen in Fig. 15. The ratio $\langle u(z;t)\rangle \big/ \langle u^*(t)\rangle$ exceeds the "usual" value from 5 up to 40 times.

3. CONCLUSIONS

The present study focused on the investigation of the behaviour of the turbulent oscillatory boundary layer in the oscillatory wave movement in the area immediately before, during and after the breaking process. The measurements of velocities inside the breaking wave were carried out in 29 profiles around the wave breaking point.

As a result of the experiments, the semi-logarithmic plots of the dimensionless velocity distribution $u^+ = \langle u(z;t)\rangle \big/ \langle u^*(t)\rangle$ were calculated for all profiles. The results show that the stationary open channel flow velocity distribution fails to describe the flow under breaking wave although previous investigations have proven that it describes the oscillatory flow in U-shaped flow tunnels relatively well. The two velocity distributions are completely different from each other.

It was also found that the flow pattern after breaking differs from the patterns observed before and during breaking.

ACKNOWLEDGEMENT

REFERENCES

1. Jonsson, I. G. Wave boundary layers and friction factors. In *Proc. 10th International Conference Coastal Engineering*. Tokyo, 1966, 127–148.
2. Kalkanis, G. Turbulent flow near an oscillating wall. *Beach Erosion Board, Technical Memo 97*, 1957.
3. Kalkanis, G. Transportation of bed material due to wave action. *US Army C E R C, Technical Memo 2*, 1964.
4. Sealth, J. F. A. Turbulent oscillatory flow over rough beds. *J. Fluid Mech.*, 1987, **182**, 369–409.
5. Nielsen, P. On the structure of oscillatory boundary layers. *Coastal Eng.*, 1985, **9**, 261–276.
6. Nielsen, P. *Coastal Bottom Boundary Layers and Sediment Transport*. World Scientific, New Jersey, London, 2005.
7. Jensen, B. L. Experimental investigation of turbulent oscillatory boundary layers. Series Paper 45, Institute of Hydrodynamics and Hydraulic Engineering (ISVA), Technical University of Denmark, 1989.
8. Kaijura, K. A model of the bottom boundary layer in water waves. *Bull. Earthquake Res. Inst.*, 1968, **46**, 75–123.
9. Grant, W. D. and Madsen, O. S. Combined wave and current interaction with a rough bottom. *J. Geophys. Res.*, 1979, **87**, 469–481.

10. Grant, W. D. and Madsen, O. S. Movable bed roughness in unsteady oscillatory flow. *J. Geophys. Res.*, 1982, **87**, 469–481.

11. Brevik, I. Oscillatory rough turbulent boundary layers. *J. Waterway Port Coastal Ocean Division, ASCE*, 1981, **107**, 175–188.

12. Rodi, W. *Turbulence Models and Their Application in Hydraulics*. International Association for Hydraulic Research, Delft, 1980.

13. Christensen, E. D. and Deigaard, R. Large eddy simulation of breaking waves. *Coastal Eng.*, 2001, **42**, 53–86.

14. Trowbridge, J. and Madsen, O. S. Turbulent wave boundary layers, I. Model formulation and first order solution. *J. Geophys. Res.*, 1984, **89**, 7989–7997.

15. Sealth, J. F. A. Velocities and shear stresses in wave-current flows. *J. Geophys. Res.*, 1991, **96**, 15237–15244.

16. Sealth, J. F. A. The suspension of sand by waves. *J. Hydraulic Res.*, 1982, **20**, 439–452.

17. Blondeaux, P. and Vittori, G. Oscillatory flow and sediment motion over a rippled bed. In *Proc. 22nd International Conference Coastal Engineering*. Delft, 1990, 2186–2199.

18. Xiuying Xing, M. E. Wave bottom boundary layer physics and bed load sediment transport in nearshore. Master Thesis, The Ohio State University, 2004.

19. Feddersen, F., Gallagher, E. L., Elgar, S. and Guza, R. T. The drag coefficient, bottom roughness, and wave breaking in the nearshore. *Coastal Eng.*, 2003, **48**, 189–195.

20. Trowbridge, J. H. and Agrawal, Y. C. Glimpses of a wave boundary layer. *J. Geophys. Res.*, 1995, **100**, 729–743.

21. Jonsson, I. G. and Carlsen, N. A. Experimental and theoretical investigations in an oscillatory turbulent boundary layer. *J. Hydraulic Res.*, 1976, **14**, 45–60.

22. Jensen, B. L., Sumer, B. M. and Fredsoe, J. Turbulent oscillatory boundary layers at high Reynolds numbers. *J. Fluid Mech.*, 1989, **206**, 265–297.

23. Stieve, M. J. F. Velocity and pressure field of spilling breakers. *Coastal Eng.*, 1980, **25**, 547–566.

24. Liiv, T. and Lagemaa, P. The variation of the velocity and turbulent kinetic energy field in the wave in the vicinity of the breaking point. Forthcoming.

25. Nadaoka, K. and Kondoh, T. Laboratory measurements of velocity field structure in the surf zone by LDV. *Coastal Eng. Japan*, 1982, **25**, 125–145.

26. Lin, P. and Liu, P. L.-F. Turbulence transport, vorticity dynamics and solute mixing under plunging breaking waves in surf zone. *J. Geophys. Res.*, 1998, **103**, 15677–15694.

27. Pedersen, C., Deigaard, R. and Sutherland, J. Measurements of the vertical correlation in turbulence under broken waves. *Coastal Eng.*, 1998, **35**, 231–249.

28. Arnskov, M. M., Fredsoe, J. and Sumer, B. M. Bed shear stress measurements over smooth bed in three dimensional wave-current motion. *Coastal Eng.*, 1993, **20**, 277–316.

29. Stansell, P. Experimental investigation of wave breaking criteria based on wave phase speeds. *J. Phys. Oceanogr.*, 2002, **32**, 1269–1283.

30. Rogers, B. D. and Dalrymple, R. A. SPH modelling of breaking waves. In *Proc. 29th International Conference Coastal Engineering*. Lisbon, 2004, 1147–1157.

31. Liu, P. C. and Babanin, A. V. Using wavelet spectrum analysis to resolve breaking events in the wind wave time series. *Ann. Geophys.*, 2004, **22**, 3335–3345.

32. Sugihara, Y., Tsumori, H. and Takasaki, A. Experimental investigation of turbulent boundary layer beneath a wind-driven surface. In *Proc. 37th International Liege Colloquium on Ocean Dynamics*. Liege, 2005.

33. Cox, D. T., Kobayashi, N. and Okayasu, A. Bottom shear stress in the surf-zone. *J. Geophys. Res.*, 1996, **101**, 337–348.

34. Krstic, R. V. and Fernando, H. J. S. The nature of rough-wall oscillatory boundary layers. *J. Hydraulic Res.*, 2001, **39**, 655–666.

35. Bryan, K. R., Black, K. P. and Gorman, R. M. Spectral estimates of dissipation rate within and near the surf zone. *J. Phys. Oceanogr.*, 2003, **33**, 979–993.

36. Liiv, T. An experimental investigation of the breaking wave characteristics in coastal regions. In *Proc. International Conference on Coastal and Port Engineering in Developing Countries, COPEDEC IV*. Rio de Janeiro, 1995, vol. 3, 2334–2343.

37. Liiv, T. Investigation of turbulence in a plunging breaker wave. *Proc. Estonian Acad. Sci. Eng.*, 2001, **7**, 58–78.

38. Liiv, U. and Liiv, T. Shear investigations of the breaking waves in the flume. In *Proc. 3rd International Conference on Hydro-Science and -Engineering*. Cottbus, Berlin, 1998, CD-ROM, 12 p.

39. Shin, S. Determination of the shear velocities, the bottom roughness and friction factors. Publications of the Oregon State University, Swash Zone Turbulence Group, Report 2, 2004, 15 p.

40. Liiv, U. Unsteady pipe flow transition to turbulence under constant acceleration. In *Proc. 10th Asian Congress of Fluid Mechanics*. Sri Lanka, 2004, CD-ROM, 7 p.

Ostsilleeruva piirikihi eksperimentaalne uurimine laine murdepunkti ümbruses

Toomas Liiv

Lainetusega kaasneva ostsilleeruva voolamise modelleerimisel on üheks tähtsamaks ja suurt praktilist huvi pakkuvaks probleemiks piirikihis tekkivate kiirusväljade muutuste kirjeldamine laineperioodi jooksul. Läbi aegade on selle küsimuse lahendamiseks välja töötatud mitmesuguseid matemaatilisi mudeleid ja teostatud hulgaliselt katseid, mis enamikul juhtudel on aga seotud horisontaalse põhjaga ühtlase voolamisega. Artiklis on kirjeldatud ostsilleeruva piirikihi eskperimentaalse uurimise tulemusi looduslikke olusid modelleerival sileda-põhjalisel kaldpinnal laine murdepunkti ümbruses.

The variation of the velocity and turbulent kinetic energy field in the wave in the vicinity of the breaking point

Toomas Liiv[a] and Priidik Lagemaa[b]

[a] Department of Mechanics, Tallinn University of Technology, Ehitajate tee 5, 19086 Tallinn, Estonia; toomas@corson.ee
[b] Marine Systems Institute, Tallinn University of Technology, Akadeemia tee 21, 12618 Tallinn, Estonia; priidik26@gmail.com

Abstract. The paper describes experimental investigation of the flow and turbulent kinetic energy under the weakly plunging breaking wave in the outer surf zone. Experiments for the present study were carried out on a surf zone model with a constant slope of $1:17$ in the vicinity of the wave breaking point. Experimental results show that the kinetic energy is largest under the wave crest and decreases rapidly after the wave crest has passed. Visualization of the flow proved that the velocity profile during backflow phases resembles the steady open channel flow, but during the onflow phases the velocity profile is unlike any other flow situation.

Key words: breaking wave, breaking point, turbulence, kinetic energy field.

1. INTRODUCTION

Experimental investigations of the processes that govern the behaviour of sediments and waves in the surf zone have lasted decades. The first investigations concentrated on the measurements of the free surface of the surf zone during the wave action. The paper [1] paid main attention to the average physical parameters of the wave, whereas the turbulent structure inside the wave was not discussed. From the latter point of view, the real insight into the mechanism of the breaking wave was gained with the introduction of different contact-free measuring techniques like laser Doppler anemometry (LDA) and particle image velocimetry (PIV). Various investigators have used the mentioned systems for measuring velocity fields and turbulent characteristics of the waves. Chang and Liu [2] measured the kinematics of the breaking waves and found that the velocity of the water particles in the wave crest exceeded the wave phase velocity

for 1.7 times. This phenomenon is even more complicated in areas of high entrainment during the breaking process.

With increasing knowledge on the breaking process, mathematicians have proposed several mathematical models to describe it. A common problem is that for accurate representation of the physical phenomenon, the model equations have to contain non-linear terms and therefore there is a necessity to use empirical relations that can only be obtained through experiments. The breaking phenomenon is by nature a non-stationary process, but in most cases, due to the lack of information, the data used is obtained from investigations of similar stationary processes. As the information on non-stationary flow is scarce, there is a great need for further experimental investigations.

The most widely used method for the determination of the velocity field and its turbulent characteristics in breaking waves is LDA. The first publication on LDA measurements in the breaking waves was [3]. Nadaoka and Kondoh [4] defined the inner and outer surf zone, based on the measured characteristics of the breaking waves in these regions. The most comprehensive publications until today are [5–7]. The data from these papers has been used by other authors for comparison and measurement verification. Ting and Kirby [6] found that in case of a plunging breaking wave there is an area of high turbulent intensity in front of the wave crest. This area was found to move perpendicular to the coast line.

The advantage of the PIV method is that it enables one to investigate coherent structures inside the flow. In the first published papers on PIV measurements, Haydon et al. [8] used local averaging to determine average velocity and velocity fluctuations, whereas Chang and Liu [9] used ensemble averaging. The shear stresses on the bottom have been mainly measured using constant temperature anemometer (CTA) techniques. The most comprehensive studies of the surf zone are [10] and [11].

In recent years, numerous experiments have been carried out in the surf zone, not only in the laboratory. The measuring instruments, mainly LDA, mechanical profiling systems, acoustic pressure sensors, video cameras, current meters etc are mounted on tripods. Feddersen and Trowbridge [12] measured the wave generated turbulence in the surf zone and developed a model that is able to reproduce the production and dissipation of turbulence during wave breaking. Trowbridge and Agrawal [13] measured the boundary layer of the wave. Their measurements indicate that there is a reduction in variance and the increase in phase relative to the flow outside the boundary layer. Feddersen and Williams [14] measured the distribution of Reynolds stresses [15] and investigated dissipation near the surf zone. Feddersen et al. [16] investigated drag coefficients, bottom roughness and wave breaking in the near shore area during a two-month campaign.

Another widely used method of investigation of the wave breaking process is mathematical modelling. The mathematical models used can generally be divided into three main groups:
1) classical, averaged wave models;
2) Boussinesq wave models;
3) Navier–Stokes model.

The first two groups of models have been relatively well described in the literature [17]. The increase of computer speed during the last decades has led to more intensive use of models, based on Navier–Stokes equations. This has initiated a separate branch of mathematical modelling, computational fluid dynamics (CFD). CFD allows modelling of different flows with utmost complicated flow kinematics, whereas the result of calculations is relatively accurate. The advantage of CFD is its high precision but the main drawback is the necessity of large computer resources.

The method is based on the Navier–Stokes equations that describe the evolution of the momentum of the water volume. The set of equations consists of the continuity equation

$$\frac{\partial u_i}{\partial x_i} = 0, \tag{1}$$

and equations for the components of the momentum as

$$\rho \frac{\partial u_i}{\partial t} + \rho u_j \frac{\partial u_i}{\partial x_j} = -\frac{\partial p}{\partial x_i} + \frac{\partial}{\partial x_j} \mu \left(\frac{\partial u_i}{\partial x_j} + \frac{\partial u_j}{\partial x_i} \right). \tag{2}$$

Here ρ is the fluid density, u_i and u_j are velocity components, p is pressure, μ is dynamic viscosity, t is time, and x_i and x_j are spatial coordinates.

When turbulent fluctuations can be neglected, relatively good results have been achieved in modelling the processes in the wave boundary layer at low Reynolds numbers using direct numerical simulation method (DNS) [17]. Another method for solving Eqs. (1) and (2) is the large eddies simulation (LES) method [18]. The difference of LES from the DNS method is that in LES the numerical grid has a larger step, and eddies with smaller scale than the grid are modelled using specific parametrizations of subgrid-scale processes. DNS and LES methods require good resolution in all three coordinates and this makes both of them very time-consuming in solving most common engineering problems.

Time-averaged Navier–Stokes equations are most commonly solved using the Reynolds-averaged Navier–Stokes equations (RANS) methods. Here the turbulent velocity u components are treated as a sum of purely averaged $\bar{u}$ and fluctuating u' components

$$u = \bar{u} \pm u' \tag{3}$$

of velocity. Substituting (3) into Eq. (2) leads to the RANS equations:

$$\rho \frac{\partial \bar{u}_i}{\partial t} + \rho \bar{u}_j \frac{\partial \bar{u}_i}{\partial x_j} = -\frac{\partial \bar{p}}{\partial x_i} + \frac{\partial}{\partial x_j} \mu \left(\frac{\partial \bar{u}_i}{\partial x_j} + \frac{\partial \bar{u}_j}{\partial x_i} \right) - \frac{\partial}{\partial x_j} \overline{\rho u'_j u'_i}. \tag{4}$$

In order to close the equations, additional information is needed to determine the Reynolds stresses

$$\tau_{ij} = -\overline{\rho u'_j u'_i}. \tag{5}$$

The analysis of the models that are used for closing the RANS equations [17] shows that the problem can be solved using for kinetic energy or turbulent viscosity coefficients that are obtained from empirical relations for stationary flow.

In order to determine the Reynolds stresses, different viscosity models are used. The most common of them are the $k - \varepsilon$ and the $k - \omega$ models, described in [19,20] (k is turbulent kinetic energy, ε is the dissipation rate of turbulent energy and ω is a variable that determines the scale of the turbulence). With relevant boundary conditions, the RANS and $k - \varepsilon$ models have successfully been used in the description of various complicated turbulent flows [21].

From the above it follows that Reynolds stresses and turbulent viscosity play a major role in closing the governing equations of the models that describe the wave breaking in the surf zone. These parameters can be interpreted in a meaningful way only with a background knowledge from experimental investigations.

Several papers describe experimental investigations of the time-dependent velocity fields in the wave breaking zone [22–25]. These investigations have unfortunately been carried out with different initial conditions, thus making it difficult to generalize the results. At the same time, there are practically no investigations on the variation of the turbulent kinetic energy in time and space in the area around the breaking point. This justifies additional experimental investigations in order to obtain more detailed description of the processes inside the breaking wave and more accurate values for the above mentioned viscosity models.

This paper continues previous investigations on wave breaking [26,27]. It focuses on the kinetic energy distribution around the wave breaking point and discusses the mechanics of the energy transport in the wave. The paper also looks into the mechanism of kinetic energy production from the point of view of local accelerations and decelerations. Presented are measurement results, obtained during the wave period, i.e. two-dimensional time-dependent fluctuating turbulent velocity components inside the breaking wave. These results allow more accurate description of the quantities used for closing Eqs. (4) and (5), and the calculation of time-dependent turbulent kinetic energy and eddy viscosity. The results have been obtained in the vicinity of the wave breaking point and thus give additional insight into the processes associated with wave breaking.

2. EXPERIMENTAL SET-UP

The aim of the experiments is the determination of the non-stationary flow field parameters at the wave breaking point and around its immediate vicinity. The experiments were performed in the wave flume of the Tallinn University of Technology to study the variation of the two-dimensional flow fields during the breaking process perpendicular to the shoreline. For this purpose regular waves were generated in the wave flume. Vertical and horizontal velocity components

under the weakly plunging breaking wave were measured with LDA. As a result of measurements in 29 sections at 1852 points along the surf zone slope perpendicular to the shoreline, the time-dependent two-dimensional flow fields were measured.

2.1. Description of the experimental set-up

The wave flume used was 0.6 m wide, 0.6 m deep and 22 m long (Fig. 1). The transparent walls of the flume were made of glass and the bottom was made of vinyl plates. Waves were generated in the section of constant depth of the flume, which was 12.45 m long. The average water depth in the constant depth section was kept equal to 0.3 m. Regular waves were generated with the flap-type wave generator with a constant wave period $T = 2.03$ s. The parameters, describing the breaking wave, are listed in Table 1. In Table 1, h_b is the water depth at the breaking point including the change of water level due to wave set-up, d_b is the still water depth at the breaking point, H_0 is the deep water wave height, L_0 is the deep water wavelength and H_b is the wave height at the breaking point. Before the measurement procedures were initiated, the waves were let to run for 30 min to allow to decrease the reflection-caused second harmonic waves and to establish an adequate wave set-up.

The measurement section was chosen so that it incorporated also the breaking point. Wave breaking was investigated on a surf zone model with constant slope of 1:17. The velocity field inside breaking waves was measured with two-component argon-ion LDA with an output power of 1.3 W. Forward scatter mode was used throughout the experiments.
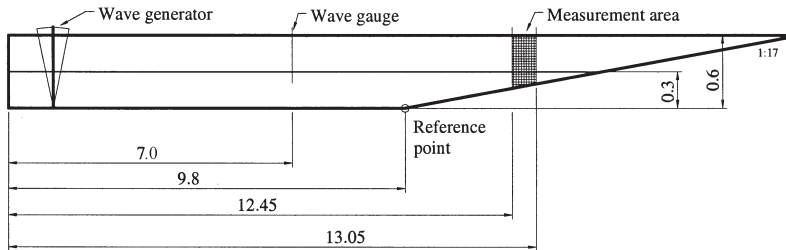
Fig. 1. Wave flume, dimensions in m.

Table 1. Parameters, describing the weak plunging breaker

T, s	h_b, m	d_b, m	x_b, m	H_0, m	H_0/L_0	H_b, m	H_b/d_b
2.0	0.106	0.111	2.90	0.072	0.012	0.118	1.06

As the LDA system allows measurement only at one point, the measurements were repeated over the vertical for all 29 sections. The measuring net had a variable step. Distance between the measuring sections was 1 cm before the breaking point and 3 cm after it. The measuring step along the vertical was 1 mm in the near-bed zone, 3 mm in the intermediate zone and 2 mm in the zone, affected directly by wave action. The lowest point was 0.05 mm above the bottom.

Wave parameters were kept constant throughout the experiments. The wave similarity was controlled with a synchronizing mechanism and analysed with methods described below. The working principle of the synchronizing mechanism is described in [27]. The wave parameters and location of the measuring points are given in Table 2.

Table 2. Location of measuring points and corresponding wave parameters

Cross-section No.	No. of measuring points on the vertical	Distance from the point A x, m	Still water depth d, m	Water depth with wave set-up h, m	Wave celerity C, m/s
29	47	3.21	0.089	0.089	0.933
28	47	3.18	0.091	0.091	0.944
27	48	3.15	0.093	0.093	0.955
26	50	3.12	0.095	0.095	0.964
25	51	3.09	0.098	0.097	0.975
24	51	3.06	0.100	0.099	0.983
23	53	3.03	0.102	0.100	0.990
22	54	3.00	0.104	0.101	0.997
21	55	2.97	0.106	0.102	1.001
20	58	2.94	0.108	0.104	1.010
19	58	2.91	0.110	0.104	1.012
18	61	2.82	0.117	0.114	1.059
17	61	2.81	0.118	0.115	1.064
16	62	2.80	0.118	0.116	1.069
15	62	2.79	0.119	0.117	1.071
14	65	2.78	0.120	0.118	1.077
13	65	2.77	0.120	0.119	1.079
12	64	2.76	0.121	0.119	1.082
11	66	2.75	0.122	0.120	1.086
10	63	2.74	0.123	0.121	1.090
9	67	2.73	0.123	0.121	1.091
8	69	2.72	0.124	0.122	1.094
7	69	2.71	0.125	0.123	1.098
6	70	2.70	0.125	0.124	1.101
5	70	2.69	0.126	0.124	1.104
4	70	2.68	0.127	0.125	1.108
3	69	2.67	0.128	0.126	1.111
2	76	2.66	0.128	0.127	1.115
1	151	2.65	0.129	0.127	1.117

2.2. Procedures

Experimental data from six channels were recorded simultaneously. The channels were connected to the computer through an analogue–digital converter. During experimental runs, horizontal and vertical velocity components, the corresponding signal dropouts, water level variation and signals from the synchronizing mechanism were saved. In order to achieve reliable results during ensemble averaging, data was collected for 151 wave periods ($T = 2.03$ s). The sampling frequency was 1000 Hz, thus for each measuring location $6 \times 306\,530$ data points were recorded. Total number of the measuring points was 1852.

In order to filter the experimental results, dropout signals were used. By measurements with the LDA system, dropouts occur when the measuring volume is not formed by the laser beams or the beam is blocked by a solid object, for instance by a sediment particle. Thus the dropout signal shows if the measured value is true or not.

The use of the signal from the synchronizing mechanism is mostly necessary for the synchronization of the data. The synchronizing mechanism was made of two stainless steel wires. The existence of electric conductivity between the wires showed whether the synchronizing mechanism was in water or not. If the synchronizing mechanism was in water, the signal value was 1 and if out of water, then 0. The location of the synchronizing mechanism was kept constant during the whole experiment. Experimental runs were started when the value of the signal had been 1 for at least 50 ms to avoid false information from possible water sprays.

A common problem with the experiments in the wave flume is how to achieve the generation of waves with a constant period. The shortcoming of the wave flume is usually the generation of reflected waves between the wave generator and the surf zone model. The easiest way to deal with the problem is to perform measurements before the reflected waves occur. In the present case it was impossible, as the number of wave periods in the experimental run was 151. For this reason the reflected wave was taken as part of the wave. In the following we investigate the behaviour of the reflected wave; 1250 wave periods were measured after the start-up of the generator. The result is depicted in Fig. 2. It can be seen from the figure that after the initial stabilization the wave period is approximately 2.02 s. After wave number 500 the wave period stabilizes at 2.03 s. This new wave period stays virtually unchanged for the rest of the working time of the generator. The mean wave period is achieved at wave 1680, i.e. 28 min after starting the wave generator. For this reason, waves were always let run at least 30 min before starting the measurements.

The turbulent flow velocity can be described as the sum of the averaged velocity and the fluctuating component:

$$u_i(t) = \langle u_i(t) \rangle + u_i'(t), \qquad (6)$$

where $u_i(t) = (u(t), v(t), w(t))$ is the measured velocity, $\langle u_i(t) \rangle$ is the averaged velocity and $u_i'(t)$ reflects turbulent fluctuations. As mentioned in the introduc-
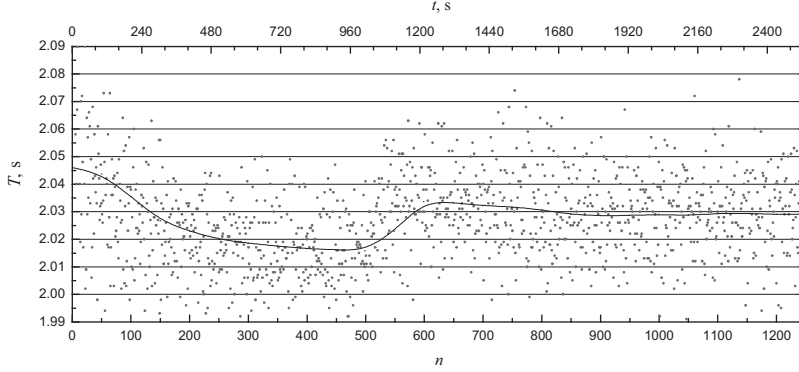
Fig. 2. Stabilization of the wave periods after the start of the wave generator; n – number of the wave.

tion, the most common way of defining the averaged velocity is the ensemble (phase) averaging. The ensemble-averaged velocity is calculated as

$$\langle u_i(t)\rangle = \frac{1}{N}\sum_{k=0}^{N-1} u_i(t+kT), \quad 0 \le t \le T, \tag{7}$$

where N is the number of waves. This method, however, requires very precise repetitions of the phenomena under investigation. Although the wave period stabilized in 30 min, this did not mean that all waves that entered the measuring section had the same period. As seen in Fig. 2, wave periods fluctuate to some extent and have a distribution as shown in Fig. 3 for 12 consequent experimental runs (1812 waves). The vertical axis gives the number of occurrences and the horizontal axes shows the wave period. The deviation from the mean period is only about ±0.03 s that makes only about 1.5% of the whole wave period. So the waves can be considered to be regular.

Since all waves did not have the same period, the usual way of ensemble-averaging was not applicable. Instead, a modified ensemble-averaging method was derived.

The first step is to find the average wave period (2.03 s) and also all individual wave periods of all waves during the experimental run. Then all waves are scaled so that they have the same length. For instance, if the period is longer ($n = 2050$ points, sampling frequency is 1000 Hz, meaning that 2050 points correspond to the wave period 2.05 s), the necessary amount of points are evenly removed from the period so that the period is exactly 2030 points. If the period is shorter than the average, the necessary amount of points is evenly added to the period. All added points are given a dropout value and they are disregarded from the analysis. All very short and long period waves (by 30 points larger or smaller
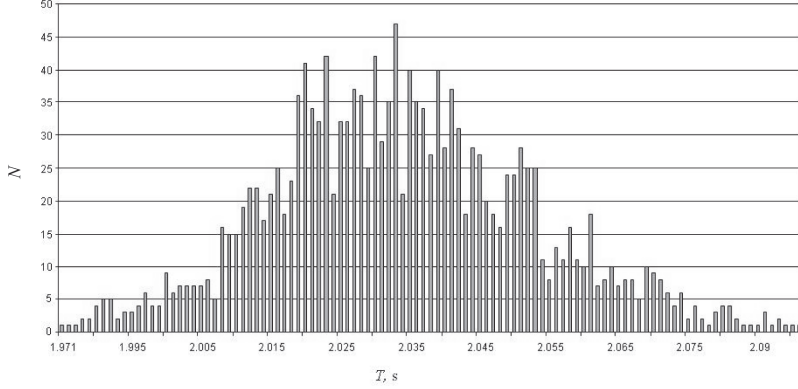
Fig. 3. Spectrum of wave periods for 12 consequent experimental runs.

than the average value) are removed from the analysis. Finally, the ensemble-average velocity is found from the equation

$$\langle u_i(t)\rangle = \begin{cases} \dfrac{1}{N}\sum_{k=0}^{N-1} u_i^*(t+kT_{\mathrm{m}})D_i(t+kT_{\mathrm{m}}), & N_D \geq 10, \\ 0, & N_D < 10, \end{cases} \qquad 0 \leq t \leq T_{\mathrm{m}}, \qquad (8)$$

where $u_i^*(t)$ is the time-scaled velocity, T_{m} is the mean wave period, $D_i(t)$ is the dropout signal and N_D is the actual number of summed values (i.e. points with $D(t)=1$). If the ensemble-averaged value is 0, then the measured data is not reliable. A similar method has also been used in [24].

According to Eq. (6), the turbulent fluctuations can be calculated as

$$u_i'(t) = u_i(t) - \langle u_i(t)\rangle. \tag{9}$$

The classical ensemble-averaging method calculates the turbulent fluctuations as

$$u_i'(t) = \frac{1}{N}\sqrt{\sum_{k=0}^{N-1} (u_i(t+kT) - \langle u_i(t)\rangle)^2}, \qquad 0 \leq t \leq T. \tag{10}$$

Similarly to the averaged velocity, the values of the root-mean square of turbulent fluctuations were found using modified ensemble-averaging

$$\langle u_i(t)\rangle = \begin{cases} \dfrac{1}{N}\sqrt{\sum_{k=0}^{N-1} (u_i^*(t+kT_{\mathrm{m}}) - \langle u_i(t)\rangle)^2 \cdot D_i(t+kT_{\mathrm{m}})}, & N_D \geq 10, \\ 0, & N_D < 10, \end{cases} \qquad 0 \leq t \leq T_{\mathrm{m}}. \tag{11}$$

50

As the LDA system used measured only two components of the velocity, the turbulent kinetic energy was calculated using the method proposed in [28]

$$k(t) = \frac{1.33}{2}(u'^2(t) + v'^2(t)).$$ (12)

2.3. Data processing

The beginning of the coordinate axes is located at the average water level at the beginning of the declined part of the bottom of the flume (Fig. 4). The measured data is presented in non-dimensional form: the horizontal coordinate x_1 is defined as

$$x_1 = \frac{x - x_b}{h_b}.$$ (13)

At the breaking point $x_1 = 0$, $x_1 > 0$ if $x > x_b$ and $x_1 < 0$ if $x < x_b$.
The dimensionless coordinate y_1 is defined as

$$y_1 = \frac{y - \eta}{h},$$ (14)

where η is instantaneous surface elevation. The surface elevation in case of breaking waves is expressed as

$$\eta_1 = \frac{\eta - \bar{\eta}}{h},$$ (15)

where $\bar{\eta}$ is the ensemble-averaged surface elevation.
The normalization of velocity components and of the turbulent kinetic energy is carried out using the local wave phase velocity C:

$$C = \sqrt{gh},$$ (16)

where g is the acceleration due to gravity.
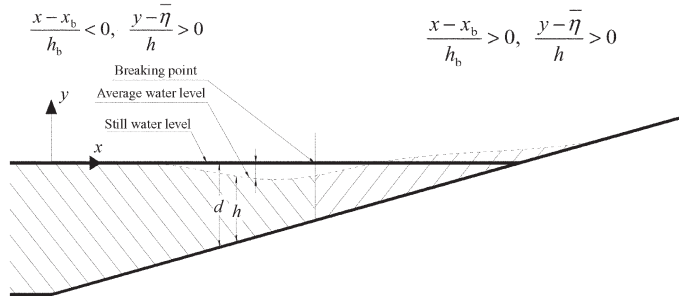
Fig. 4. Definition of flow parameters.

3. EXPERIMENTAL RESULTS

3.1. Time series

Figure 5 shows the surface elevation, ensemble-averaged horizontal and vertical velocity components and turbulent kinetic energy in different cross-sections. The measurements were performed in 29 cross-sections, from which three are chosen to be depicted in the present article: $(x - x_b)/h_b = -2.36$, $(x - x_b)/h_b = 0.09$ and $(x - x_b)/h_b = 2.17$. These cross-sections characterize the situation before breaking, during the initial breaking process and after the breaking has occurred.

The surface elevation is depicted in Figs. 5A to 5C. It can be seen that the surface elevation in different cross-sections is not constant. In comparison with the inner surf zone measurements in [7] and [29], where the value $(\eta - \bar{\eta})/h$ was almost constant, the surface elevation in the outer surf zone changes considerably, especially in the region of initial breaking. Here the maximum surface elevation is equal to the average water depth and minimum surface elevation is 1.5% of the average water depth. This result agrees with [6]. The ratio of the wave height to the water depth H/h is 1.13 that is remarkably larger than the usual value (about 0.8) of the wave breaking parameter.

Figures 5D to 5F show the variation of the ensemble-averaged horizontal velocity component during one wave period. The horizontal velocity component follows the variation of surface elevation. There is a secondary crest after the velocity maximum. This secondary wave is generated by the backflow of water from the shoreline. Similar secondary waves have been described also in [6].

Before the wave breaks, the maximum of the horizontal component reaches about $0.4C$ in all cross-sections. After the crest, this similarity between the cross-sections disappears. The non-dimensional horizontal velocity varies between $0.15C$ and $0.8C$.

Close to the still water level, the horizontal velocity component is zero. This means that at this location no reliable data is available. In the present case it means that the measuring volume was not formed, due to the fact that the laser beams were out of the water in the wave trough. In most of the studies this data is not presented.

Figures 5G to 5I show the variation of the ensemble-averaged vertical velocity component. The maximum value of the vertical velocity is always reached during the maximum acceleration of the horizontal velocity. The maximum of the vertical component moves along the wave crest, in front of it. This is the location, where backflow from the previous wave and the onshore movement of the new wave meet and where water has nowhere else to go than upwards. The maximum acceleration of the horizontal velocity can be explained by the sudden reversal of the flow.

From the experimental data it can be concluded that during the maximum deceleration of the horizontal velocity component the vertical velocity in the upper layers of the water column achieves its minimum value. This result
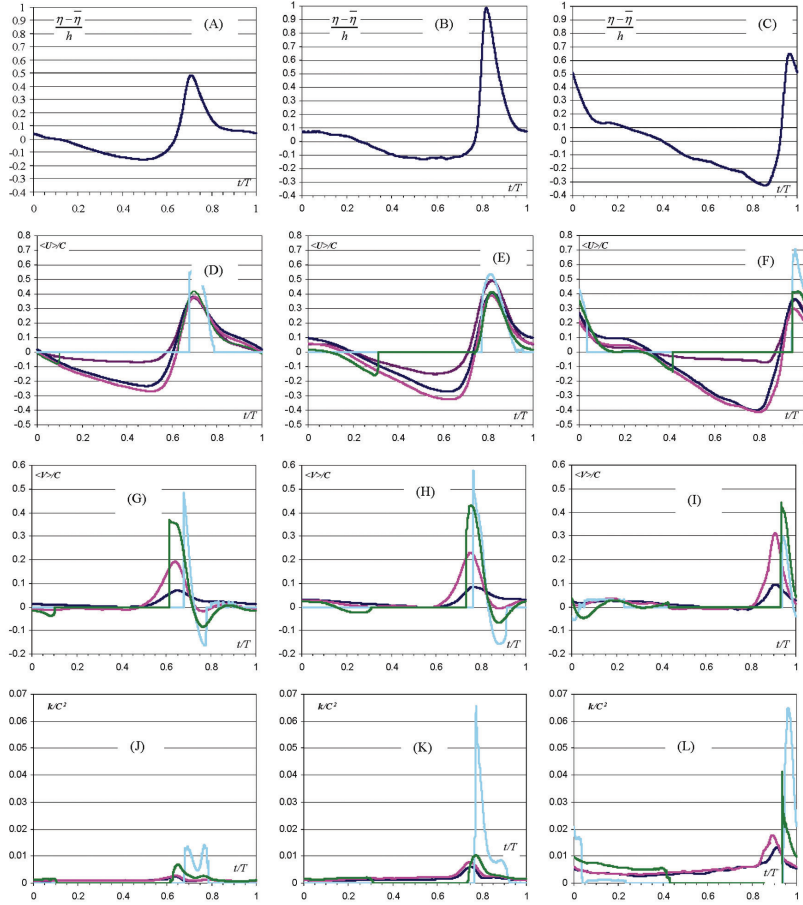
Fig. 5. Surface elevation (A–C), horizontal velocity component (D–F), vertical velocity component (G–I) and turbulent kinetic energy (J–L) in cross-sections $(x - x_b)/h_b = -2.36$ (left column), $(x - x_b)/h_b = 0.09$ (centre column) and $(x - x_b)/h_b = 2.17$ (right column) at the heights:
—— $(y - \bar{\eta})/h = -0.99$, —— $(y - \bar{\eta})/h = -0.89$, —— $(y - \bar{\eta})/h = -0.54$,
—— $(y - \bar{\eta})/h = -0.17$, —— $(y - \bar{\eta})/h = 0.18$.
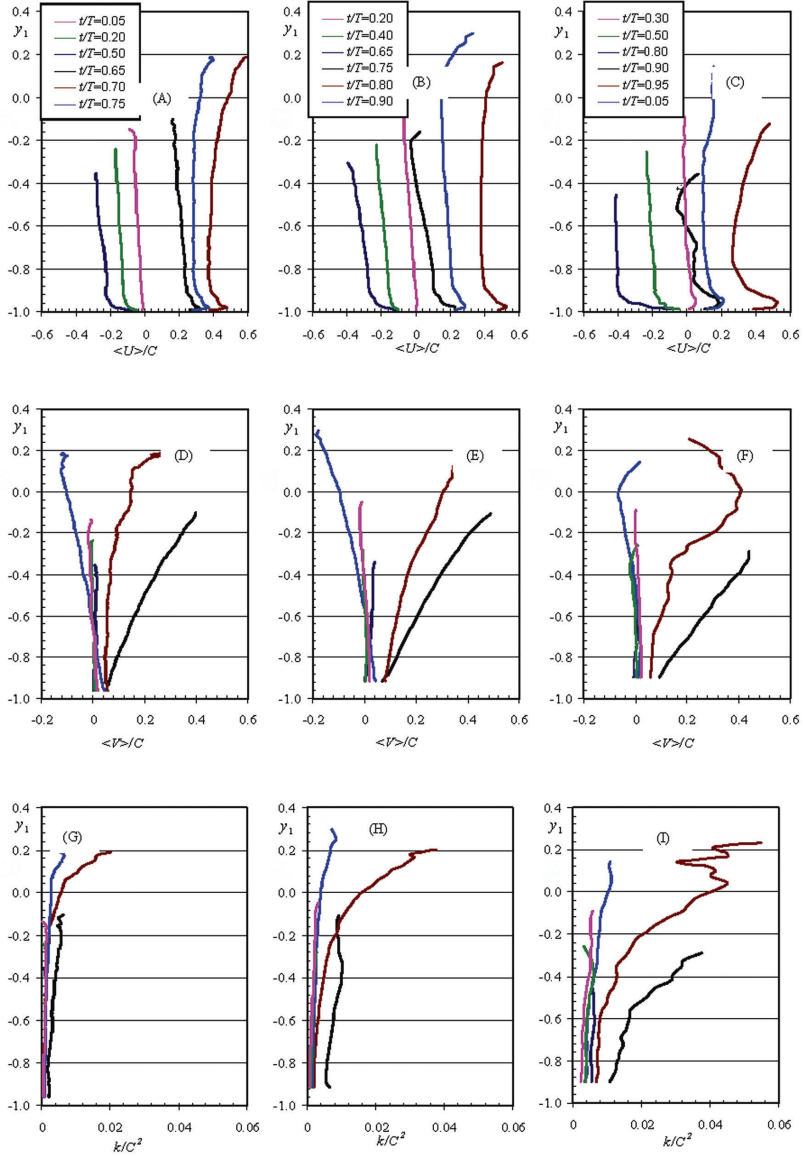
Fig. 6. Ensemble-averaged horizontal (A–C) and vertical (D–F) velocity and turbulent kinetic energy (G–H) profiles; left column: $(x - x_b)/h_b = -2.36$; middle column: $(x - x_b)/h_b = 0.09$; right column: $(x - x_b)/h_b = 2.17$. ,

54

supports the Marker and Cell (MAC) method [30], which has been used to model the processes on the coastline. In MAC method all computational elements are given as markers, which move according to the calculated velocity field.

The maximum value of the vertical component of velocity in the intermediate layers of the water column is about $0.2C$ before the breaking point, which is in good agreement with earlier investigations [6]. Near the still water level the value is about $0.5C$. After the breaking point, during the backflow phase of the wave, the value of the vertical velocity component in all layers approaches zero.

The time series of the turbulent kinetic energy are presented in Figs. 5J to 5L. The kinetic energy has two local peaks. They correspond to local extremes of the vertical velocity component and also to the maximums of the acceleration and deceleration of the horizontal velocity component. While before breaking the energy levels before and after the wave crest are approximately equal, then as the breaking process develops, the kinetic energy precedes the wave crest. This is one of the major differences between spilling and plunging breakers. According to [19], the energy maximum inside the spilling breaker moves behind the wave crest.

Before breaking, the level of turbulent kinetic energy is low. The energy is generated only in the upper layers of the water column, reaching there the level of about $0.015C^2$ under the wave crest. When breaking is initiated, the energy level grows considerably and reaches also the bottom layer. This suggests that the wave front has plunged into the wave crest in front of it. After the breaking point the maximum measured kinetic energy was about $0.65C^2$. It is also interesting to follow the development of the levels of turbulent kinetic energy along the surf zone model. The energy before the wave crest at $(x - x_b)/h_b = -2.36$ and immediately after breaking at $(x - x_b)/h_b = 0.09$ have a value less than about $0.001C^2$. In the third cross-section, at $(x - x_b)/h_b = 2.17$, the level of turbulent kinetic energy before the wave crest has increased nearly by 5 times. In this cross-section large-scale eddies have reached the bottom and the mixing processes have carried the turbulent kinetic energy all over the water column.

3.2. Ensemble-averaged profiles

Figure 6 depicts vertical distributions of the horizontal and vertical ensemble-averaged velocities and turbulent kinetic energy at different moments. Similarly to Fig. 5, the profiles under investigation are located at $(x - x_b)/h_b = -2.36$, $(x - x_b)/h_b = 0.09$ and $(x - x_b)/h_b = 2.17$.

Figures 6A to 6C depict the variation of the horizontal velocity component at different time moments in the three above mentioned profiles. There are two types of lines in the figures. The lines coloured pink, green and dark blue represent the backflow from the beach; lines coloured black, brown and light blue represent the onflow towards the beach. The flow profiles during backflow resemble the classical steady flow profiles in open channels. During onflow towards the beach, the velocity profiles are remarkably different from the steady open channel flow. The measurements show that during the onflow, the horizontal velocity of the

water particles is larger in the near-bed zone and in the layers close to the water surface than in the intermediate layers. This can be explained with the backflow of water that decelerates the water particles in the intermediate zone to such a level that an almost homogeneous flow pattern is formed in the given zone. The Boussinesq type wave models for the beach make the same assumption [31].

The ensemble-averaged distributions of the vertical velocity component are shown in Figs. 6D to 6F. Similarly to the horizontal velocity component, the backflow values of the vertical velocity component resemble open channel flow. During backflow the value is approximately zero. During the wave phases, when the flow is directed towards the shore, the vertical velocity changes linearly from zero at the bottom to about $0.4C$ above the still water level. This means that under the wave crest water is "pulled" into the crest during wave propagation and the shoaling process (brown and black lines). The light blue line represents the phase of the wave when water is intensively flowing out from the wave crest. This results in the increase of the negative (directed towards the bottom) flow velocity. This phenomenon is especially pronounced in the profiles near the breaking point at $(x - x_b)/h_b = 0.09$, where the velocity reaches about $0.2C$. At $(x - x_b)/h_b = 2.17$ this value is more than twice smaller. This suggests that the wave has entered the area of wave setup.

Figures 6G to 6I show the distribution of turbulent kinetic energy. It can be noticed that before breaking (G) the level of kinetic energy is low. There is only a slight increase of turbulent kinetic energy in the wave crest. The next figures (H and I) show how the kinetic energy diffuses towards the bottom layers. This phenomenon becomes first evident under the crest and as the wave progresses also during the backflow phases.

3.3. Variation of the turbulent kinetic energy across the surf zone

In the present study the measured profiles of the turbulent kinetic energy are close enough to give a qualitative picture of its variation over the whole measured area. As mentioned before, the horizontal step between the profiles was 10 mm before the breaking point and 30 mm after it.

Figure 7 gives the time-averaged variation of the turbulent kinetic energy across the surf zone at different non-dimesional heights above the bottom. These values have been obtained during the analysis of turbulent fluctuations using Eq. (12). The analysis of measured data shows that the level of turbulent kinetic energy is increased as we approach the shore. Figure 7 shows clearly that after the wave has plunged into the trough, the level of turbulent kinetic energy increases, especially above the still water level.

The level of the kinetic energy and also turbulence intensity are low until the wave crest plunges. The plunging point is probably characterized by especially high values of turbulence intensity, but due to the high level of air entrainment it is impossible to measure it using LDA techniques. It has been suggested that the intensity of turbulence there is more that ten times higher than in other parts of the wave.
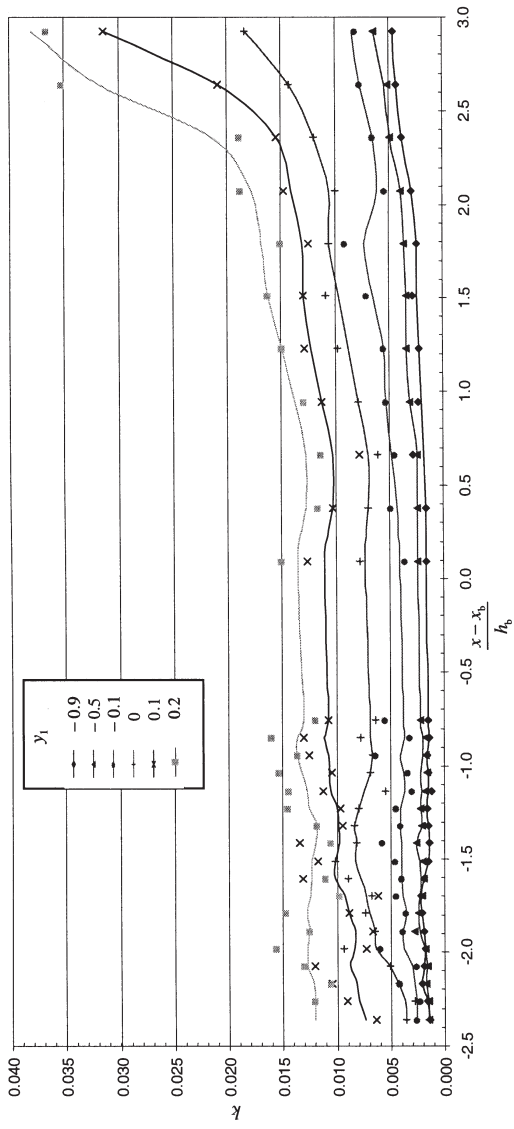
Fig. 7. Time-averaged variation of turbulent kinetic energy perpendicular to the coastline at different heights above the bottom.

57

The development of PIV methods and computer graphics has led to the usage of field graphs in the description of breaking waves [32,33]. The advantage of field graphs in comparison to conventional methods is that it enables one to follow the qualitative nature of the breaking process. The field graphs in the case of LDA measurements are usually not presented as there is not sufficiently data. In the case of the present experimental run, the measured data had a sufficiently high spatial resolution to make it possible to present field graphs.

3.4. Velocity vector and turbulent kinetic energy fields around the breaking point

Figures 8 to 13 present velocity vectors and turbulent kinetic energy fields for the measured area under the breaking wave. As the vertical resolution of measurements is very high, only every third point is depicted. The figures show also the still water level, instantaneous surface profile and the wave flume bottom. In the white area between the surface profile and the coloured kinetic energy plots the measurements did not give reliable data due to high air entrainment or lack of laser beams in the water. In order to get a better understanding of the processes involved, the length scale of the vectors in all the figures is kept the same. Due to this, very low velocities are represented by an arrow that shows the direction of the flow.

At $t/T = 0.4$ and 0.5 there is backflow all over the measuring section. Here the flow resembles very much analogues flows in open channels. The same could be concluded from the flow profiles in Fig. 6. The first signs of the arrival of the wave crest appear at $t/T = 0.6$ when the surface starts to elevate and the magnitude of the vertical component of velocity becomes comparable with the horizontal component. At $t/T = 0.7$, the wave crest has entered the measuring section. At this time moment the process of meeting the flows towards and from the shore can easily be followed. This process eventually results in the increase of the water column in the wave and the breaking of the wave. There is always an area in front of the wave crest, where water particles move towards the surface perpendicular to the wave movement direction. This phenomenon is caused by the collision of the water masses moving towards each other. This movement is more intense near the still water level. Figures 12 and 13 show that the movement of water particles in the upper layers of the water column behind the wave crest is directed slightly downwards, showing that the lowering water surface presses water particles down.

Figure 5 shows that at time moments when vertical movement of water particles precedes the crest, the horizontal component of velocity is zero and it changes the sign.

The obtained velocity fields lead to the conclusion that there is one large-scale vortice under the breaking wave with its vertical dimension approximately equal to the water depth and the horizontal dimension approximately equal to the wave amplitude.
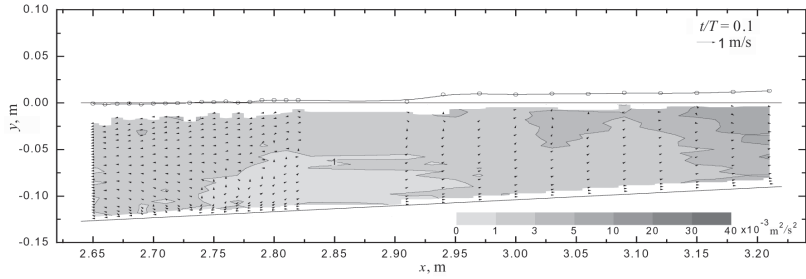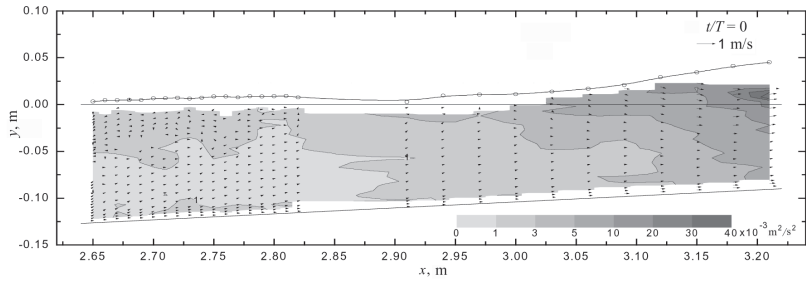
Fig. 8. Turbulent kinetic energy and velocity field at *t/T* = 0.0 and 0.1.
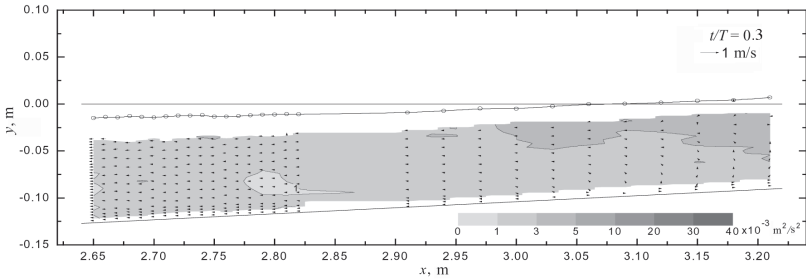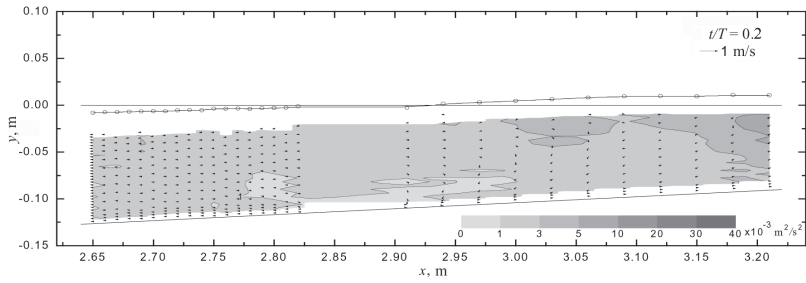
Fig. 9. Turbulent kinetic energy and velocity field at *t/T* = 0.2 and 0.3.
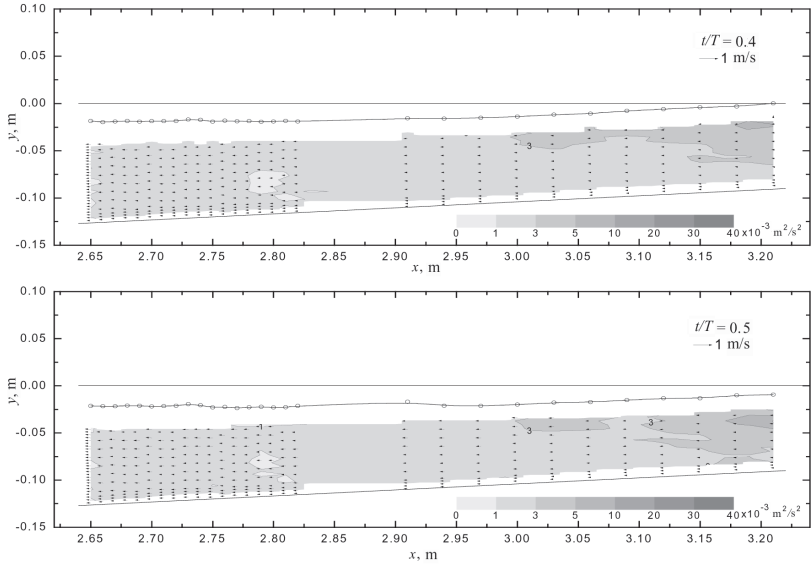
Fig. 10. Turbulent kinetic energy and velocity field at *t/T* = 0.4 and 0.5.
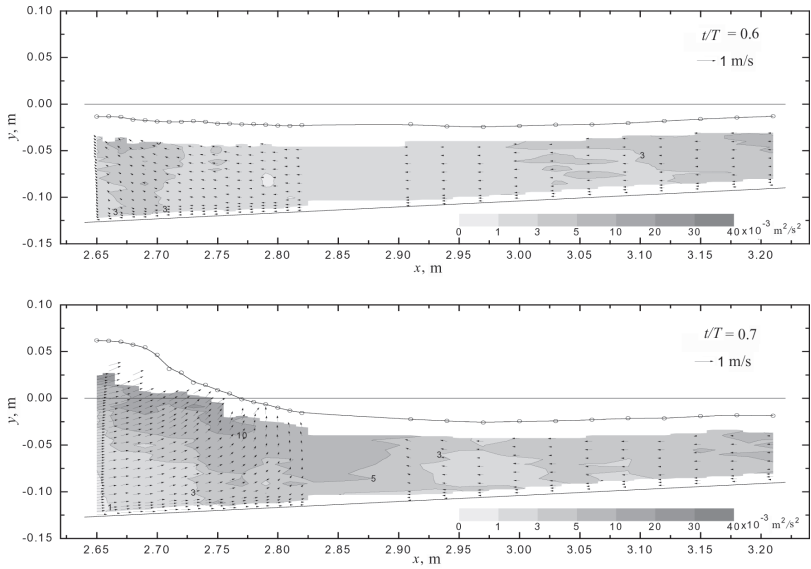
Fig. 11. Turbulent kinetic energy and velocity field at *t/T* = 0.6 and 0.7.
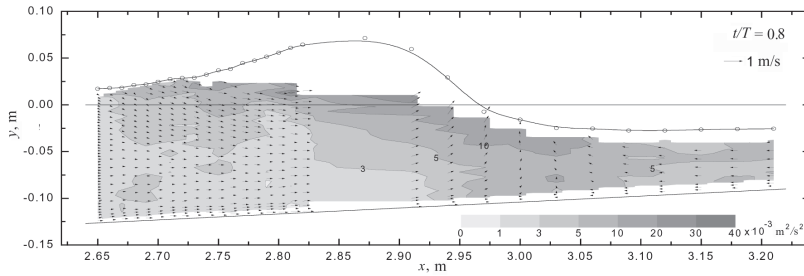
Fig. 12. Turbulent kinetic energy and velocity field at $t/T = 0.8$ and 0.85.
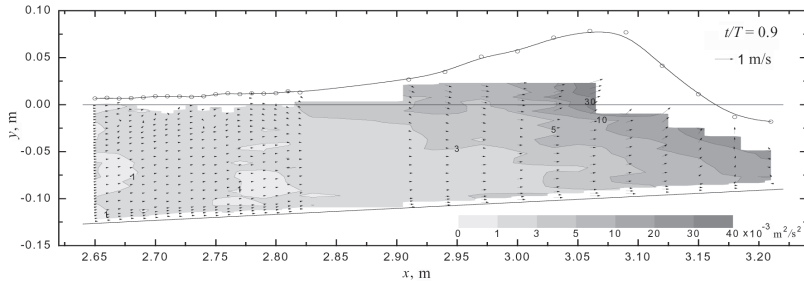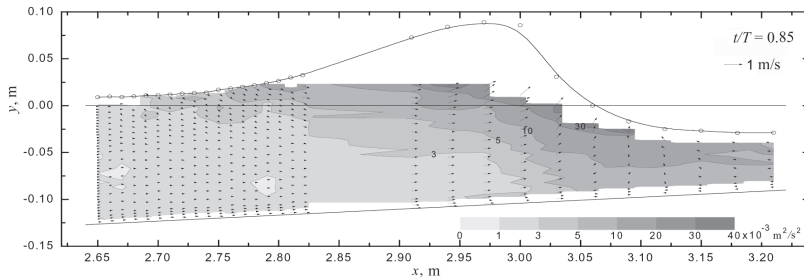
Fig. 13. Turbulent kinetic energy and velocity field at $t/T = 0.9$.

Besides the velocity vector fields, Figs. 8 to 13 present also turbulent kinetic energy fields in the breaking wave. In order to show both very low and high values of turbulent kinetic energy, a non-linear scale has been used. To the knowledge of the authors, similar graphs have not been published earlier.

Higher values of the turbulent kinetic energy are concentrated in the area under and before the wave crest (cf $t/T = 0.7$ to 0.9). The shoreward moving wave crest generates more and more energy that through dispersion spreads towards the bottom. At $t/T = 0.7$, when the crest is situated before the breaking point $(x = 2.90 \, \text{m})$, the turbulence, generated in the wave crest, starts spreading downwards. It reaches the bottom at $t/T = 0.9$.

The area with the largest values of turbulent kinetic energy is located at the wave crest. Figure 5 shows that the generation of the turbulent energy takes place in front of the crest, where the acceleration of the horizontal velocity component is the largest. This fact shows that energy is drawn from the generation zone and carried along with the wave.

The second area with a relatively high turbulent energy level is located behind the wave crest. Figure 5 shows that in this area the horizontal velocity is decelerating. The increase of turbulent fluctuations and hence also of turbulent kinetic energy has been noticed also by other authors [34]. The third area of generation of turbulence is the bottom boundary layer. Since during the present experimental run the smooth bottom was used, the increase of turbulent energy due to the bottom boundary layer is not large. It has been shown that the generation of turbulence by the boundary layer even in case of rough bottoms is neglible in comparison with the generation from the wave crest. Turbulent energy is therefore concentrated in the wave crest and in the rest of the wave there is practically no turbulent energy [6]. Turbulence is generated in front of the wave crest, drawn into it and carried on by it. Most of the turbulent energy dissipates behind the wave and during the breaking process. The same conclusion was also made in [19].

4. CONCLUSIONS

The present study concentrated on the behaviour of the plunging breaking wave in the outer surf zone. Experiments were carried out in the wave flume with a smooth bottom. The surf zone model had a constant slope of 1:17. Water particle velocities were measured with LDA technology.

During wave phases, when flow is directed away from the shoreline, the ensemble-averaged profiles of the horizontal velocity component resemble the profiles of the steady open channel flow. During the phases, when flow is directed towards the shore, the horizontal velocity of the water particles is larger in the near-bed zone and in the layers close to the water surface than in the intermediate layers.

The ensemble-averaged vertical velocity component gains its maximum value simultaneously with the maximum acceleration of the horizontal velocity component. In the upper layers of the water column, behind the wave crest the vertical component of velocity is always negative, and during backflow phases the value is close to zero.

As a result of the experimental investigations, two-dimensional flow and energy fields have been calculated. These allow to make the following conclusions.

– The turbulent kinetic energy has two local maximums that correspond to the extreme values of the vertical and horizontal accelerations.
– Before the breaking point, the time-averaged turbulent kinetic energy is practically constant. It starts increasing from the breaking point and has a sudden increase immediately before the crest plunges into the preceding trough.

- After the breaking point, the maximum value of the turbulent energy is located at the crest, from where it spreads all over the water column. This is different from the spilling breaking wave, where the turbulent fluctuations do not reach the bottom.
- There is always an area with water particles with purely vertical velocity, travelling in front of the wave crest. This phenomenon is more evident in the area immediately under the stillwater level.
- The turbulent kinetic energy, generated in the crest during the breaking process, dissipates immediately after the wave has passed.

ACKNOWLEDGEMENT

REFERENCES

1. Svendsen, I. A. and Hansen, J. B. Determination up to breaking of periodic waves on a beach. In *Proc. 16th Coastal Engineering Conference*. Hamburg, 1976, 477–496.
2. Chang, K.-A. and Liu, P. L.-F. Experimental investigation of turbulence generated by breaking waves in water of intermediate depth. *Phys. Fluids*, 1999, **11**, 3339–3400.
3. Stieve, M. J. F. Velocity and pressure field of spilling breaker. In *Proc. 17th Coastal Engineering Conference*. Sydney, 1980, 574–566.
4. Nadaoka, K. and Kondoh, T. Laboratory measurements of velocity field in the surf zone by LDV. *Coastal Eng. Japan*, 1982, **25**, 125–146.
5. Ting, F. C. K. and Kirby, J. T. Observation of undertow and turbulence in a laboratory surf zone. *Coastal Eng.*, 1994, **24**, 51–80.
6. Ting, F. C. K. and Kirby, J. T. Dynamics of surf zone turbulence in a strong plunging breaker. *Coastal Eng.*, 1995, **24**, 177–204.
7. Ting, F. C. K. and Kirby, J. T. Dynamics of surf-zone turbulence in spilling breaker. *Coastal Eng.*, 1996, **27**, 131–160.
8. Haydon, T. R., Hann, D. B., Davies, P., Greated, C. A. and Barnes, T. C. D. Turbulence structure in surf zone. In *Proc. 25th International Conference on Coastal Engineering*. Orlando, FL, 1996, 214–220.
9. Chang, K.-A. and Liu, P. L.-F. Measurements of breaking waves using particle image velocimetry. In *Proc. 25th International Conference on Coastal Engineering*. Orlando, FL, 1996, 527–537.
10. Deigaard, R., Mikkelsen, M. B. and Fredsoe, J. Measurements of the bed shear stress in the surf zone. *Progress Report*, ISVA, Techn. Univ. Denmark, Lyngby, 1991, **73**, 484–497.
11. Cox, D. T., Kobayashi, N. and Okayasu, A. Bottom shear stress on the surf zone. *J. Geophys. Res.*, 1996, **101**, 14337–14348.
12. Feddersen, F. and Trowbridge, J. H. The effect of wave breaking on surf-zone turbulence and alongshore currents: a modelling study. *J. Phys. Oceanogr.*, 2005, **35**, 2187–2202.
13. Trowbridge, J. H. and Agrawal, Y. C. Glimpses of wave boundary layer. *J. Geophys. Res.*, 1995, **100**, 20729–20743.
14. Feddersen, F. and Williams, A. J. III. A direct estimation of the Reynolds stress vertical structure in the near shore. *J. Atmos. Ocean. Techn.*, 2007, **24**, 102–116.
15. Bryan, K. R., Black, K. P. and Gorman, R. M. Spectral estimates of dissipation rate within and near the surf zone. *J. Phys. Oceanogr.*, 2003, **33**, 979–993.

16. Feddersen, F., Gallagher, E. L., Guza, R. T. and Elgar, S. The drag coefficient, bottom roughness and wave-breaking in the nearshore. *Coastal Eng.*, 2003, **48**, 189–195.

17. Fredsoe, J. and Deigaard, R. *Mechanics of Coastal Sediment Transport*. World Scientific, Singapore, 1992.

18. Songdong Shao. Simulation of breaking wave by SPH method coupled with $k - \varepsilon$ model. *J. Hydr. Res.*, 2006, **44**, 338–349.

19. Lin, P. and Liu, P. L. F. Turbulence transport, vorticity dynamics and solute mixing under plunging breaking waves in surf zone. *J. Geophys. Res.*, 1998, **103**, 15677–15694.

20. Lin, P. and Liu, P. L. F. A numerical study of breaking waves in surf zone. *J. Fluid Mech.*, 1998, **359**, 239–264.

21. Rodi, W. *Turbulence Models and Their Application in Hydraulics*. IAHR, Delft, 1980.

22. Nadaoka, K., Hino, M. and Koyano, Y. Structure of turbulent flow under breaking waves in the surf zone. *J. Fluid Mech.*, 1989, **204**, 359–387.

23. Pedersen, C., Deigaard, R. and Sutherland, J. Turbulence measurements under broken waves. *Progress Report*, ISVA, Techn. Univ. Denmark, Lyngby, 1993, **74**, 81–97.

24. Petti, M. and Longo, S. Turbulence experiments in swash zone. *Coastal Eng.*, 2001, **43**, 1–24.

25. Ting, F. C. K. Laboratory study of wave and turbulence velocities in a broad-banded irregular wave surf zone. *Coastal Eng.*, 2001, **43**, 183–208.

26. Liiv, T. An experimental investigation of the breaking wave characteristics in coastal regions. In *Proc. International Conference on Coastal and Port Engineering in Developing Countries COPEDEC IV*. Rio de Janeiro, 1995, vol. 3, 2334–2343.

27. Liiv, T. Investigation of turbulence in a plunging breaker wave. *Proc. Estonian Acad. Sci. Eng.*, 2001, **7**, 58–78.

28. Stieve, M. J. F. and Wind, H. G. A study of radiation stress and set-up in the nearshore region. *Coastal Eng.*, 1982, **6**, 1–25.

29. Svendsen, I. A. Analysis of surf zone turbulence. *J. Geophys. Res.*, 1987, **92**, 5115–5124.

30. Sakai, T., Mizutani, T., Tanaka, H. and Tada, Y. Vortex formation in plunging breakers. In *Proc. International Conference on Coastal Engineering*. Taipei, Taiwan, 1986, vol. 1, 711–723.

31. Schäffer, H. A., Madsen, P. A. and Deigaard, R. A Boussinesq model for waves breaking in shallow water. *Coastal Eng.*, 1993, **20**, 185–202.

32. Takikawa, K., Yamada, F. and Matsumoto, K. Internal characteristics and numerical analysis of plunging breaker on a slope. *Coastal Eng.*, 1997, **31**, 143–161.

33. Christensen, E. D. and Deigaard, R. Large eddy simulation in breaking waves. *Coastal Eng.*, 2001, **42**, 53–86.

34. Aitsam, A., Daniel, E. and Liiv, U. Investigation of the velocity distribution and shear stresses in decelerated pipe flow. *Proc. Estonian Acad. Sci. Phys. Math.*, 1990, **39**, 290–295.

Murdlaine hüdrodünaamilise kiirusvälja ja kineetilise energia muutumine laine murdepunkti ümbruses

Toomas Liiv ja Priidik Lagemaa

On vaadeldud lainetust lainerennis, mille põhja kalle on 1:17. Kasutades LDA-mõõtmisi, on uuritud laine perioodi jooksul kahemõõtmelist kiirusvälja, murdlaine kiiruse horisontaal- ja vertikaalkomponendi aegridu ning hetkväärtusi eri ajamomentidel. Kõik mõõtmised on teostatud murdepunkti ümbruses kokku 29 ristlõikes. Mõõtmistulemuste töötlemise põhjal on määratud turbulentse kineetilise energia muutumine risti rannajoonega ja kahemõõtmeline kiiruse vektorväli.

DISSERTATIONS DEFENDED AT
TALLINN UNIVERSITY OF TECHNOLOGY ON
CIVIL ENGINEERING

1. **Heino Mölder**. Cycle of investigations to improve the efficiency and reliability of activated sludge process in sewage treatment plants. 1992.

2. **Stellian Grabko**. Structure and properties of oil-shale Portland cement concrete. 1993.

3. **Kent Arvidsson**. Analysis of interacting systems of shear walls, coupled shear walls and frames in multi-storey buildings. 1996.

4. **Andrus Aavik**. Methodical basis for the evaluation of pavement structural strength in Estonian Pavement Management System (EPMS). 2003.

5. **Priit Vilba**. Unstiffened welded thin-walled metal girder under uniform loading. 2003.

6. **Irene Lill.** Evaluation of Labour Management Strategies in Construction. 2004.

7. **Juhan Idnurm**. Discrete analysis of cable-supported bridges. 2004.

8. **Arvo Iital**. Monitoring of Surface Water Quality in Small Agricultural Watersheds. Methodology and optimization of monitoring network. 2005.

9. **Liis Sipelgas**. Application of satellite data for monitoring the marine environment. 2006.

10. **Ott Koppel**. Infrastruktuuri arvestus vertikaalselt integreeritud raudtee-ettevõtja korral: hinnakujunduse aspekt (Eesti peamise raudtee-ettevõtja näitel). 2006.

11. **Targo Kalamees**. Hygrothermal criteria for design and simulation of buildings. 2006.

12. **Raido Puust**. Probabilistic leak detection in pipe networks using the SCEM-UA algorithm. 2007.

13. **Sergei Zub**. Combined treatment of sulfate-rich molasses wastewater from yeast industry. Technology optimization. 2007.

14. **Alvina Reihan**. Analysis of long-term river runoff trends and climate change impact on water resources in Estonia. 2008.

15. **Ain Valdmann**. On the coastal zone management of the city of Tallinn under natural and anthropogenic pressure. 2008.

16. **Ira Didenkulova**. Long wave dynamics in the coastal zone. 2008.

17. **Alvar Toode**. DHW consumption, consumption profiles and their influence on dimensioning of a district heating network. 2008.

18. **Annely Kuu**. Biological diversity of agricultural soils in Estonia. 2008.

19. **Andres Tolli**. Hiina konteinerveod läbi Eesti Venemaale ja Hiinasse tagasisaadetavate tühjade konteinerite arvu vähendamise võimalused. 2008.

20. **Heiki Onton**. Investigation of the causes of deterioration of old reinforced concrete constructions and possibilities of their restoration. 2008.

21. **Harri Moora**. Life cycle assessment as a decision support tool for system optimisation – the case of waste management in Estonia. 2009.

22. **Andres Kask**. Lithohydrodynamic processes in the Tallinn Bay area. 2009.

23. **Loreta Kelpšaitė**. Changing properties of wind waves and vessel wakes on the eastern coast of the Baltic Sea. 2009.

24. **Dmitry Kurennoy.** Analysis of the properties of fast ferry wakes in the context of coastal management. 2009.

25. **Egon Kivi**. Structural behavior of cable-stayed suspension bridge structure. 2009.

26. **Madis Ratassepp**. Wave scattering at discontinuities in plates and pipes. 2010.

27. **Tiia Pedusaar**. Management of lake Ülemiste, a drinking water reservoir. 2010.

28. **Karin Pachel**. Water resources, sustainable use and integrated management in Estonia. 2010.

29. **Andrus Räämet**. Spatio-temporal variability of the Baltic Sea wave fields. 2010.

30. **Alar Just**. Structural fire design of timber frame assemblies insulated by glass wool and covered by gypsum plasterboards. 2010.